TUNABLE CPW RING RESONATOR-BASED BANDPASS FILTERS UTILIZING RF MEMS VARACTORS

by

Ahlam Mohammad Ebrahim Pish Dast

A Thesis Presented to the Faculty of the
American University of Sharjah
College of Engineering
in Partial Fulfillment
of the Requirements
for the Degree of

Master of Science in
Electrical Engineering

Sharjah, United Arab Emirates

January 2017

Approval Signatures

We, the undersigned, approve the Master's Thesis of Ahlam Mohammad Ebrahim Pish Dast.

Thesis Title: Tunable CPW Ring Resonator-Based Bandpass Filters Utilizing RF MEMS Varactors.

Signature **Date of Signature** (dd/mm/yyyy)

_____ _____

Dr. Maher Bakri Kassem
Assistant Professor, Department of Electrical Engineering
Thesis Advisor

_____ _____

Dr. Oualid Hammi
Associate Professor, Department of Electrical Engineering
Thesis Committee Member

_____ _____

Dr. Taha Landolsi
Professor, Department of Computer Science and Engineering
Thesis Committee Member

_____ _____

Dr. Nasser Qaddoumi
Head, Department of Electrical Engineering

_____ _____

Dr. Ghaleb Husseini
Associate Dean for Graduate Affairs and Research
College of Engineering

_____ _____

Dr. Richard T. Schoephoerster
Dean, College of Engineering

_____ _____

Dr. Mohamed El-Tarhuni
Vice Provost Graduate Studies

Acknowledgements

Firstly, I am grateful to Allah for His tremendous support, and guidance; for bestowing on me good health and wellbeing that were necessary to complete this thesis. I want to thank my husband, my parents and brothers for their unceasing encouragement, support and attention. I also want to thank my advisor; Dr. Maher Bakri-Kassem for guiding and helping me in order to make this thesis a well done achievement. Also, I want to acknowledge the Electrical Engineering Department of the American University of Sharjah for providing me the support of receiving the graduate teaching assistantship. Finally, I want to thank all my friends and colleagues for their support.

To my husband and parents …

Abstract

Radio Frequency (RF) Micro-Electro-Mechanical Systems (MEMS) switches are mostly used in many applications such as: tunable filters, phase shifters and oscillators because they offer wide bandwidth, low insertion loss, excellent isolation and outstanding linearity in comparison with their electronic counterparts. The objective of this research is to design and implement tunable RF MEMS based bandpass filters (BPF) using coplanar waveguide (CPW) ring resonator with both frequency control, and to achieve tunable BPF that demonstrate low insertion loss, high return loss, high quality factor, and compact size. Tunable bandpass filters that are RF MEMS based have the potential to advance wireless communications and radar systems due to their superior RF performance in comparison with conventional tunable filters. Four new types of bandpass filters using CPW technology with open ring resonators are proposed in this work which being tuned using RF MEMS capacitive switches to achieve wide tuning range with multiple DC biasing circuits. The advantage of designing the filter with CPW structure is having the ground plane and the signal conductor on the same level. This feature allows achieving compact structures in comparison with microstrip technology and will allow the integration with other technology such as RF MEMS. Two tunable ring resonators and two second order BPF are introduced in this thesis. The ring resonator that is the basic block of the proposed tunable filters is of a circular shape and open type where the RF MEMS capacitive switches are placed in the open area of the ring resonator between the edges to tune the electrical length and achieve tunability. For the second order BPF, two ring resonators are coupled with two couplers and a CPW waveguide. All proposed filters are built on an Aluminum Oxide (Al2-O3) ceramic substrate with the thickness of 675 μm. The first and second designs of tunable ring resonator are designed at 2 GHz. These two designs are used in wireless communications, WiMAX (Worldwide interoperability Microwave Access), mobile GSM and ISM bands. The third and fourth designs of tunable bandpass filter are designed at 20 GHz, and they can be used in mobile satellite applications.

Search Terms: RF MEMS Capacitive Switches, CPW Technology, Ring Resonator, BPF

Table of Contents

List of Figures

List of Tables

List of Abbreviations

ADS - Advanced Design System

BPF - Band-Pass Filter

CAD - Computer Aided Design

CPW - Co-Planar Waveguide

CR - Cognitive Radio

EM - Electro-Magnetic

HFSS - High Frequency Structural Simulator

IL - Insertion Loss

MEMS - Micro-Electro-Mechanical System

Q - Quality Factor

RF - Radio Frequency

RL - Return Loss

TEM - Transverse Electro-Magnetic

UHF - Ultra High Frequency

VHF - Very High Frequency

Chapter 1: Introduction and Literature Review

1.1. Introduction

The fundamental concept of microwave engineering was developed because of the radar which was the first major application of microwave technology. The frequencies in the range of 100 MHz to 1000 GHz introduce the field of radio frequency (RF) and also of microwave engineering. There are different frequency ranges which span from very high frequency (VHF) to ultra-high frequency (UHF), but in the case of microwaves, the frequencies used are between 3 and 300 GHz, with a corresponding electrical wave length between $\lambda = 10$ cm and $\lambda = 1$ mm [1] The RF and microwave frequency bands are shown in the electromagnetic spectrum of Fig 1.1.

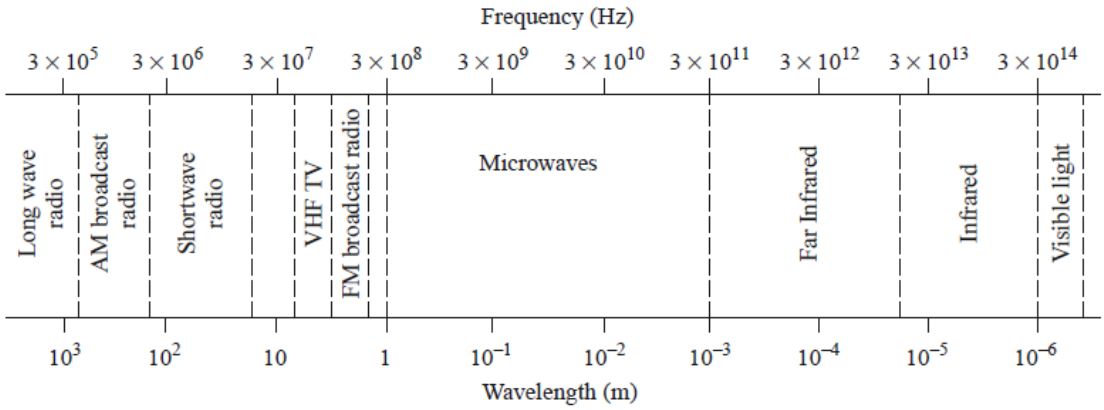

Fig 1.1: Different frequency bands in electromagnetic spectrum

In 1873, the first modern electromagnetic theory was formulated by James Clerk Maxwell. The idea behind this theory was derived from electromagnetic energy. During the period 1885 to 1887, the Maxwell's formulation was cast in its modern form by Oliver Heaviside, in which he removed many of the mathematical complexities of Maxwell's theory and introduced vector notation and provided a foundation for practical applications of guided waves and transmission lines [1]

During the recent years, the significant and continuing developments are in high frequency solid state devices, microwave integrated circuits, computer aided design techniques, and the applications of RF and microwave technology to wireless communications. The radio technology growth was restricted to the HF (High

Frequency) and to VHF (Very High Frequency) range in the early 1900s, because of the lack of reliable microwave sources and other components[1]

Microwave filters are used to provide frequency selectivity in mobile and satellite communications, radar, electronic warfare, and remote sensing systems operating at microwave frequencies. In general, the electric performance of the filter is described in terms of its insertion loss, return loss, frequency selectivity (or attenuation at rejection band), group delay variation in the passband, and so on [2] The filter should be designed such that there is a small insertion loss, large return loss for impedance matching with interconnecting components, and high frequency selectivity to prevent interference.

There are four types of filter designs which are the Butterworth (maximally flat), Chebyshev (equal ripple in the passband), inverse Chebyshev (equal ripple in the stopband) and elliptic (equal ripple in the passband and stopband) [2] The Chebyshev filters are widely used in filter design; because the Chebyshev response has a fairly good frequency selectivity compared to Butterworth response for the same order, however, Butterworth has better phase response.

Wireless communications systems have been demanding tighter requirements in terms of electrical specifications as well as drastic reductions of manufacturing costs and development times [3] Electrically tunable or reconfigurable microwave devices, such as filters, are in great demand in existing and future radio frequency (RF) front-ends as many wireless communication systems become more and more complex in an increasingly crowded radio spectrum environment [4] The major issue of designing the filter is to improve both electrical and mechanical performance. Moreover, the main function for filter designers is to reduce the size and volume of the filter. Dielectric resonators have always been a good choice for this purpose. The advantages of dielectric resonators are their small sizes and high temperature stability. Also, creating the dual mode technique in filters; will help reduce the volume and mass of microwave filters.

There are advantages of coplanar waveguide (CPW) over microstrip, which are: wider range of realizable impedances, less dispersion, and easier to integrate with solid state devices with no need of connection via grounding [6] In some CPW filter

designs, additional bond-wires or air-bridges are used to connect two ground planes on both sides of the signal conductor, so the grounds are in the same polarity.

There are advantages of transmission lines used in filters which are compact, low cost, and capable of being easily integrated with active circuit devices, such as diodes and transistors, to form microwave integrated circuits.

A ring resonator consists of a closed loop of transmission line. It acts as a bandpass filter. Ring resonators are used to measure dispersion, phase velocity, and dielectric constant [7] In general, the resonance happens at frequencies at which the circumference of the ring is equal to a whole number, *n*, of guided wavelengths on the transmission line. The advantages of ring resonator are low radiation loss, high Q value and dual modes.

The tunable filter design technique, which is the aim of this thesis, is another microwave filter design technique since recent broadband receiving and transmitting systems have increased the demand for frequency tunability of microwave components. Tuning the filter which is changing the center frequency is done by switching from one filter to the other, so in this case the number of the filters inside the system should be equal to the number of the channels. There are different types of planar technologies for the tuning filters which are: 1) semiconductor (silicon, GaAs) varactor diodes; 2) p-i-n diodes; 3) ferroelectric varactors; and 4) RF microelectromechanical systems (RF-MEMS) devices. Tuning range, tuning speed, and tuning linearity are the most important parameters for tunable filters. Varactor tuning technique is used for fast tuning speed, as it can be easily integrated on coplanar waveguide and microstrip structure. The varactors are non-linear devices, so the large input signals generate harmonics. Small size, fast tuning speed, and low insertion loss are the advantages of MEMS capacitive switches, but they create narrow tuning range due to poor capacitance ratio.

High quality factor, high power and high selectivity microwave tunable bandpass filters have become indispensable components for modern multiband communication systems due to rigorous specification requirements.

In general, there is no perfect tunable filter with all advantages mentioned before in the same time. The most concerning point for designing the tunable filter is to change both the center frequency of the filter and the bandwidth with minimal

insertion loss and maximum return loss. The tunable filer should have the same performance for all channels with different center frequencies.

Finally, for all kinds of filters, reducing the size of the filter has always received a great attention. Recent solid state device technologies have made it possible to implement miniaturized electronic circuits including microwave devices and components [8]. The number of resonators used in the filter has the large dimension of the distributed filter stems. Moreover, many researchers made a lot of efforts to develop the topologies of miniaturized resonators [8]

In this thesis, a novel tunable CPW open ring resonator bandpass filter is designed and implemented on HFSS and ADS simulation. In the following section, the published papers for ring resonators design and CPW filters are introduced with frequency responses. Chapter two is about the theory background of designing the filters, ring resonator and general information about CPW transmission line and resonators. Then, chapter three and four introduce the novel design structure and design steps with simulation results for two different center frequencies. Layout simulations and their circuit model simulations with calculation of quality factor of the filter are included in the same chapters three and four as well. Moreover, chapter five summarizes and compares the obtained results with that previously reported in the literature. Finally, chapter six concludes this thesis and gives recommendations for a future works.

1.2. Literature Review

Many different design structures and configurations are available in the literature; wide band ring resonator [9] coupled ring resonator [10] tri-mode bandpass filter [11-12], transversal resonator array bandpass filter [13] square ring resonator bandpass filter [14] varactor tuned ring resonator bandpass filter [15] dual band ring resonator bandpass filter [16] tunable bandpass filter with constant bandwidth [17] tunable filter-antenna ring resonator [18] and wideband bandpass filter with dual-mode ring resonator [19] They have been all designed and implemented in microstrip structures technology with various material in substrate and signal plane.

The dual-mode resonator microstrip filter was firstly introduced by Wolff in 1972 [20] It became an attractive subject for research in wireless communication systems. It includes microstrip technology with almost symmetrical shape for gaining

dual-mode and resonant frequencies. Microstrip ring resonators are widely used in antennas, bandpass filters, oscillators, couplers and mixers [21] Compact size and high quality factors are the advantages of designing bandpass filter using dual-mode ring resonator.

A new asymmetric ring resonator wideband microstrip bandpass filters is designed under multiple resonances [9] The structure of this filter is squared ring with two capacitive coupling elements at perpendicular positions. Due to the symmetrical design of this squared ring resonator filter, the filter has even and odd modes, which has different structure for each modes. On even mode, the two sides of the schematic design become open circuited, but in case of odd mode, the two end sides become short circuited.

Bandpass filter using ring resonator with quasi elliptic function and very large bandwidth around 0.5 GHz is presented in [10] This design presents a new coupled ring resonator with symmetrical shape which makes the filter operate in dual (even/odd) modes. In addition to the symmetric plane of the input/output feeds, two open stubs are connected to the inner ring to move a transmission zero from mid-passband to the lower transition band.

In [11] a spiral shape resonator with short and open stub is used to design high selectivity triple mode microstrip bandpass filter. The structure of this filter consists of spiral half-wavelength resonator loaded with two short stubs and a T-type open stub. Because of the symmetrical shape of resonator, the filter can be analyzed by odd and even mode methods to find resonant frequencies of the resonator. The layout is designed by using microstrip resonators and Rogers TMM10 substrate with thickness of 1 mm.

Another planar microstrip tri-mode bandpass filter using center stub loaded spiral resonator is introduced in [12] which is almost the same as [11] In here, half wavelength spiral resonator center loaded with two T-shaped open stubs has been used to design a new tri-mode bandpass filter. The resonator of this filter has been controlled by tuning the electrical length of the spiral resonators and T shaped stubs.

A microstrip filter structure using transversal resonator array and fully canonical bandpass filter is proposed in [13] which is made by the parallel arrangement of even and odd mode half wavelength resonators. Multiple transmission

zeros achieved by controlling of external quality factors for multiple resonators, without using any couplings between adjacent non adjacent resonators [13]

A microstrip square ring resonator is designed, fabricated and measured for a low loss bandpass filter by using two asymmetrically loaded open circuited stubs [14] In this design, the stop-band characteristics of ring resonator is used to develop a bandpass filter. The center frequency of this filter appears at 2.4 GHz with bandwidth of 1.4 GHz. The equivalent circuit model of the filter is also designed with almost identical S-parameters response. Parallel coupled lines are introduced at the input and output feed lines of the ring resonator for the improvement of the rejection band zone. All the simulations done in this paper are carried out using both time domain and frequency domain full wave simulators.

A tunable microstrip ring resonator bandpass filter with center frequency of 2.5 GHz is designed to have tunable bandwidth for the mid-upper passband bandwidth [15] Mid-upper passband bandwidth is tuned by varying capacitance of four shunt varactors, but the mid-lower band is almost fixed. In this design, equivalent serial capacitor is used to design open stub which is attached to the ring resonator. All the EM simulations is this work are done in HFSS.

In [16] a bandpass filter is designed by using dual-band ring resonator based on two pairs of first and second order degenerate resonant modes. The frequency response of the filter has two transmission poles in both passbands. Firstly, in order to excite the two first order degenerate modes and create multiple transmission zeros, two capacitors or parallel coupled lines are placed at two non-orthogonally excited positions along a ring resonator. Then, for two second order degenerate modes to excite, a set of perturbations is used on the ring resonator. In this ring resonator, four and eight open circuited stubs are loaded symmetrically along the ring, which makes the filter excite two poles in the second passband.

A microstrip tunable second order bandpass filter is designed with constant bandwidth by using switchable varactor tuned resonators [17] A combination of electric and magnetic coupling is developed to get a near constant absolute bandwidth across the tuning range. The switchable tunable resonators and switchable feed lines are used to utilize a wide tuning range and compact size.

A compact filter-antenna with tunable frequency band is designed and simulated in [18] which is used for interweave cognitive radio (CR) systems. A microstrip ring resonator bandpass filter is designed with antenna. The tuning of this design is done by using single varactor diode, and it has simple biasing voltage which has a small effect on the filter-antenna performance. According to the results, filter-antenna is able to tune over a wide operating band of 1.43 GHz.

A bandpass filter using dual mode square ring resonator is designed in [19] with a multiple mode parallel coupled line structure, which is used for vehicular radar systems. There are transmission zeros in the lower and upper stopbands of the filter. The frequency response of this filter has a sharp rejection near the passband, and extremely wide stopband. A parallel coupled line is used in millimeter wave.

In this thesis, CPW ring resonator is used to design first and second order bandpass filter. The tuning of this filter is done by using RF MEMS capacitive switches, which is placed at the ring resonator. The Aluminum Oxide (Al2-O3) ceramic substrate is used to design this filter with thickness of 675 μm. The filter is designed for two different ring resonator radios which operate at two different center frequencies. The smaller of overall size of the filter is the main benefit of using CPW technology.

1.3. Thesis Organization

Chapter two contains the basics of microwave filters which are the main parameters like polynomials, coupling matrix, transmission lines, resonators and quality factor. Moreover, different types of microwave filters will be discussed along with their frequency responses. In chapter three, the first and second order microwave bandpass filters at 2 GHz center frequency are designed and simulated in both HFSS and ADS software for layout and schematic designs. RF MEMS capacitive switches are used to tune the filter. Chapter four introduces the same novel design but for 20 GHz center frequency. In chapter five, the results of both layout and schematic are compared to each other and with prior art. Finally, in chapter six, the conclusion of the thesis and future works are discussed.

1.4. Thesis Contribution

The novelty of this thesis is to design microwave filter in CPW structure by using ring resonator. The other advantage of this work is to get better return loss and

insertion loss for the filter design. The main achievement of this thesis is to show the advantages of using CPW technology, which makes a smaller overall size of the layout design. By comparing this work with other available literature, this filter provides better performance in insertion loss and return loss with overall reduced in size.

Chapter 2: Microwave Filters Theory Background

In this chapter, microwave filters basics which are polynomials and different types of microwave bandpass filters such as maximally flat, equal ripple, elliptic function, and linear phase will be covered in detail. Coupling matrix, transmission lines, resonators, and quality factor will be also explained. At the end of the chapter, RF MEMS and their advantages will be discussed.

2.1. Filter Network Theory

The microwave filter is used in many electronic systems such as mobile, radio, satellite communications and radar [20] The function of filters is to select or reject signal at different frequencies for the certain application frequencies. Also, the physical realization of microwave filters may vary, while the circuit network theory is common to all [21]

RF and microwave filters can be designed in many ways and each of these are designed based on the requirement of the filters. In general, microwave filters are two port networks used to control the frequency response in an RF or microwave systems. They allow the frequency in the range of pass-band to pass, and attenuate the rest of signals which are out of their pass-band. The first step of designing microwave filter is explained in next section.

2.1.1. Filter design using polynomials. First of all, to begin the filter design using insertion loss method is to define the low pass transfer function which is a ratio of output voltage to input voltage, which may be written as [22]

$$\frac{V_{out}}{V_{in}} = \frac{a_m S^m + a_{m-1} S^{m-1} + \cdots + a_1 S + a_0}{b_n S^n + b_{n-1} S^{n-1} + \cdots + b_1 S + b_0} = t(S) \qquad (1)$$

Where S= σn + jΩ is the normalized complex frequency. This is the common variable used in Laplace transformation theory. In order to have a stable system, the denominator of t(s) must be Hurwitz (the roots of the denominator must be in the left half plane complex frequency domain). By evaluating the transfer function t(s) at S = jΩ, the ratio of the output amplitude to the input amplitude can be created. S = jΩ is a

sinusoidal frequency, while the letter Ω represents real angular frequencies but the letter S is said to represent complex frequencies.

If the output amplitude of a sinusoidal is smaller than the amplitude at the input, then the signal is said to have been attenuated, and the signal is in terms of decibels (dB) as shown in Eq. 2, and this expression can be written as Eq. 3 by defining the transfer function t(s) [22]

$$A(\Omega) = 20\log\left|\frac{V_{in}(j\Omega)}{V_{out}(j\Omega)}\right| \tag{2}$$

$$A(\Omega) = 20\log|t(j\Omega)| \tag{3}$$

It is a common practice to consider functions that are ratios of input to output, so it can be expressed by Eq. 4, then from Eq. 3, the attenuation of filter can be described by Eq. 5.

$$H(S) = \frac{1}{t(S)} = \frac{b_n S^n + b_{n-1}S^{n-1} + \cdots + b_1 S + b_0}{a_n S^n + a_{n-1}S^{n-1} + \cdots + a_1 S + a_0} = \frac{E(S)}{P(S)} \tag{4}$$

$$A(\Omega) = 20\log|H(j\Omega)|. \tag{5}$$

H(S) is referred to a function of input *P(S)*/output *E(S)* transfer function. In the passband of a filter, the approximated shape is usually a constant. To simplify the constant value, it can be normalized to unity which is approximately equal to one. It is suitable to remove this constant term and instead use the characteristic function *K(S)* defined by Eq. 6. From Eq. 4, it is shown that *H(S)* and *K(S)* have the same denominator polynomial, so *K(S)* can be expressed by Eq. 7 which *F(S)* is a function of input/output transfer function. Finally, the attenuation of the network will be written as Eq. 8 [21]

$$H(S)H(-S) = 1 + K(S)K(-S) \tag{6}$$

$$K(S) = \frac{F(S)}{P(S)} \tag{7}$$

$$A(\Omega) = 10\log|H(j\Omega)|^2 = 10\log(1 + |K(j\Omega)|^2) \tag{8}$$

As a result, from Eq. 8, when either H(jΩ) or K(jΩ) is infinite, the attenuation is infinite. However, just when K(jΩ) is zero, there is an attenuation zero. In this case, the characteristic function is more useful; because it removes the unity constant and focuses more on the attenuation zeros (reflection zeros) and attenuation poles (transmission zeros).

2.2. Microwave Bandpass Filter

The definition of filter is to control the frequency response at a certain point in an RF or microwave system by providing transmission at frequency within the passband of the filter and attenuation in the stopband of the filter [21] There are different frequency responses of filter which are low-pass, high- pass, bandpass, and band- reject characteristics. Applications can be found in almost any type of RF or microwave communication, radar, or test and measurement systems [20]. Sophisticated computer-aided design (CAD) tools based on the insertion loss method are used for most microwave filter design.

Next section provides the frequency characteristics of periodic structures, which consist of a transmission line or waveguide periodically loaded with reactive elements. Image parameter method is to design the filter which consists of a cascade of simpler two port filter sections to provide the desired cutoff frequencies and attenuation characteristics but not allow the specification of a particular frequency response over the complete operating range. Therefore, while the technique is very simple, the design of filters using this method must be repeated many times to achieve the desired results. The other method is called insertion loss method, which uses network synthesis techniques to design filters with a completely specified frequency response. In this method, first the low-pass filter prototypes are normalized in terms of impedance and frequency, then transformations are applied to convert the prototype designs to the desired response type frequency range, and impedance level.

2.2.1. Periodic structure of filter. An example of a periodic structure is an infinite transmission line or waveguide periodically loaded with reactive elements. Depending on the transmission line media being used, various forms of periodic structure can take. Often, the loading elements are formed as discontinuities in the line itself, but in any case they can be modeled as lumped reactance in shunt or series on a transmission line, as shown in Fig 2.1 and Fig 2.2 [23] Periodic structures

support slow-wave propagation (slower than the phase velocity of the unloaded line), and have passband and stopband characteristics similar to those of filters; they find application in traveling-wave tubes, masers, phase shifters, and antennas [20]

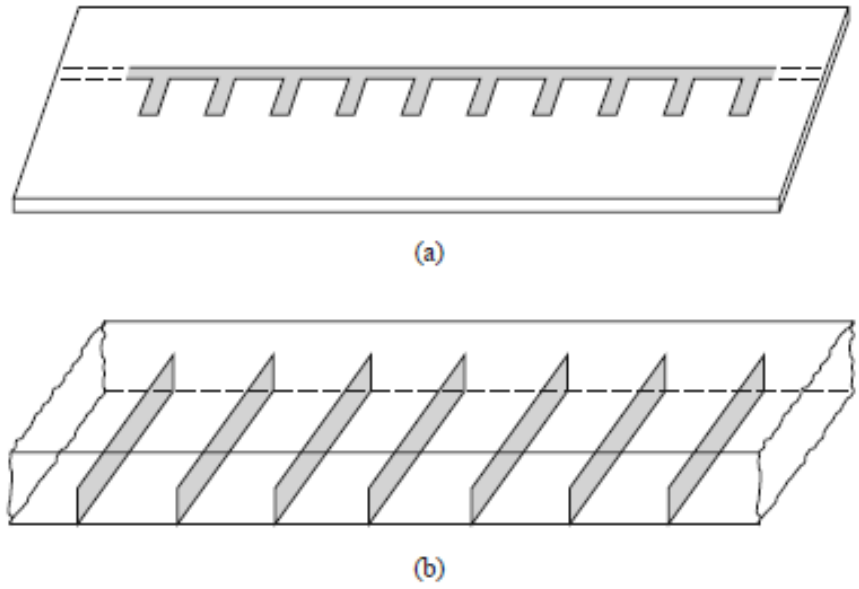

Fig 2.1: Examples of periodic structures. (a) Periodic stubs on a microstrip line. (b) Periodic diaphragm in a waveguide [20]

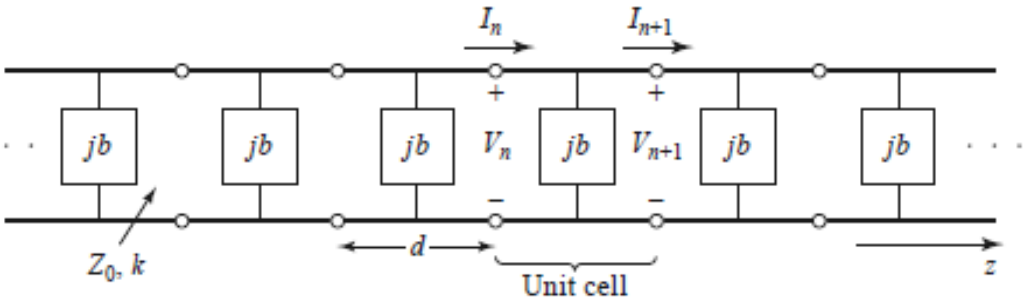

Fig 2.2: Equivalent circuit of a periodically loaded transmission line. The unloaded line has characteristic impedance $\boldsymbol{Z}_\circ$ and propagation constant K [20]

2.2.2. Filter design using image method The filter design using image method is to calculate the input and output impedances. The image impedance of the filter using image method is same as transmission line characteristic impedance. There is a relation between image parameters and the general circuit parameters, whose transmission properties can be defined in terms of their image parameters. The example of image properties of the L-section network is shown in Fig 2.3 [24]

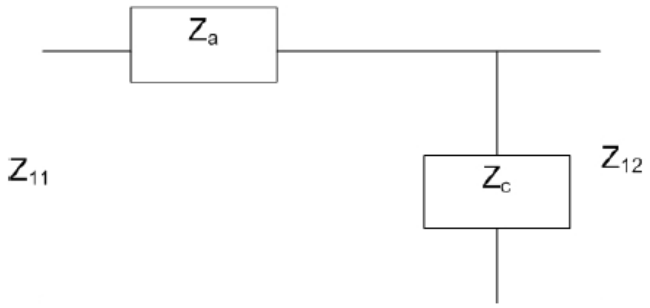

Fig 2.3: L section network [21]

$$Z_{11} = \sqrt{Z_a(Z_a + Z_c)} \tag{9}$$

$$Z_{12} = \frac{Z_a Z_c}{\sqrt{Z_a(Z_a + Z_c)}} \tag{10}$$

$$\gamma = coth^{-1}\sqrt{1 + Z_c/Z_a} \tag{11}$$

Z_{11}, Z_{12} and γ are the image parameters, where Z_a and Z_c are the transmission properties of the L-section network.

2.2.3. Filter design using network synthesis method. In this method, the transfer function of the circuit is used to design a filter. The transmission coefficient is an example of the transfer function. By using the transfer function, the input impedance of a circuit can be found, then expanded to give the element values of the circuit. There are many methods that come up with network synthesis methods, but the most common is insertion loss method [25]

A perfect filter would have zero insertion loss in the passband, infinite attenuation in the stopband, and a linear phase response (to avoid signal distortion) in the passband [26] This kind of filter does not exist in practice, so compromises must be made which is the art of filter design. The image parameter method is useful for some applications, but there is no methodical way of improving the design. However, the insertion loss method has a high degree of control over the passband and stopband amplitude and phase characteristics, with a systematic way to synthesize a desire response. According to the types of response, the different filter types of this method can be used. For example, for minimum insertion loss, a binomial response could be used; a Chebyshev response would satisfy a requirement for the sharpest cutoff. The

different filter prototypes are described in this part, and the order of the filter is equal to the number of reactive elements [24]

Insertion loss method can be used for low-pass, high-pass, band-pass and band-stop filters. There are different responses between insertion loss, sharp cut-off and good phase response, so it can be divided into maximally flat, equal ripple, elliptic function and linear phase filter responses [27] A filter response using the insertion loss method is defined by the insertion of a device in a transmission line, or power loss ratio, P_{LR} as shown in Eq. 12. The insertion loss (IL) in dB is described by Eq. 13. $|\Gamma(\omega)|^2$ is an even function of ω; so it can be expressed as a polynomial in ω^2, thus, the equation will be as shown in Eq. 14. Here, *M* and *N* are real polynomials in ω^2 and the power loss ratio equation then can be written as given in Eq. 15 [21]

$$P_{LR} = \frac{Power\ available\ from\ source}{Power\ delivered\ to\ load} = \frac{P_{inc}}{P_{load}} = \frac{1}{1 - |\Gamma(\omega)|^2} \tag{12}$$

$$IL = 10 \log P_{LR} \tag{13}$$

$$|\Gamma(\omega)|^2 = \frac{M(\omega^2)}{M(\omega^2) + N(\omega^2)} \tag{14}$$

$$P_{LR} = 1 + \frac{M(\omega^2)}{N(\omega^2)} \tag{15}$$

Maximally flat response is also called binomial or Butterworth response, and it provides the flattest possible passband response for a given filter complexity. The expression of loss-pass filter is:

$$P_{LR} = 1 + K^2 \left(\frac{\omega}{\omega_c}\right)^{2n} \tag{16}$$

From Eq. 16, *n* is the order of the filter, and ω_c is the cutoff frequency. The passband response is from ω=0 to ω =ω_c; at the band edge the power loss ratio is 1 + K^2. As common, it is chosen as the -3dB point, K will be equal to one. For ω >ω_c, the attenuation and frequency have proportional effect, as shown in Fig 2.4.

Equal ripple or the Chebyshev polynomial is used to specify the insertion loss of an n^{th} order low-pass filter which can be expressed by Eq. 17. Minimizing the error between the idealized and the actual filter characteristics over the range of the filter is the property of Chebyshev filters.

$$P_{LR} = 1 + K^2 T_N^2 \left(\frac{\omega}{\omega_c}\right) \tag{17}$$

From Eq. 17, the sharper cutoff will result, although the passband response will have ripples of amplitude 1 + K² as shown in Fig 2.4.

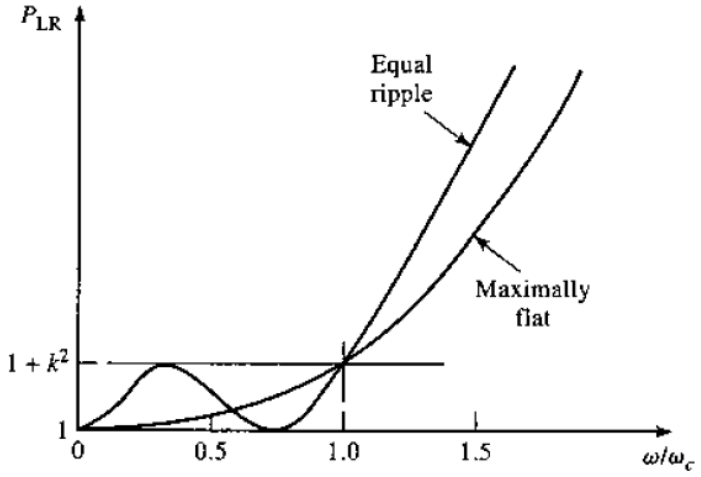

Fig 2.4: Maximally flat and equal ripple low pass filter responses (N=3) [21]

Both the maximally flat and equal ripple responses have an increased attenuation in the stopband. In case of elliptic function filters, they have minimum stopband attenuation, and equal ripple responses in the passband as well as in the stopband, as shown in Fig 2.5. A_{max} is the maximum attenuation in the passband, and A_{min} is the minimum attenuation in the stopband.

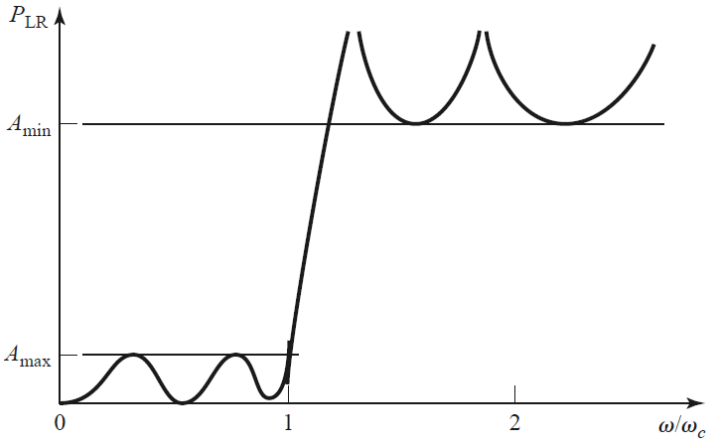

Fig 2.5: Elliptic function LPF response [21].

The filters mentioned above specify the amplitude response, but in some applications such as multiplexing filters for communication systems, it is important to have a linear phase response in the passband to avoid signal distortion. A linear phase

characteristic can be written as Eq. 18. Ø (ω) which is the phase of the voltage transfer function of the filter, and p is a constant. Maximally flat function is the group delay for a linear phase response filter which is described by Eq. 19.

$$\emptyset(\omega) = A\omega\left[1 + p\left(\frac{\omega}{\omega_c}\right)^{2n}\right] \tag{18}$$

$$\tau_d = \frac{d\emptyset}{d\omega} = A\left[1 + p(2N+1)\left(\frac{\omega}{\omega_c}\right)^{2n}\right] \tag{19}$$

2.3. Coupling Matrix

2.3.1. General circuit model of filter. The coupling matrix (in the early 1970s) was extracted from the voltage current relationship of the equivalent circuit model [28] Fig 2.6 is the equivalent circuit model of a narrow band bandpass prototype. The source of this circuit has an open circuit voltage e_s with resistance R_s and terminated by the load R_L. The circuit model is collected of lumped element series resonators which are coupled by transformers. i represents the current flowing in each series resonator. Self-inductance and capacitance of each resonator are 1 H and 1 F. This results in a center frequency of 1 rad/s and the couplings are normalized for a bandwidth of 1 rad/s [11] Each loop is coupled to every other loop through mutual couplings and these couplings are assumed to be frequency independent because of the narrow band approximation. The circuit prototype in Fig 2.6 is the voltage current relationship for each loop which can be combined into the matrix form that is convenient to manipulate as follows:

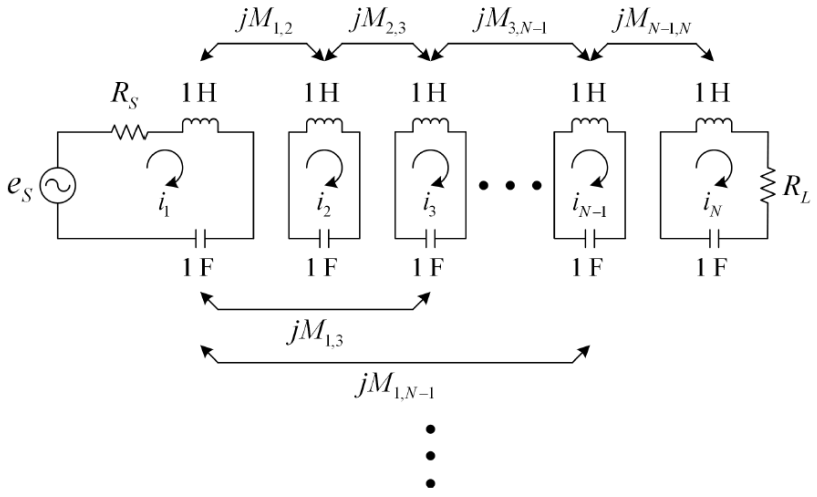

Fig 2.6: A bandpass circuit prototype for an $\boldsymbol{N^{th}}$ order filter [1]

$$\begin{bmatrix} e_S \\ 0 \\ \vdots \\ 0 \\ 0 \end{bmatrix} = \begin{bmatrix} R_S + j(\omega - \frac{1}{\omega}) & jM_{1,2} & \cdots & jM_{1,N-1} & jM_{1,N} \\ jM_{2,1} & j(\omega - \frac{1}{\omega}) & \cdots & jM_{2,N-1} & jM_{2,N} \\ \vdots & \vdots & \ddots & \vdots & \vdots \\ jM_{N-1,1} & jM_{N-1,2} & \cdots & j(\omega - \frac{1}{\omega}) & jM_{N-1,N} \\ jM_{N,1} & jM_{N,2} & \cdots & jM_{N,N-1} & R_L + j(\omega - \frac{1}{\omega}) \end{bmatrix} \begin{bmatrix} i_1 \\ i_2 \\ \vdots \\ i_{N-1} \\ i_N \end{bmatrix} \quad (20)$$

The simplified form of Eq. 20 voltage-current relationship is [29]:

$$E = AI = \left(j\left(\omega - \frac{1}{\omega}\right)U + R + jM\right)I \quad (21)$$

E is the matrix in left-hand side of Eq. 21 and *U* is the identity matrix. *I*, *R*, and *M* are:

$$I = \begin{bmatrix} i_1 \\ i_2 \\ \vdots \\ i_{N-1} \\ i_N \end{bmatrix} \quad (22)$$

$$R = \begin{bmatrix} R_S & 0 & \cdots & 0 & 0 \\ 0 & 0 & \cdots & 0 & 0 \\ \vdots & \vdots & \ddots & \vdots & \vdots \\ 0 & 0 & \cdots & 0 & 0 \\ 0 & 0 & \cdots & 0 & R_L \end{bmatrix} \quad (13)$$

$$M = \begin{bmatrix} 0 & M_{1,2} & \cdots & M_{1,N-1} & M_{1,N} \\ M_{2,1} & 0 & \cdots & M_{2,N-1} & M_{2,N} \\ \vdots & \vdots & \ddots & \vdots & \vdots \\ M_{N-1,1} & M_{N-1,2} & \cdots & 0 & M_{N-1,N} \\ M_{N,1} & M_{N,2} & \cdots & M_{N,N-1} & 0 \end{bmatrix} \quad (24)$$

M is called the coupling matrix.

As all series resonators have the same resonators, and thus the same resonant frequency, the filter of the equivalent circuit model is a synchronously tuned circuit. For asynchronously tuned filter, the bandpass prototype is done by including

hypothetical frequency-invariant reactive elements in each series resonator as shown Fig 2.7 in. The coupling matrix is [29]:

$$M = \begin{bmatrix} M_{1,1} & M_{1,2} & \cdots & M_{1,N-1} & M_{1,N} \\ M_{2,1} & M_{2,2} & \cdots & M_{2,N-1} & M_{2,N} \\ \vdots & \vdots & \ddots & \vdots & \vdots \\ M_{N-1,1} & M_{N-1,2} & \cdots & M_{N-1,N-1} & M_{N-1,N} \\ M_{N,1} & M_{N,2} & \cdots & M_{N,N-1} & M_{N,N} \end{bmatrix} \quad (25)$$

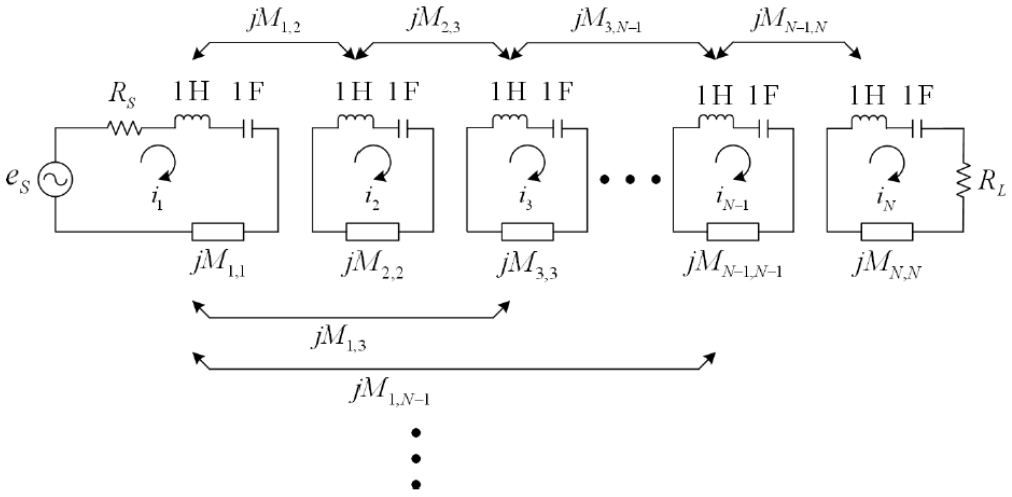

Fig 2.7: A bandpass circuit prototype for an $\boldsymbol{N^{th}}$ order filter

The purpose of synthesizing microwave resonator filters is finding this coupling matrix along with R_S and R_L with given low-pass transfer function. So the voltage-current relationship for bandpass prototype should be expressed by low-pass terminology. The low-pass to bandpass transformation is [29]

$$\Omega = \frac{\omega_0}{\Delta\omega}\left(\frac{\omega}{\omega_0} - \frac{\omega_0}{\omega}\right) \quad (26)$$

$$E = AI = (j\Omega U + R + jM)I = (SU + R + jM)I \quad (27)$$

Where $\omega_{\circ}$ and $\Delta\omega$ are the center frequency and the bandwidth in rad/s of the bandpass filter. Fig 2.8 shows the voltage-current relationship for the bandpass topology. By replacing the series resonators by inductors, the bandpass prototype can be transformed to the low-pass prototype, Fig 2.8.

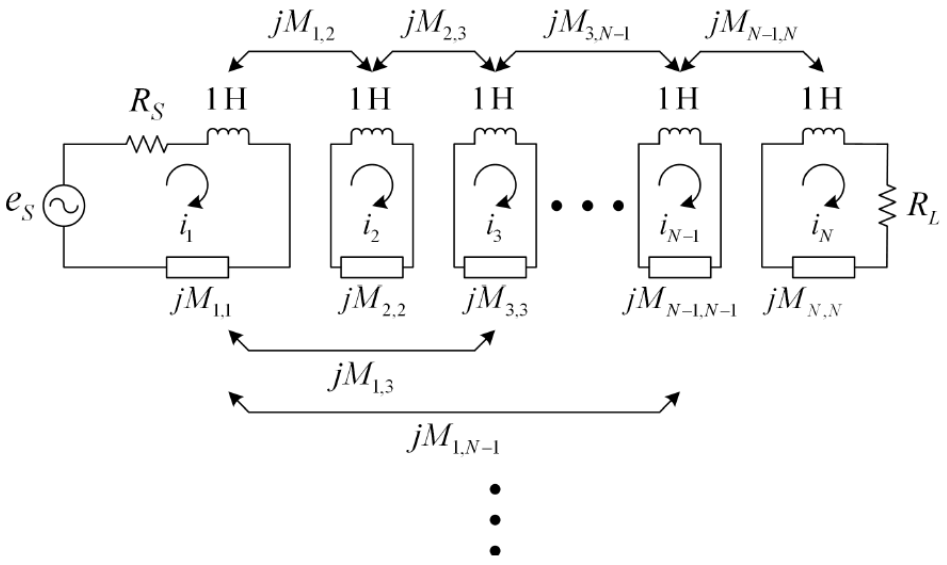

Fig 2.8: A low-pass circuit prototype for an $\boldsymbol{N^{th}}$ order filter [29].

2.3.2. Filter scattering parameter. In Fig 2.9, the low-pass circuit prototype operates between a voltage source generating e_s Volts and an internal impedance of R_s Ohms and a load impedance of R_L Ohms. The general circuit including the source and load terminations can be represented by the impedance matrix A as shown in Fig 2.9. This impedance matrix can also be divided into the matrix's purely resistive and purely reactive parts by Eq. 28. The impedance matrix Z is a purely reactive network which operates between a voltage source with internal impedance R_s and a load R_L. The current in each loop is described by Eq. 29 [30]

$$A = R + jM + SU = R + Z \tag{28}$$

$$I = A^{-1} E \tag{29}$$

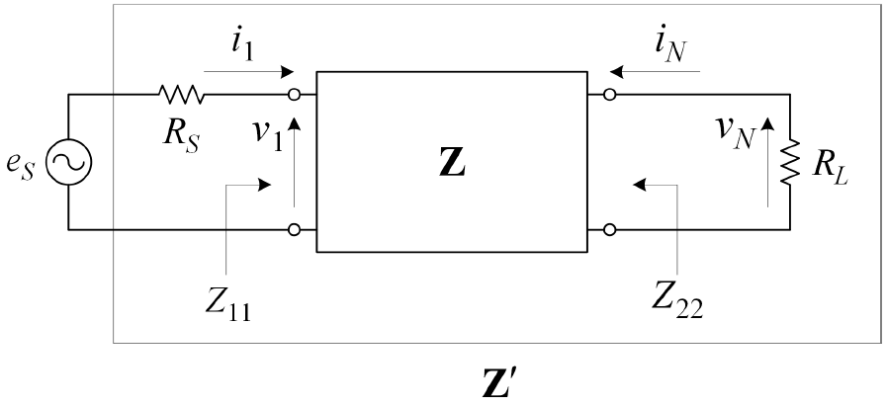

Fig 2.9: A circuit network for an $\boldsymbol{N^{th}}$ order filter [1]

Where A is the network open-circuit impedance matrix with the source and load impedances included. $Z_{11} = v_1/i_1$ is the impedance looking in at the input port, while the potential divider at the input port gives Z_{11} and Eq. 30 produces i_1 . Then, Z_{11} can be expressed by Eq. 30 and then reduced to Eq. 31. As a result, the reflection coefficient at the input and output can be expressed by Eq. 32 and 33.

$$Z_{11} = \frac{v_1}{i_1} = \frac{e_S Z_{11}}{Z_{11} + R_S} \frac{1}{e_S A_{1,1}^{-1}} \tag{30}$$

$$\frac{1}{Z_{11} + R_S} = A_{1,1}^{-1} \tag{31}$$

$$S_{11} = 1 - 2R_S A_{1,1}^{-1} \tag{32}$$

$$S_{22} = 1 - 2R_L A_{N,N}^{-1} \tag{33}$$

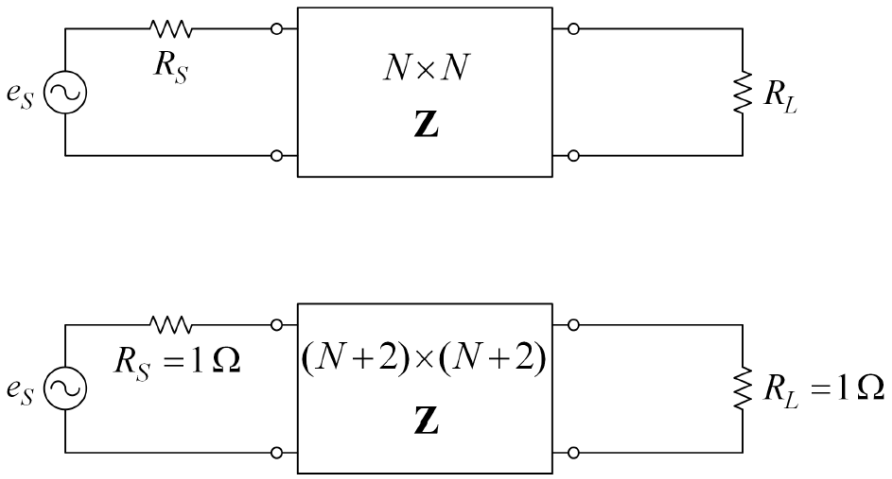

Fig 2.10: A circuit network for an Nth order filter (a) by using the NxN matrix (b) using the (N+2) x (N+2) matrix [1]

2.3.3. Square coupling matrix. In general, the source and load terminations are nonzero, and by inserting impedance inverters $M_{S,1}$ and $M_{n,1}$ of impedance values $\sqrt{Rs}$ and $\sqrt{RL}$ on the source and load side of the network which can be normalized to unity impedance [28] These inverters can be written as $N \times N$ matrix $(N + 2) \times (N + 2)$ creating matrix.

$$M = \begin{bmatrix} 0 & M_{S,1} & 0 & \cdots & 0 & 0 & 0 \\ M_{S,1} & M_{1,1} & M_{1,2} & \cdots & M_{1,N-1} & M_{1,N} & 0 \\ 0 & M_{1,2} & M_{2,2} & \cdots & M_{2,N-1} & M_{2,N} & 0 \\ \vdots & \vdots & \vdots & \ddots & \vdots & \vdots & \vdots \\ 0 & M_{1,N-1} & M_{2,N-1} & \cdots & M_{N-1,N-1} & M_{N-1,N} & 0 \\ 0 & M_{1,N} & M_{2,N} & \cdots & M_{N-1,N} & M_{N,N} & M_{N,L} \\ 0 & 0 & 0 & & 0 & M_{N,L} & 0 \end{bmatrix} \quad (34)$$

From Eq. 34, $M_{S,1}$ is equal to $\sqrt{Rs}$ and $M_{N,1}$ is equal to $\sqrt{RL}$. The general matrix form is included coupling between the source and/or load terminations, and the internal nodes within the core $N \times N$ matrix. Also, there is source/load coupling $M_{S,1}$ in order to fully realize filter functions. The $(N+2) \times (N+2)$ coupling matrix is:

$$M = \begin{bmatrix} 0 & M_{S,1} & M_{S,2} & \cdots & M_{S,N-1} & M_{S,N} & M_{S,L} \\ M_{S,1} & M_{1,1} & M_{1,2} & \cdots & M_{1,N-1} & M_{1,N} & M_{1,L} \\ M_{S,2} & M_{1,2} & M_{2,2} & \cdots & M_{2,N-1} & M_{2,N} & M_{2,L} \\ \vdots & \vdots & \vdots & \ddots & \vdots & \vdots & \vdots \\ M_{S,N-1} & M_{1,N-1} & M_{2,N-1} & \cdots & M_{N-1,N-1} & M_{N-1,N} & M_{N-1,L} \\ M_{S,N} & M_{1,N} & M_{2,N} & \cdots & M_{N-1,N} & M_{N,N} & M_{N,L} \\ M_{S,L} & M_{1,L} & M_{2,L} & & M_{N-1,L} & M_{N,L} & 0 \end{bmatrix} \quad (35)$$

For this matrix, the voltage-current relationship can be expressed by Eq. 36, and the transmission and reflection coefficients are given by Eq. 37 and 38.

$$E = AI = (R + j\Omega W + jM)I \quad (36)$$

$$S_{21} = 2\,.\,A^{-1}_{N+2,1} \quad (37)$$

$$S_{11} = 1 - 2\,.\,A^{-1}_{1,1} \quad (38)$$

2.4. Theory Background of Transmission Lines

The transmission lines introduce the connection from one port to another port, which work like wire in circuit design theory [21] Transmission lines can operate in different frequencies and resistivity substrate. Moreover, there are three modes depending on which are the slow wave mode, skin effect mode and dielectric quasi

TEM mode. There is the same circuit model for all types of transmission lines. In this section, the transformation from transmission line to its circuit model is presented by using Maxwell's equations [32]

Lumped element and distributed element of transmission line. There is a main difference between transmission line theory and circuit theory which is electrical size. On circuit theory, the physical dimensions are assumed much smaller than the electrical wavelength, but in case of transmission line theory, the size of the wavelengths is the main part [32]. There are two ways to transfer the transmission line to the circuit model which are lumped element and distributed element. On lumped element, the voltage and current do not change over the physical dimension of the elements, but in distributed elements, voltage and current magnitude and phase will be changed by transmission line's length, so the components become more dependent on the frequency. The lumped element equivalent circuit is shown in Fig 2.11.

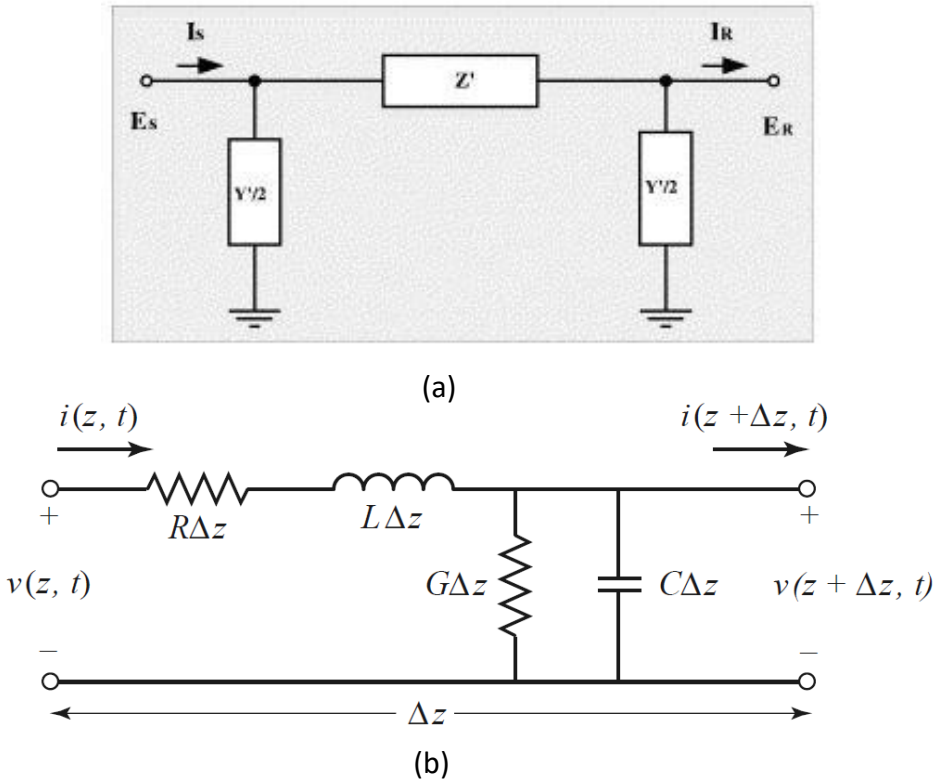

Fig 2.11: (a) Distributed Element example, (b) Equivalent Circuit of lumped element [1]

In here, *R* is the series resistance per unit length, *L* is series inductance per unit length, *G* is shunt conductance per unit length and *C* is shunt capacitance per unit length.

There are some equations, which are used in this part to relate the transmission line to its circuit model. The complex propagation constant equation is expressed by Eq. 39, and the characteristic impedance $Z_\circ$ is written as Eq. 40. The wavelength (λ) and phase velocity (v_{ph}) of the line are described as Eq. 41 and 42 [33]

$$\gamma = \alpha + j\beta = \sqrt{(R + j\omega L)(G + j\omega C)} \tag{39}$$

$$Z_\circ = \frac{R + j\omega L}{\gamma} = \sqrt{\frac{R + j\omega L}{G + j\omega C}} \tag{40}$$

$$v_{ph} = \frac{\omega}{\beta} = \lambda f \tag{41}$$

$$\lambda = \frac{2\pi}{\beta} \tag{42}$$

2.4.1. Transmission line resonator. The distributed elements are mostly used for designing the transmission lines, because the ideal lumped elements of the circuit are usually impossible to achieve at microwave frequencies [34] In this section, different transmission lines with various length and terminations (open or short circuited model) are presented. The transmission lines in here are included with losses due to the effect they have on quality factor.

2.4.1.1. ***Short circuited λ/2 transmission line.*** The length of this type of transmission line is λ/2 at the resonance frequency and it has characteristic impedance $Z_\circ$, propagation constant β and attenuation constant α. The short circuited λ/2 transmission line is shown in Fig 2.12.

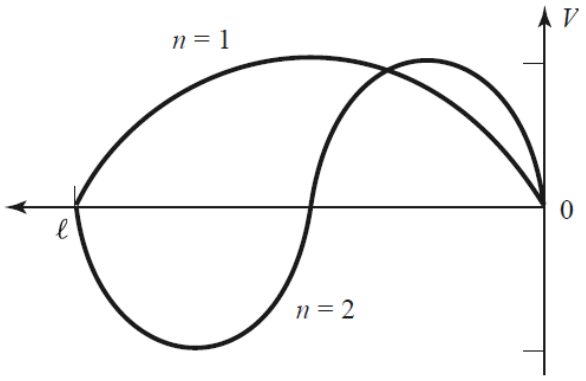

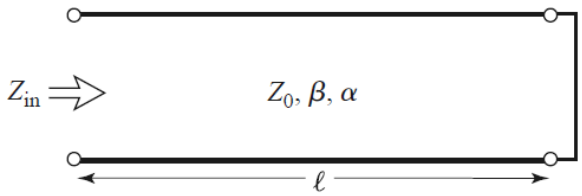

Fig 2.12: Short circuited λ/2 transmission line [1].

The equations used in short circuited λ/2 transmission line are expressed as follow:

$$Z_{in} = Z_\circ \frac{\tanh \alpha l + j \tan \beta l}{1 + j \tan \beta l \tanh \alpha l} \tag{43}$$

$$\beta l = \frac{\omega l}{v_{ph}} = \pi + \frac{\Delta\omega\pi}{\omega_\circ} \tag{44}$$

$$l = \frac{\lambda}{2} = \frac{\pi v_{ph}}{\omega_\circ} \tag{45}$$

For lossless transmission line α is zero. The series RLC resonant circuit and unloaded quality factor $Q_\circ$ equations are in the next sections.

2.4.1.2. ***Short circuited λ/4 transmission line.*** In this part, the length of transmission line is changed, so the equations can be expressed by:

$$Z_{in} = Z_\circ \frac{1 - j \tanh \alpha l \cot \beta l}{\tanh \alpha l - j \cot \beta l} \tag{46}$$

$$\beta l = \frac{\pi}{2} + \frac{\pi\Delta\omega}{2\omega_\circ} \tag{47}$$

$$R = \frac{Z_\circ}{\alpha l}, C = \frac{\pi}{4\omega_\circ Z_\circ}, L = \frac{1}{\omega_\circ^2 C} \tag{48}$$

$$Q_\circ = \omega_\circ RC = \frac{\pi}{4\alpha l} = \frac{\beta}{2\alpha} \tag{49}$$

2.4.1.3. ***Open circuited λ/2 transmission line.*** In most microstrip circuits, the open circuited length of transmission line are used, as shown in Fig 2.13. The behavior of this type of resonator is like a parallel resonant circuit. The equation of input impedance of open circuited λ/2 transmission line is the same as the short circuited design. The propagation constant equation is:

$$\beta l = \pi + \frac{\pi\Delta\omega}{\omega_\circ} \tag{50}$$

The equivalent RLC circuit equations are:

$$R = \frac{Z_\circ}{\alpha l}, C = \frac{\pi}{2\omega_\circ Z_\circ}, L = \frac{1}{\omega_\circ^2 C} \tag{51}$$

$$Q_\circ = \omega_\circ RC = \frac{\pi}{2\alpha l} = \frac{\beta}{2\alpha} \tag{52}$$

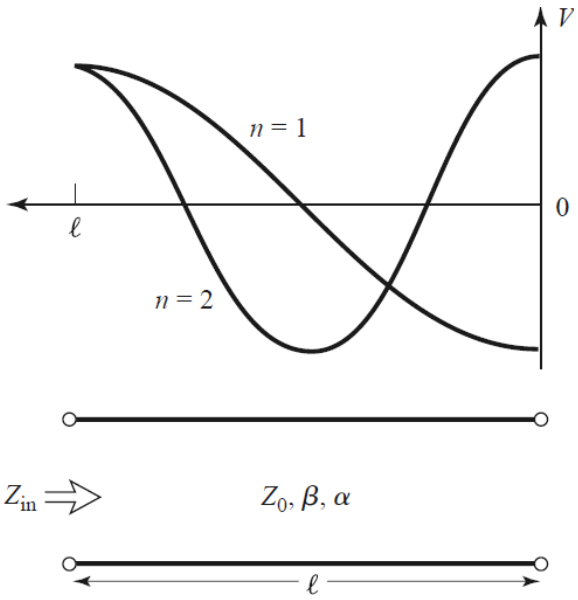

Fig 2.13: Open Circuited λ/2 Transmission Line [1]

2.4.2. Coplanar waveguide (CPW) transmission line. A structure of the CPW transmission line consists of a thin film center conductor with ground plane on both sides of the conductor on low loss dielectric substrate [35] as depicted in Fig 2.14.

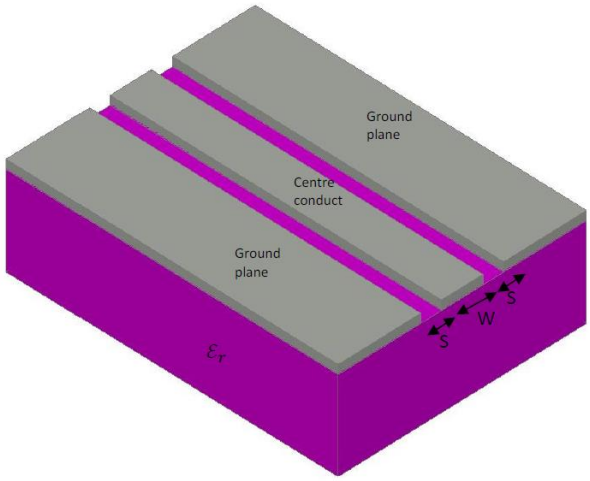

Fig 2.14: Structure of CPW transmission line [36].

The width of the center conductor is defined as *W* and the gap from the center strip and ground plane is *S*. The ratio of the conductor width (*W*) to the gap width (*S*) and the relative dielectric constant (ε_r) affect the characteristic impedance ($Z_\circ$) of the CPW [20]. The characteristic impedance ($Z_\circ$) and the phase velocity (v_{ph}) of the CPW can be found from the following equations [37]:

$$Z_\circ = \frac{1}{C_{cpw} v_{ph}} \tag{53}$$

$$v_{ph} = \left(\frac{2}{\varepsilon_{eff} + 1}\right)^{0.5} C \tag{54}$$

$$\varepsilon_{eff} = \frac{\varepsilon_r + 1}{2} \tag{55}$$

The capacitor per unit length (C_{cpw}) of CPW can be found by using conformal mapping technique. ε_{eff} is the effective dielectric constant of the substrate and *C* is the velocity of light in free space. Another important parameter for the CPW transmission line is propagation constant (β) and it can be expressed by Eq. 56, which λ_s is the wavelength of the signal.

$$\beta = \frac{2\pi}{\lambda_s}\sqrt{\varepsilon_{eff}} \tag{56}$$

The total attenuation of the signal that propagates through the CPW is dependent on the attenuation due to the dielectric losses (α_d) in the substrate and attenuation due to conductor losses (α_c) in the center conductor and ground planes, so: $\alpha_{total} = \alpha_d + \alpha_c$.

2.5. Resonator

An ideal resonant circuit consists of capacitor and inductor which is known as LC circuit, Fig 2.15 [1] By connecting capacitor and inductor together, the result circuit is known as electrical resonator. The function of LC circuits is to produce signals at a certain frequency. These circuits are used in filters, tuners, oscillators and frequency mixers.

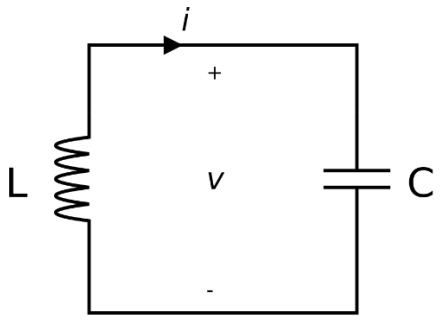

Fig 2.15: LC circuit model [1].

Resonators are used to generate waves of specific frequencies. They can be used to select specific frequencies from a signal. The applications of resonator are in oscillators and transformers (to create microwave signal), filters, radar equipment, microwave relay stations, satellite communication, microwave oven and particle accelerators [34]

2.5.1. Resonance of Resonator. When the frequency and magnitude of the capacitor and inductive reactance are equal, the resonance occurs. The resonant frequency of LC circuit is:

$$f_\circ = \frac{1}{2\pi\sqrt{LC}} \tag{57}$$

Resonators are used to perform different types of RF microwave components like oscillators, filters and phase shifters. There are different types of resonators which are categorized by the shape of the resonators and its performances. The examples of resonators are coaxial, dielectric, crystal, ceramic, and ring resonator (RR) and more. So, it is important for designers to understand the characteristics of the various types of resonators. In this thesis, the ring resonator is used to design the filter.

2.5.2. Microwave ring resonator. Many microwave devices are designed based on ring resonator circuits, for example; oscillators, filters, antennas and mixers. The structure of the ring resonators consists of metallic ring in circular or square shape, which is carved or etched on dielectric substrates. Ring resonators are designed in closed and open metallic ring. For open ring resonators, there is a small gap, so the capacitor has a high value [38]

The parameters of the ring resonators depend on the resonant frequency, and the structure has the ability of presenting resonance at frequencies much larger than its size [39] Fig 2.16 shows the example of the square ring resonator.

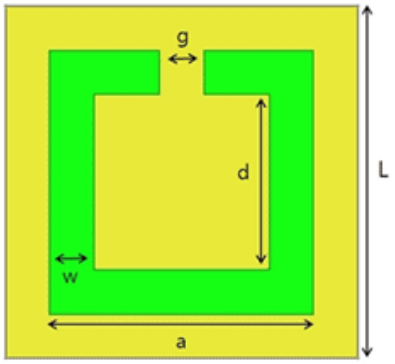

Fig 2.16: Example of square ring resonator [38].

As shown in Fig 2.17, the parameters of this ring are: the inner radius *R*, the thickness *w*, the height *h*, and the gap width *g*. The inductance *L* and the capacitance *C* are used to design the sub-wavelength split ring resonator [40]

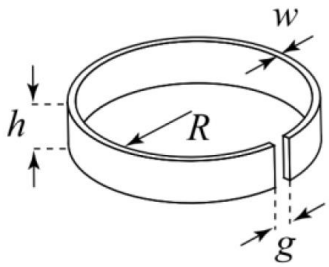

Fig 2.17: Open circular ring resonator [40].

The resonance frequency, inductance and capacitor gap equations are:

$$f_\circ = \frac{1}{2\pi\sqrt{LC}} \tag{58}$$

$$L = \mu_\circ R_m(\ln\frac{8R_m}{h+w} - 0.5) \tag{59}$$

$$C_{gap} = \varepsilon_\circ\left[\frac{wh}{g} + \frac{2\pi h}{\ln\left(\frac{2.4h}{w}\right)}\right] \tag{60}$$

$\mu_\circ$ is the permeability of free space and R_m is the mean radius of the ring, $R_m = R + w/2$.

2.6. Loaded and Unloaded Quality Factor

Quality factor in general determines the quality of the device, and the quality is defined in here as low loss. There are loaded quality factor and unloaded quality factor of resonators. Return loss and insertion loss are used to calculate quality factor [41-43].

The information of the conductivity of the metal walls as well as the dielectric loss tangent for resonators that are loaded with dielectric materials are needed to find the accurate value of unloaded quality factor. By using high conductivity metals like gold, copper and silver, high quality factor can be achieved.

In narrow bandpass filter design, loaded quality factor (Q_L) is one of the important parameters, which can mainly affect the shape of the passband response of a filter. There are two ways to find the loaded quality factor which are equations of its circuit model or from a full wave electromagnetic (EM) simulation [43]

The loaded quality factor is found from the insertion loss information of frequency response which is expressed by Eq. 61, and return loss information is used to find the unloaded quality factor which is written as Eq. 62.

$$Q_L = \frac{f_\circ}{\Delta f} \tag{61}$$

$$Q_u = \frac{w_\circ}{\Delta w} \tag{62}$$

2.7. Micro Electro Mechanical System (MEMS)

Micro-Electro-Mechanical Systems (MEMS) devices are compact in size devices in micrometer scale and has the electrical and the mechanical domains coupled together and built using microfabrication. The physical dimensions of MEMS can be measured from below one micron on the lower end of the dimensional spectrum, to several millimeters [44-46]. There are different types of MEMS devices which can be seen in simple structures with no moving elements. Also, they can be seen in extremely complex electromechanical systems with many moving elements. MEMS devices and circuits are used for various functions including sensors and actuators [47] They can also be integrated with microelectronics.

MEMS capacitive switches compared with other semiconductor devices have many advantages like low loss, very high quality factor at mm-wave frequencies, high power handling capability, and low power consumption. RF MEMS device has two parts: the electrical part and the actuation part. The mechanical movements are done from electrostatic, piezoelectric, or thermal force. The common method which is mostly used is electrostatic actuation, because it has virtually zero power consumption, small electrode size, thin layers used, short switching time, and provides the possibility of biasing the switch using high resistance bias lines.

There are three different standard technologies for MEMS capacitive switches designs, which are parallel plate structure, an inter digital structure and MEMS switches capacitance banks [47] On parallel plate structure, the different values of capacitance can be achieved by providing DC bias and by making the gap between the parallel plates vertically changed. On second technology, the change of gap is horizontally between the comb fingers, and finally the last one develops MEMS switches to select the required capacitance from fixed valued capacitance banks [48]

2.8. Design Steps

The overall design of tunable bandpass filter using CPW ring resonator will be presented in this section. The first step for this process is to choose the structure technology and the center frequency which can be used for wireless applications, so the spected filters should operate around 2 GHz and 20 GHz. The radius of the ring resonator should be calculated by having fixed value of frequency and thickness of resonator. Different types of input/output port coupling are found, which in this thesis edge input/output coupling is used to design the first order bandpass filter. The filter design consists of two open ring resonators with two couplers and a CPW waveguide in between. In this thesis, gold material is used for resonator and Aluminum Oxide (Al2-O3) ceramic substrate with fixed standard thickness. To get the main goals of this work, the overall design should go through optimization. At the end, by using RF MEMS capacitive switches the tuning of the filter is done and it should be the same function performance. Next section contains the specification of bandpass filter with expected results.

2.9. Bandpass Filter Specification

The summary of the specification and expected results of bandpass filter is listed in Table 2.1. Most filters are designed in microstrip technology, but the CPW technology filters are an active area in research. This work is a novel design for bandpass filter using CPW ring resonator. The input/output ports are normlized to 50 ohm such that to get the perfect matching.

Table 2.1: Filter specifications

Design Parameters	Specificatios
Technology	CPW
Center Frequnecy	2 and 20 GHz
Expected Bandwidth for 2 GHz	1 GHz
Expected Bandwidth for 20 GHz	2 GHz
Return Loss (for both)	< -20 dB
Insertion Loss (for both)	>-2 dB
Quality Factor	15
Input Port (Impedance)	50 Ohm
Output Port (Impedance)	50 Ohm

Chapter 3: Tunable RF MEMS Capacitive Switches Bandpass Filter Using CPW Ring Resonator for Low Frequency

In this chapter, CPW ring resonator is used to design a bandpass filter operating at 2 GHz center frequency with both schematic and layout designs. The schematic design of filter is developed and simulated in ADS software, and the 3D structure of the proposed design is simulated in HFSS.

3.1. Overall Design of Filter

The first step of this work is to choose the type of technology which the filter should be designed with. The CPW structure has been chosen for this filter design, with which the signal plane conductor and ground plane are on same level. As a result, lower characteristic impedances can be developed with compact size. The impedances of the device can be found by the separation distance from signal plane to ground plane. The advantages of the CPW structure, compared to microstrip structure, are many. After deciding on the technology, the resonator type is an important parameter for this filter. There are different types of resonators; each of them has various functionality. Depending on the type of filter and center frequency, the resonator shape is implemented and designed. The ring resonator has a response of a bandpass filter. The new model of the bandpass filter using open ring resonator in CPW structure is designed and simulated for both in circuit simulator and EM simulator. The open ring resonator with edge coupling on both sides is designed on a CPW structure. The gap in the ring resonator acts like a capacitor, which can be replaced by RF MEMS capacitive switches to achieve tunability.

3.1.1. Design technology. The challenging part of the design in all filters is to reduce the overall size of the layout. By using CPW technology, the size of the design will become smaller than other used technologies. Because the signal plane and ground plane are in the same level, other technologies can be easily integrated with the filter including MEMS devices and flipped chip microelectronic ICs. Bond wires or bridges are needed for connecting both grounds on the two sides of the signal plane in order to maintain the same polarity for grounding. The other types of technologies that were used for designing filters are: microstrip, CPW, stripline and slotline. Firstly, the aim of this thesis is to come up with bandpass filters that are tunable and exhibit compact sizes, therefore the CPW technology has been chosen to

design the proposed bandpass filters. Also, the radius of the ring resonator has been chosen depending on center frequency.

The design schematic of this filter is developed and implemented in ADS software by using the distributed elements of transmission lines. All the sizes of the transmission lines are calculated and then simulated to get the bandpass filter response operating with center frequency of 2 GHz. The optimization method is implemented to achieve the best possible RF performance including all the losses of the metal and substrate. The 3D structure is built in HFSS tool and the response is simulated by introducing the metal and substrate materials. Gold metal is used with Alumina substrate by having the fixed thickness size. In this chapter, all the steps of designing the first order bandpass filter with the obtained responses are introduced.

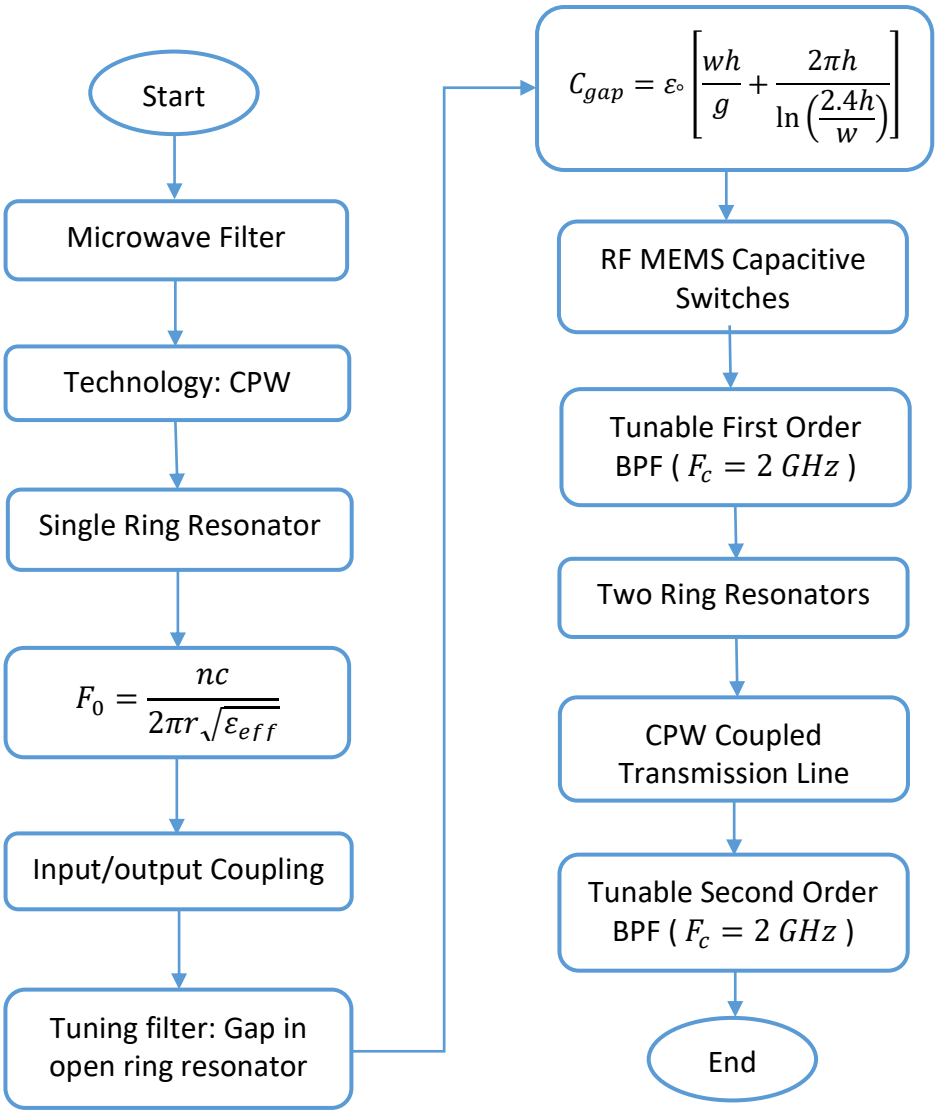

Fig 3.1: Design steps of this thesis

From Fig 3.1, n is the order number, r is the radius of the ring resonator and ε_{eff} is the effective dielectric constant.

3.1.2. Filter bandwidth. The bandwidth of any filter is defined as a frequency range that exists below 3 dB of the maximum center or resonant peak. The following figure shows the ideal bandpass filter response. The ideal bandpass filter can be used to filter out certain frequencies that lie within a particular band of frequencies, for example, noise cancellation. Bandpass filters have two reactive components, the capacitors, in their circuit model, so they are known as second order filters. The two capacitors are placed one in low pass circuit and another capacitor in the high pass circuit.

$$BW = F_H - F_L \tag{63}$$

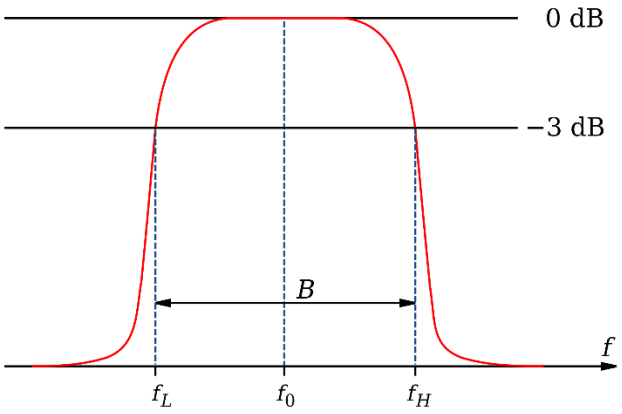

Fig 3.2: Ideal bandpass filter response

3.1.3. Insertion loss and return loss of filter. The Insertion loss, S_{21}, is the ratio in power that will lost in the passband which is resulting from the insertion of the device in an ideal transmission line that is matched from both sides, and it is usually defined in dB.

The Return loss,S_{11}, defines the ratio of the power, at port number one, that is reflected from the device inserted in an ideal transmission line. The reflection is defined in dB.

3.1.4. Input/ Output coupling in microwave filter. There are different types of coupling for input and output ports such as capacitive gap coupling, edge

coupling, inductive coupling etc. In this work, edge coupling, coupled line coupler, with electrical length of half wavelength is used. It is important to control the space from the ring resonator and the edge coupling. The gap between edge coupling and ring resonator can be represented in lumped element model that can be used in tuning. The gap structures at the input/output coupling cannot get tight coupling and they are sensitive to fabrication tolerance, which leads to high insertion loss. The structure of this kind of model acts in three distinct sections: the input/output lines, the coupling structures, and the ring resonator.

3.1.5. Separation gap in transmission line. The gap in transmission line is shown in Fig 3.3 with its circuit model. The circuit model of the gap in transmission line is designed with three capacitors in π-network model which are C_g and C_p. By using the closed form equation mentioned above or circuit simulator as ADS, the values of the capacitors can be calculated.

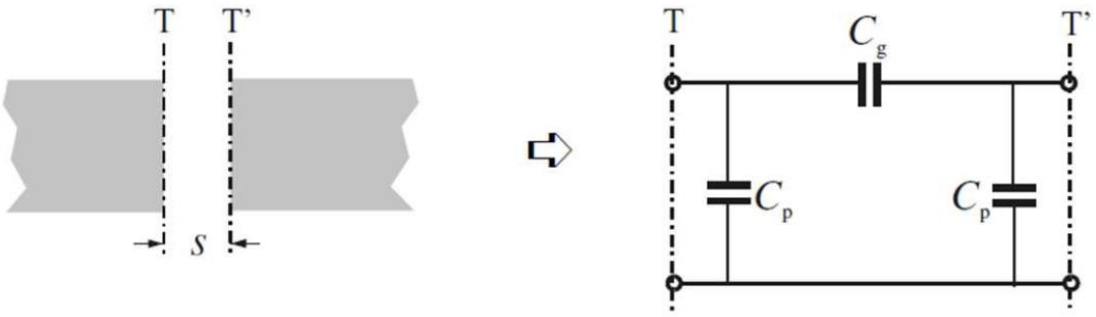

Fig 3.3: Equivalent circuit model of the gap in a transmission line

3.2. First Order BPF Circuit Model

The circuit model of this microwave bandpass filter is designed and simulated in ADS. The circuit model is created by dividing the layout into four parts of λ/4 transmission lines as shown in Fig 3.4. The first and second parts are the same as coupled line couplers of CPW transmission lines type, while the third part is simple one transmission line. Finally, the fourth part includes two transmission lines with π-network capacitor model which is designed for a gap in the transmission line. This gap is used to tune the filter by changing the gap or the capacitive coupling through the RF MEMS Varactors. In schematic design, only the result with changing the gap is simulated, to approximate the RF MEMS Varactors mission in the circuit simulator

in ADS. The input and output ports are normalized to 50 Ohms. The final result has been optimized to get the best frequency response of the filter.

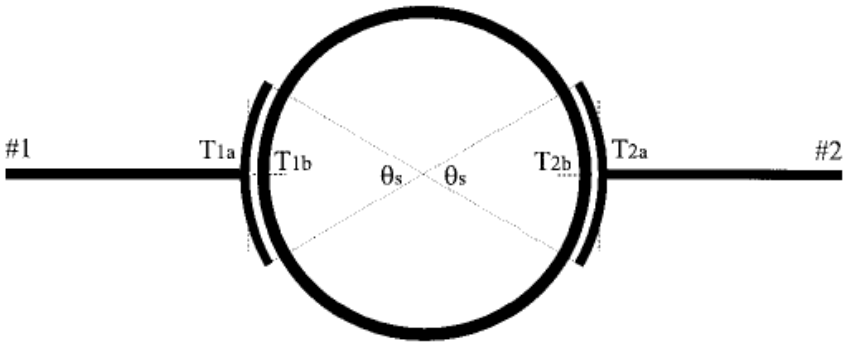

Fig 3.4: Simple ring resonator design with edge coupling

3.2.1. Schematic design (Circuit Model). The circuit model of this first order bandpass filter using CPW ring resonator has been designed and simulated in ADS. The overall design is shown in Fig 3.5. The built-in CPW transmission lines and library are used. The CPW transmission lines in ADS are designed such that the gap from conductor to ground, width, length and thickness of transmission lines can be controlled. The main design of this thesis is circular ring resonator, but in here the ring resonator is in square shape, and that is because of the build in CPW transmission lines library which has limited shape designs. As a result, the frequency response of circuit model of this design will be slightly different from its layout design. Firstly, for designing the circuit model of ring resonator, the sizes of the transmission lines are calculated for the certain center frequency which in this part is for 2 GHz. Then, for better result, the optimization process in ADS is used.

The circuit model is shown in Fig 3.5, and all used components are CPW transmission lines from ADS library. The circuit model is divided into six parts which model number one is a simple CPW transmission line, however, model number two is the gap in the ring which in here only the gap changed manually to check the tunability of the filter and later is used for tuning purpose through integrating a an RF MEMS Varactors. Coupled line coupler, which is the edge coupling element, of CPW type is shown in model number three in the same figure. The input and output ports that is connected to the ground are shown in model number four, which are normalized to 50 Ohms. Number five is the CPW transmission line which is open

from both sides, and number six is the stub CPW transmission line closed from one side. The substrate and conductor materials are defined in this design.

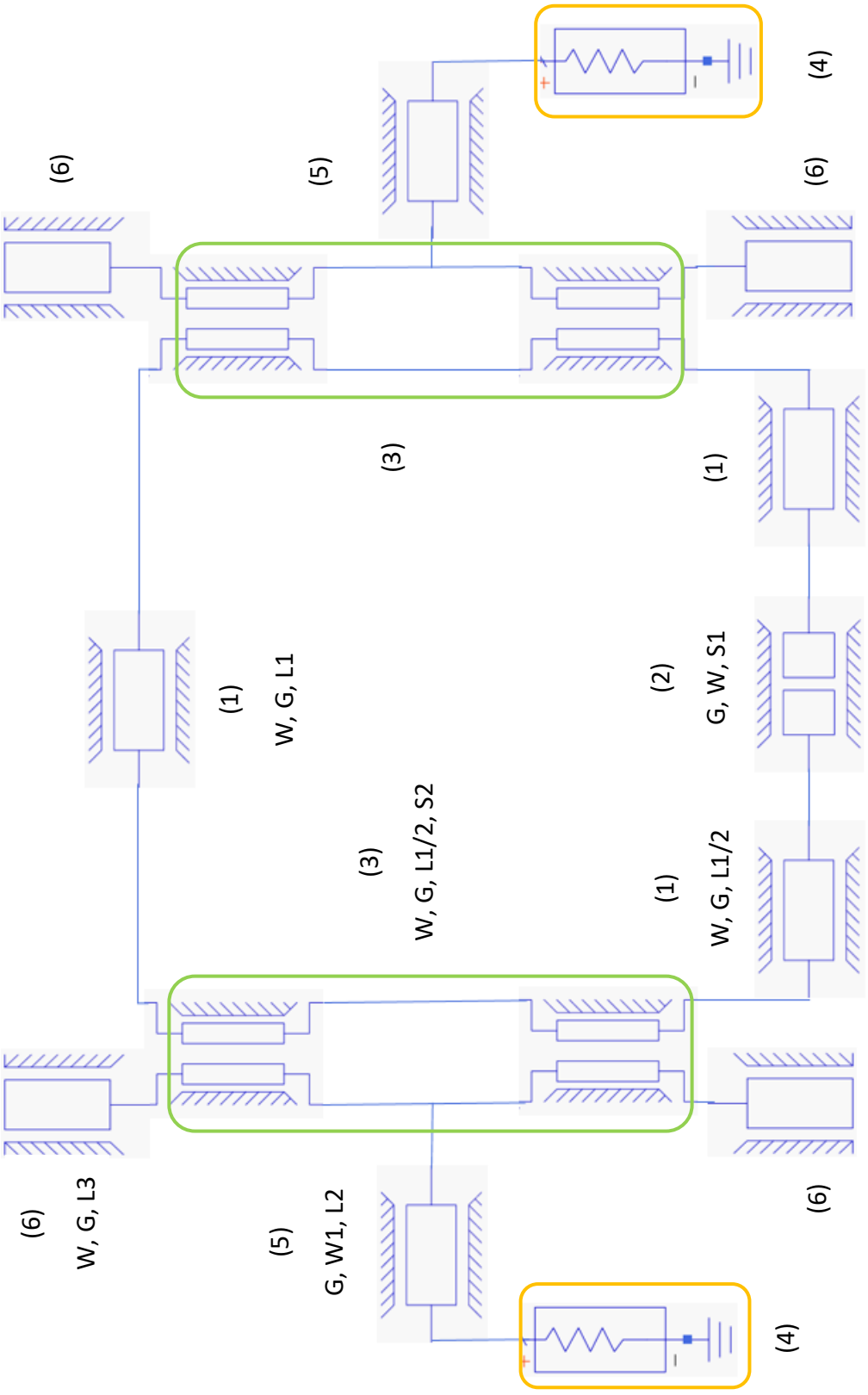

Fig 3.5: Schematic design of filter in ADS

3.2.2. Simulation result of circuit model. The simulation result for insertion loss and return loss is shown in Fig 3.6. From the result, the center frequency of this filter is at 2 GHz with bandwidth of around 0.3 GHz. Fig 3.7 shows insertion loss and return loss values, which are 0.5 dB and 23 dB, respectively.

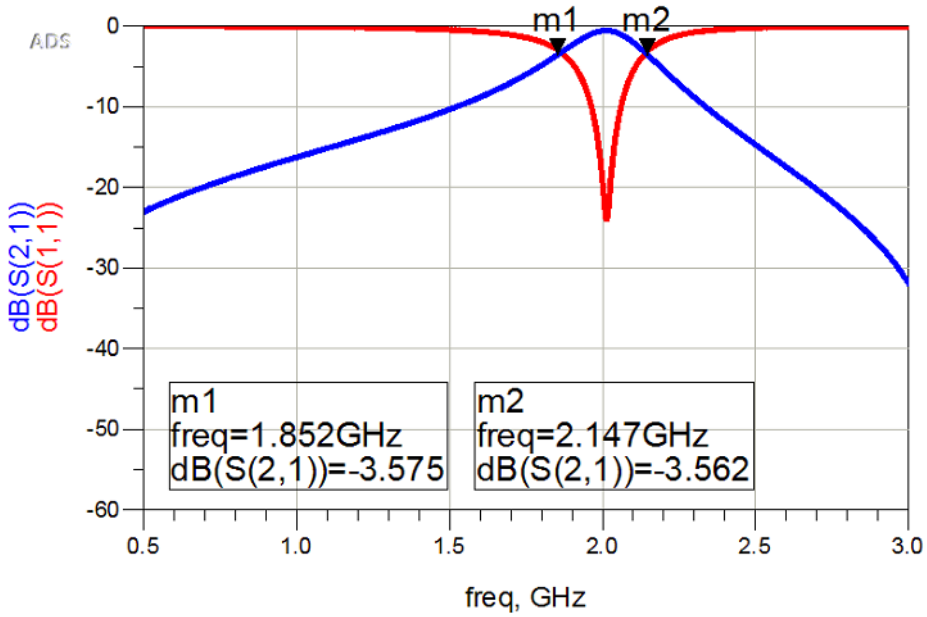

Fig 3.6: Simulated first order BPF in ADS

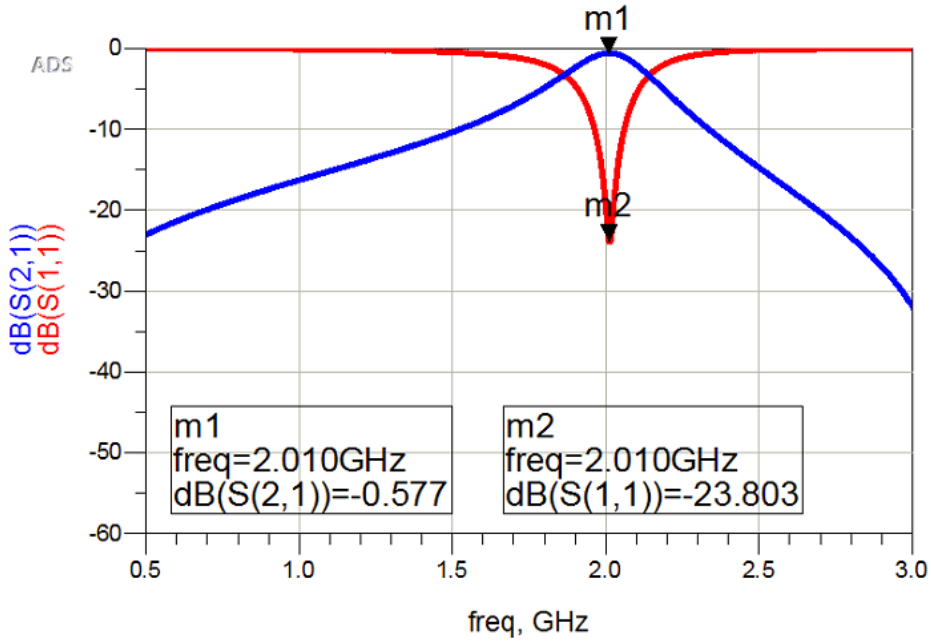

Fig 3.7: Simulated insertion loss and return loss parameters in ADS

3.2.3. Simulation of tuning BPF for circuit model. The next step is to run the simulation for different values of separation gap to get tuning process. The gap in the ring resonator has been changed from 100 µm to 200 µm with step size of 50 µm. In Fig 3.8 it is clear that by changing the gap, the center frequency will change by keeping the same response of the filter. The center frequencies are varied from 2 GHz to 2.12 GHz with different bandwidth for each center frequencies. The frequency response of the filter should be near to the ideal frequency response, so the lower return loss and the insertion loss close to zero is the purpose of this design.

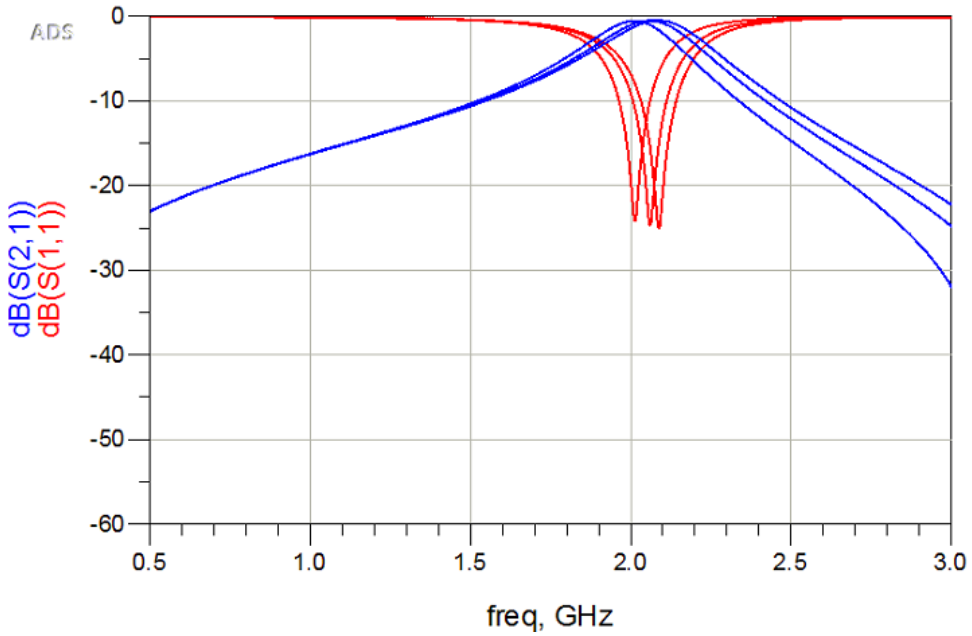

Fig 3.8: Simulated tunability of first order BPF with different gap sizes in ADS

The optimization process is used on simulation results in ADS to enhance the obtained RF performance. The ADS has a built in optimization process for any design, this process is done to get the final frequency response close to the ideal design. As a result, the values of return loss and insertion loss are defined in the process for the fixed bandwidth and the best frequency response is achieved. Because this design has a different variables in the transmission lines, so there are too much control in the design to get the best result. The next part is to calculate the loaded and unloaded quality factor which is of the aim of this thesis, and then the schematic design of second order BPF for low center frequency is designed by introducing another ring resonator.

3.2.4. Calculated loaded and unloaded quality factor. The loaded quality factor of the filter can be found from the S_{11} simulation result, and the unloaded quality factor is calculated from the S_{21} simulation result. From the simulation results in ADS, the following values are calculated:

$$Q_L = \frac{2}{2.147 - 1.852} = 6.78$$

$$Q_u = \frac{2}{2.03 - 1.98} = 40$$

3.3. Second Order BPF Circuit Model

The second order BPF is designed by introducing another ring resonator which is connected by one CPW transmission line between two ring resonators. The numbers of resonators used in the design define the number of order in the filter. The same size and dimensions of the first ring resonator are used to design the second ring resonator. The input is edge coupled to the first ring resonator then coupled again to a transmission line in between the two rings, then the output is edge coupled to the second ring resonator. The second order BPF has been designed to have a center frequency at 2 GHz. Moreover, an optimization technique is applied on the obtained results to fine tune the RF performance. The same simulations process are done for this design.

The CPW transmission line between the two ring resonators is chosen such that the losses are minimal. The length and the gap between the signal conductor and the ground planes of the transmission line are found to control the bandwidth of the obtain filter. As a result, this transmission line is an important element in fine-tuning the inner coupling of the second order BPF. The dimensions of this CPW transmission line were optimized in the ADS to obtain the best possible RF performance.

Fig 3.9 shows the circuit model of second order BPF designed in ADS which is modeled by two square ring resonators connected by simple CPW transmission line. The simulation results of return loss and insertion loss using the circuit simulator are presented in the next sections. Also the loaded quality factor and unloaded quality factor are calculated from the final frequency responses of the filter after optimization process.

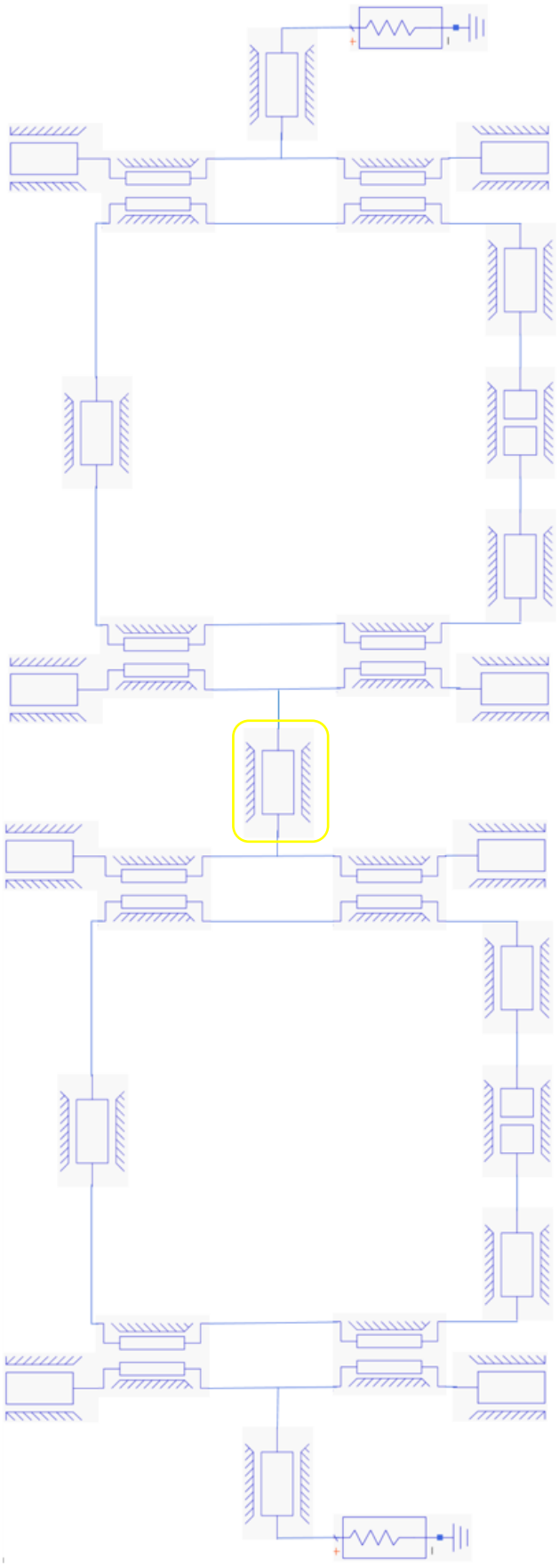

Fig 3.9: Circuit model of the second order BPF in ADS

3.3.1. Simulation results of the lumped element model in ADS. The second order BPF frequency response is shown in Fig 3.10. The center frequency is at 2 GHz with bandwidth of 0.3 GHz. Fig 3.11 shows that the Insertion Loss is around 0.94 dB, and the return loss is 29.25 dB. The results proved that by increasing the number of order of filter, the performance of the filter will improve (better insertion and return loss).

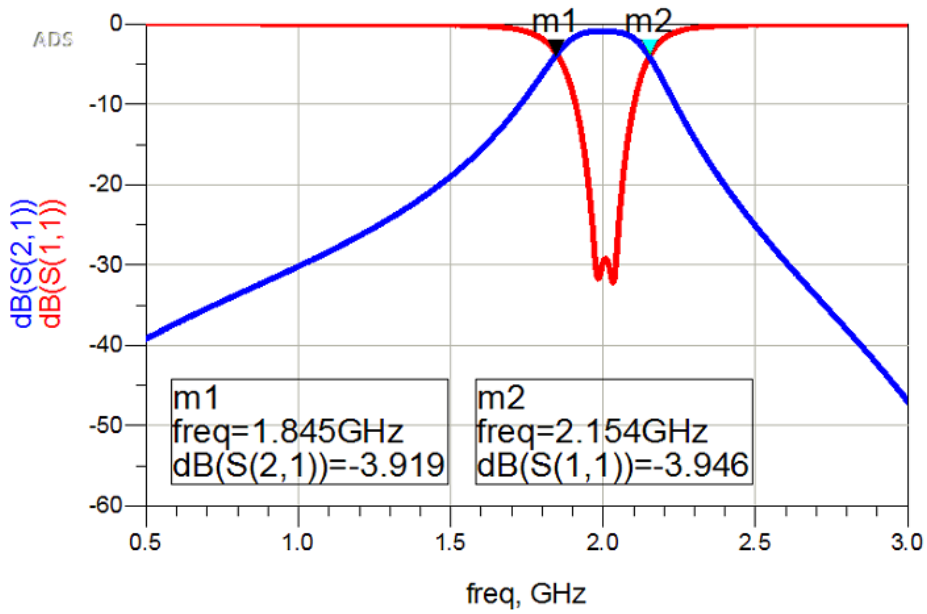

Fig 3.10: Extracted bandwidth of second order BPF in ADS

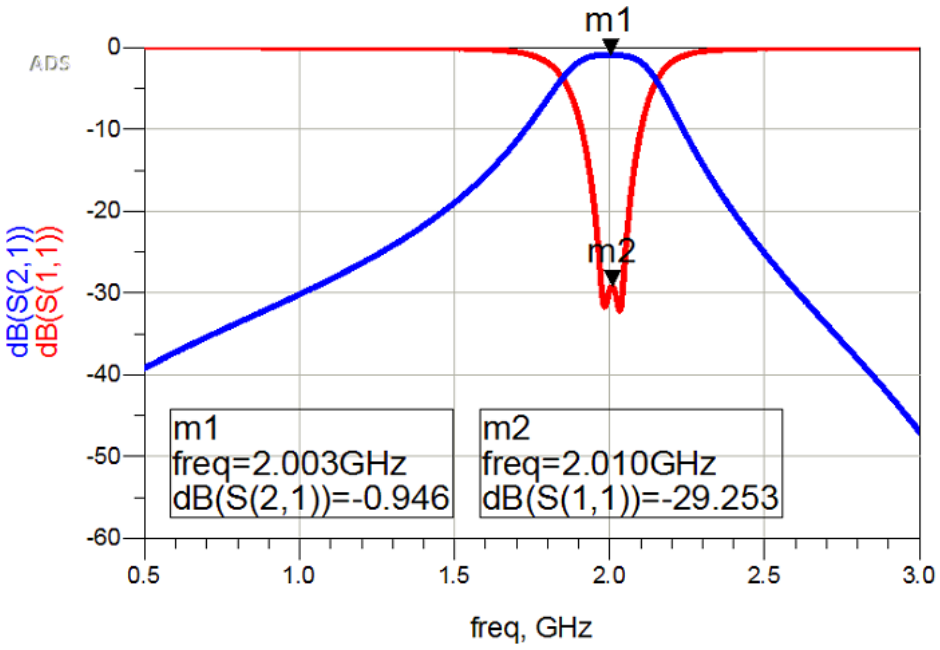

Fig 3.11: Extracted insertion loss and return loss for second order BPF in ADS

3.3.2. Calculated loaded and unloaded quality factor. The lumped element model of the second order BPF is simulated in ADS using the circuit simulator. Fig 3.12 and Fig 3.13 show the points used to calculate the loaded and unloaded quality factor. The calculated values are as follow:

$$Q_L = \frac{2}{2.154 - 1.845} = 6.47$$

$$Q_u = \frac{2}{2.049 - 1.968} = 24.69$$

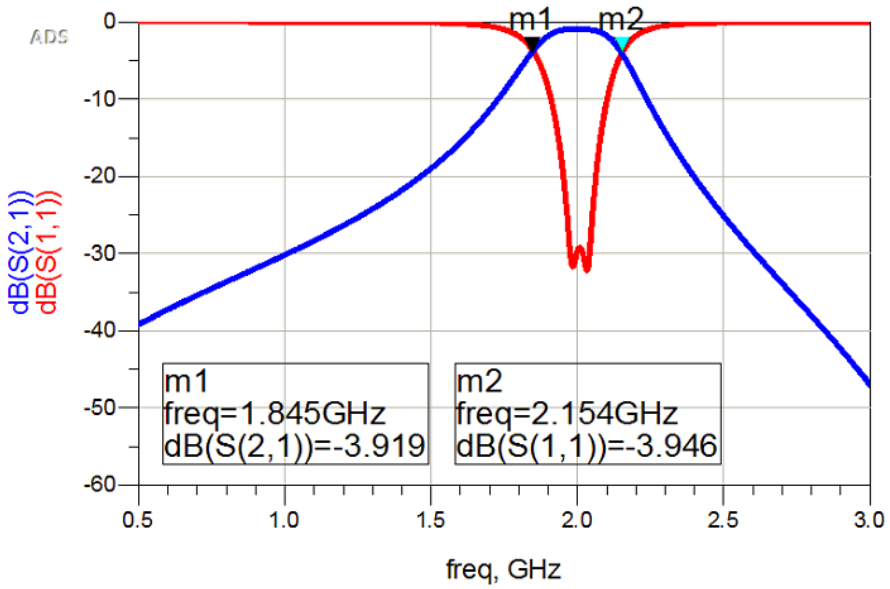

Fig 3.12: Extracted loaded quality factor for second order BPF in ADS

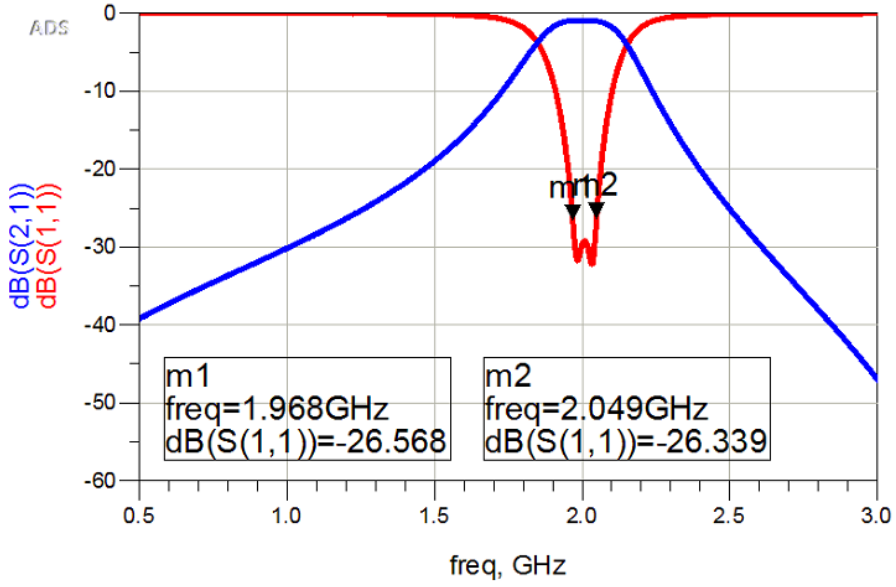

Fig 3.13: Extracted unloaded quality factor for second order BPF in ADS

3.4. First Order BPF 3D Model in HFSS

The dimensions obtained in ADS are used to build the 3D model in the EM simulator which is a FEM based that uses the frequency domain. The parameters are the radius of the ring, the width and thickness of the signal conductor, the length and the gap and length of the coupled line coupler. Since the lumped element model of the ring resonator is of a square shape in ADS, slightly different values are expected to be obtained in the EM model. The thickness of signal and ground plane is set to be 2 μm with gold material, and the material of the substrate is Alumina with a thickness of 675 μm. The overall size of the first order BPF is 15 mm x 15 mm. Fig 3.14 and Fig 3.15 show the top and the side views of the designed filter in HFSS, respectively.

It is observed in the figures that the yellow conductors are the rings and the edge coupling while the ground planes are chosen to be of a gray color along with the air bridges for illustration purposes. The substrate is chosen to be made of a green color. The air box size of filter in HFSS should be six times bigger than the thickness of the substrate. In Fig 3.15, the air box is cut in smaller size due to show the overall design of the filter in the report.

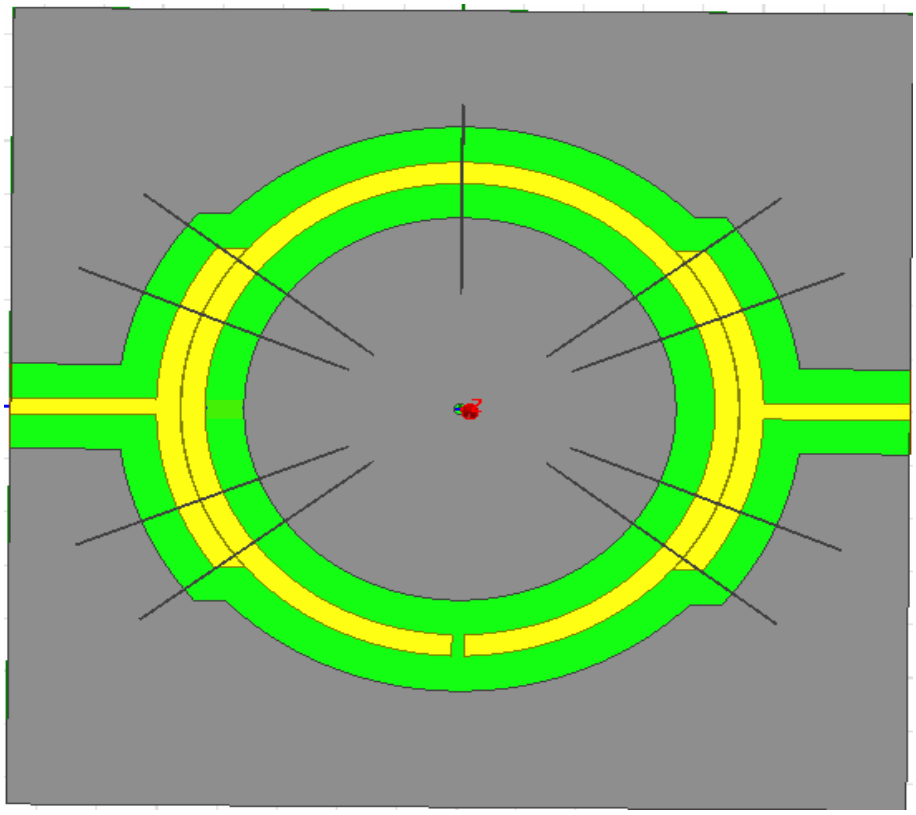

Fig 3.14: Top view of the filter in HFSS

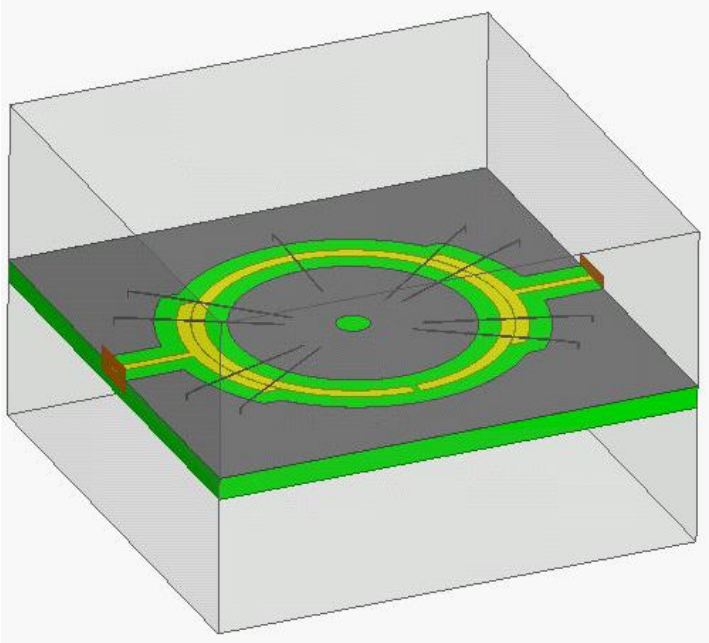

Fig 3.15: Tilted view of the filter in HFSS

3.4.1. EM simulation results of 3D model in HFSS. The S-parameters, S_{11} and S_{21}, of the simulated single resonator are shown in Fig. 3.16. The simulation is performed over the frequency range from 0.5 to 3.5 GHz. The center frequency is at 2 GHz with bandwidth of 0.59 GHz. The result shows that the insertion loss is around 0.5 dB at 2 GHz, and the return loss is around 25 dB at the same frequency. Fig 3.17 shows obtained response of the RF response when the gap in the ring resonator is changed from 100 μm to 200 μm in 50 μm step.

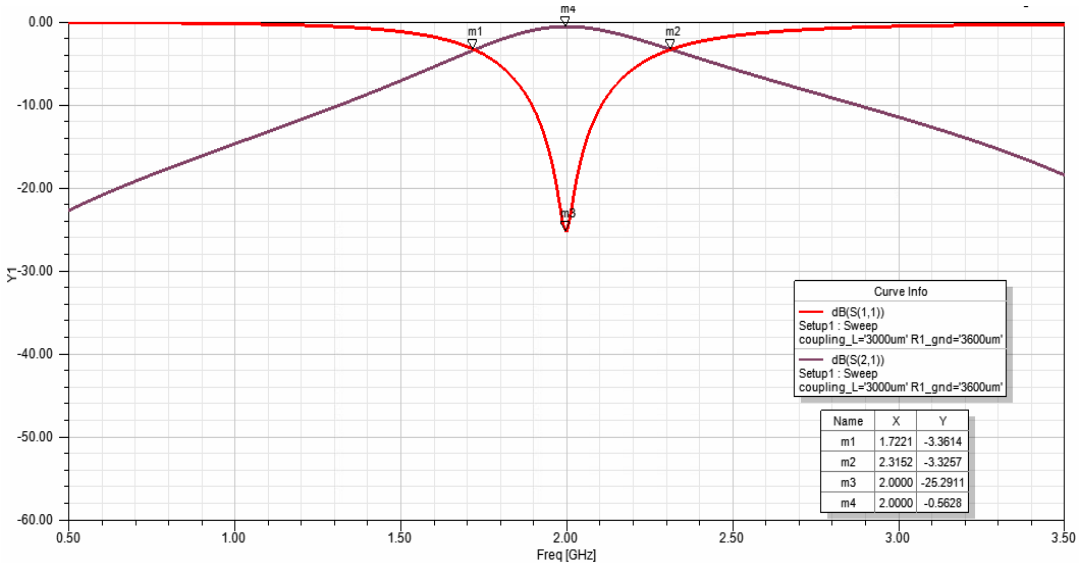

Fig 3.16: Simulated first order BPF in HFSS

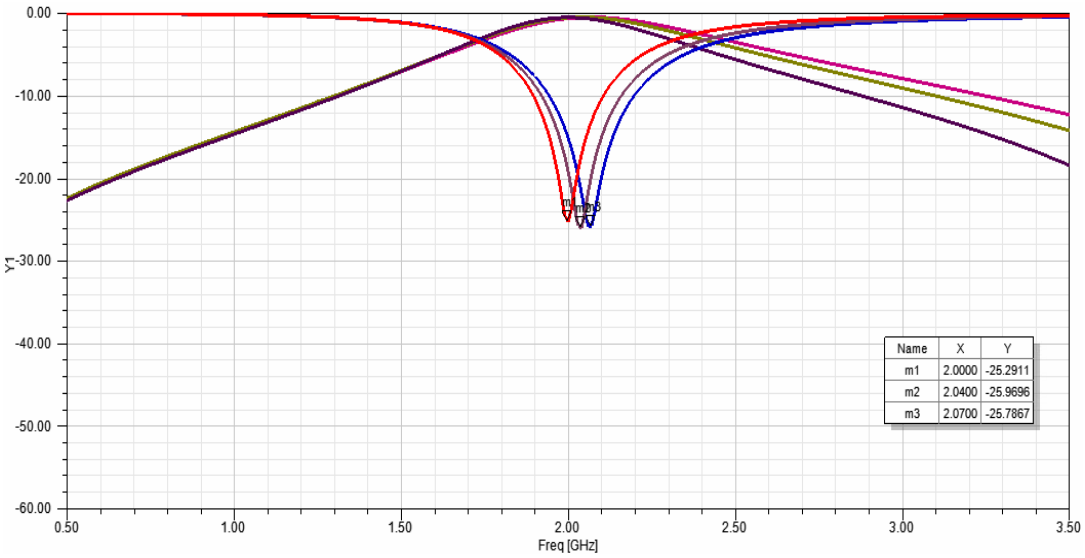

Fig 3.17: Simulated tunability of single resonator in HFSS

3.4.2. Calculated loaded and unloaded quality factor (QF). The loaded and unloaded quality factors are found from the results of the EM simulation. It is noted that the quality factor of the 3D design is worse than the simulated quality factors obtained from ADS.

$$Q_L = \frac{2}{2.315 - 1.722} = 3.38$$

$$Q_u = \frac{2}{2.03 - 1.97} = 33.33$$

3.4.3. RF MEMS varactor design. The gap in the ring resonator can be utilized to tune the resonator by loading it with an RF MEMS varactor. There are different models of RF MEMS varactors such as: analog, and digital. In this work, an analog cantilever beam model is designed and simulated to tune the filter. The beam has dimensions of 1000 μm and 300 μm with an overlap of 300 μm and 100 μm as shown in Fig. 3.18. Different values of capacitance due to the overlap area can be achieved by varying the gap between the tip of the beam and the other side of the ring resonator. Fig 3.18 shows the RF MEMS varactor that is designed in HFSS for this filter. The final design of the first order BPF with the RF MEMS varactor is shown in Fig 3.19. In Fig 3.20, the RF performance of the resonator is illustrated with a gap of 2.5 μm.

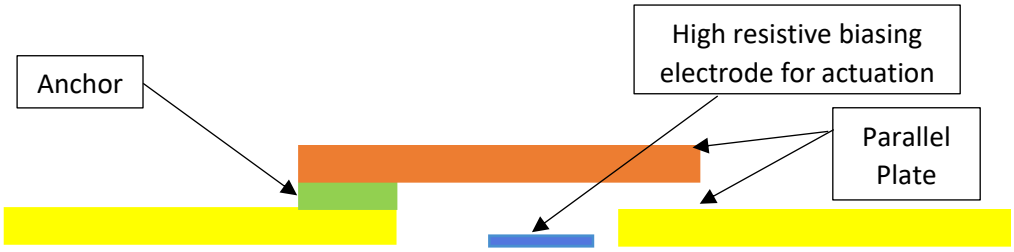

Fig 3.18: RF MEMS varactor model in HFSS

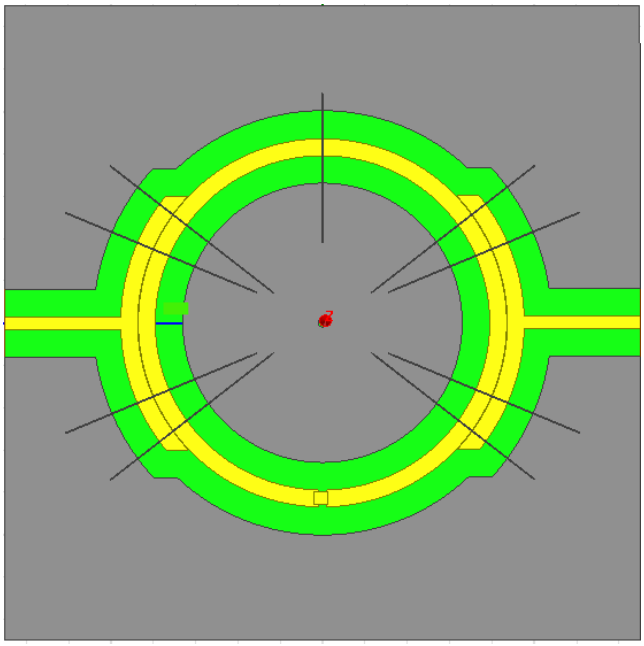

Fig 3.19: Final design of first order BPF with RF MEMS varcator

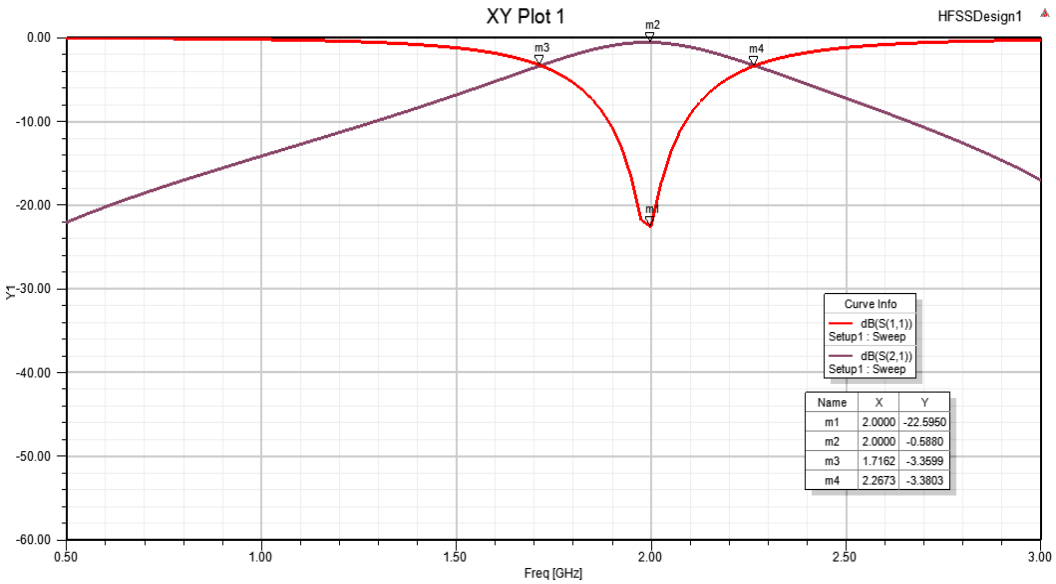

Fig 3.20: Simulated first order BPF using RF MEMS varcator

The tuning process is done by changing the gap between the tip of the cantilever beam and the bottom electrode which the other side of the ring resonator from 2.5 μm down to 1.8 μm. Fig 3.21. shows the RF performance of the resonator where the center frequency is varying from 1.7 GHz to 2 GHz with an extra loss of approximately 1 dB in the Insertion Loss. The rejection band for each tuned filter is changed, which is due to the change of capacitor for each simulation.

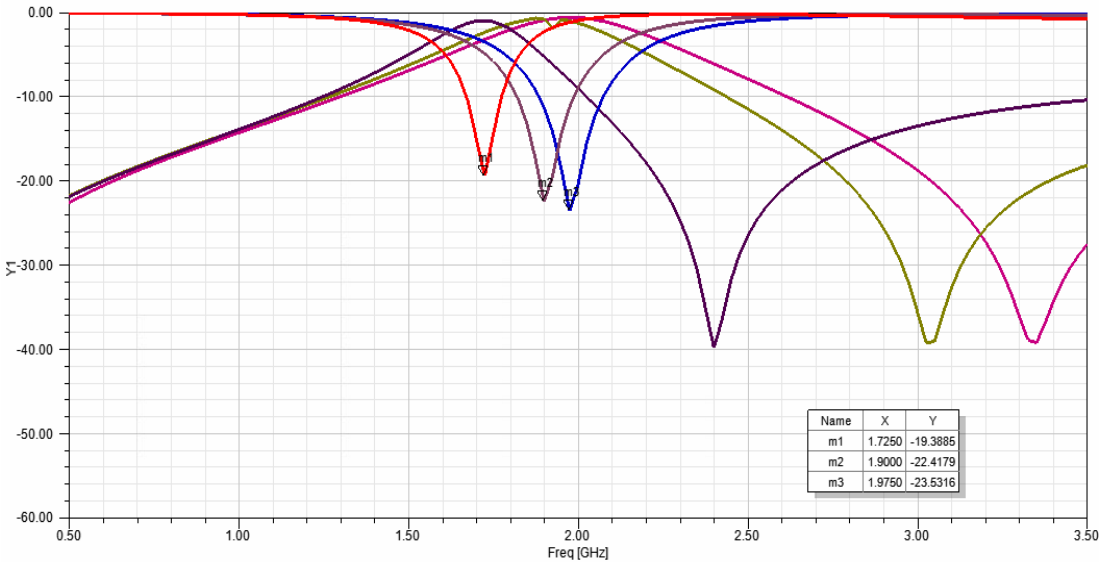

Fig 3.21: Simulated Tunability of the first order BPF using an RF MEMS varactor

3.5. Second Order BPF 3D Design in HFSS

The 3D design of the second order BPF is designed and simulated in HFSS software with the values closed to the circuit model design values. Because of the square shape ring resonator in the circuit model, the values will be slightly different from here. The design is based on two ring resonators that are connected by a transmission line from output of the first ring to the input of the second ring as shown in Fig 3.22. All the resonators sizes are the same as first order BPF with the same substrate and the conductor materials. The air bridges are also the same as the first order design, which are used to keep the polarity of the ground. The air box containing the filter design varies from -10000 µm to 20000 µm. First, the filter is simulated with an air gap between the ring resonators then the air gap is loaded with the RF MEMS varactor for tuning purposes. The two ring resonators are separated by 4000 µm transmission line and the overall size of the filter is 15 mm x 30 mm.

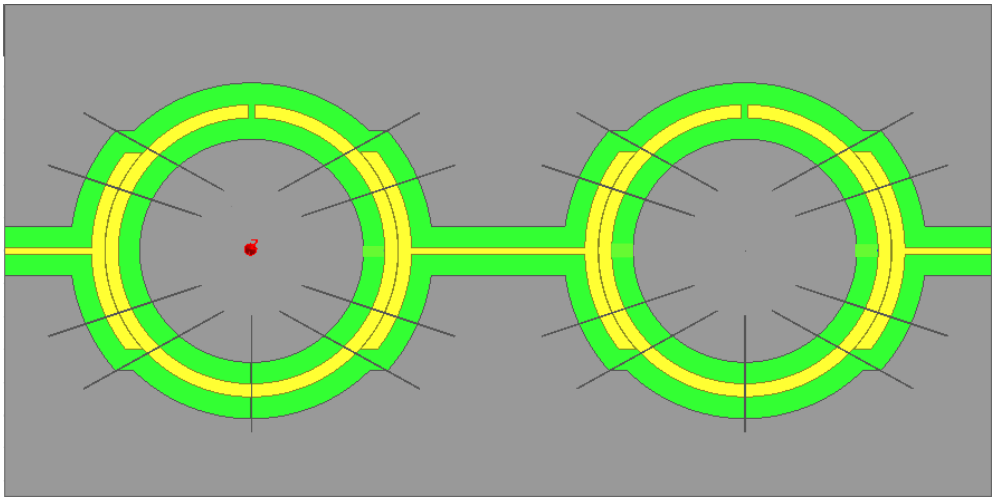

Fig 3.22: Second order BPF 3D model with conventional gap

3.5.1. Simulation results of the 3D design in HFSS. The second order BPF is simulated in HFSS software and the return loss and insertion loss results are displayed in Fig 3.23. The center frequency is appeared at 2.04 GHz with a return loss of 26.29 dB and an insertion loss of 1.12 dB. The bandwidth of the filter is 0.39 GHz, which is a smaller bandwidth than the first order BPF. The transmission line, between the two ring resonators, controls the inner coupling and as a result the bandwidth, the insertion loss, and the return loss. The tuning of the filter is obtained through varying the gap between the tip of the cantilever beam and the other side of the ring resonator as shown in Fig 3.24.

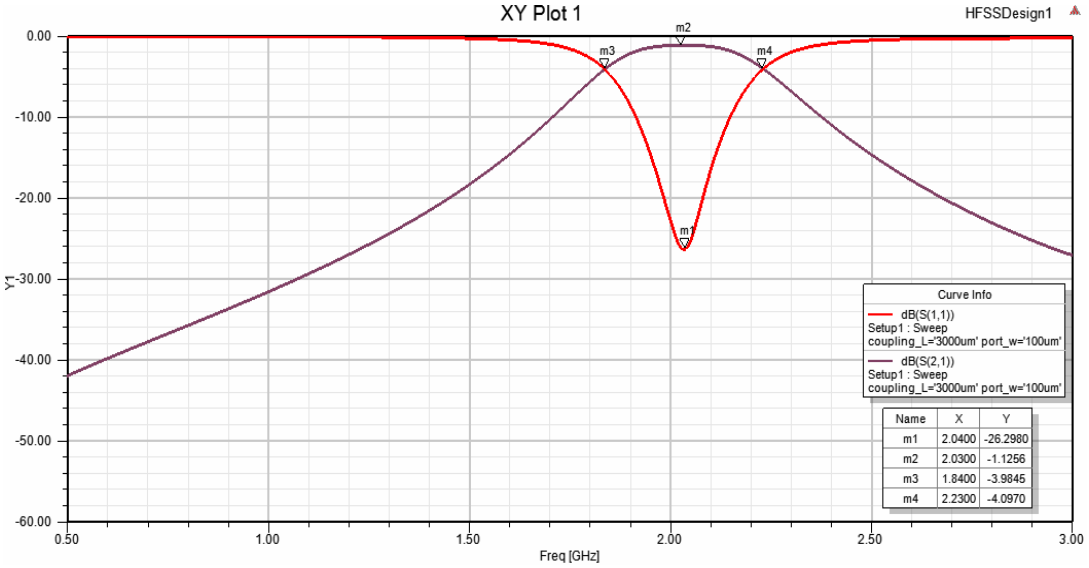

Fig 3.23: Simulated second order BPF with a conventional gap

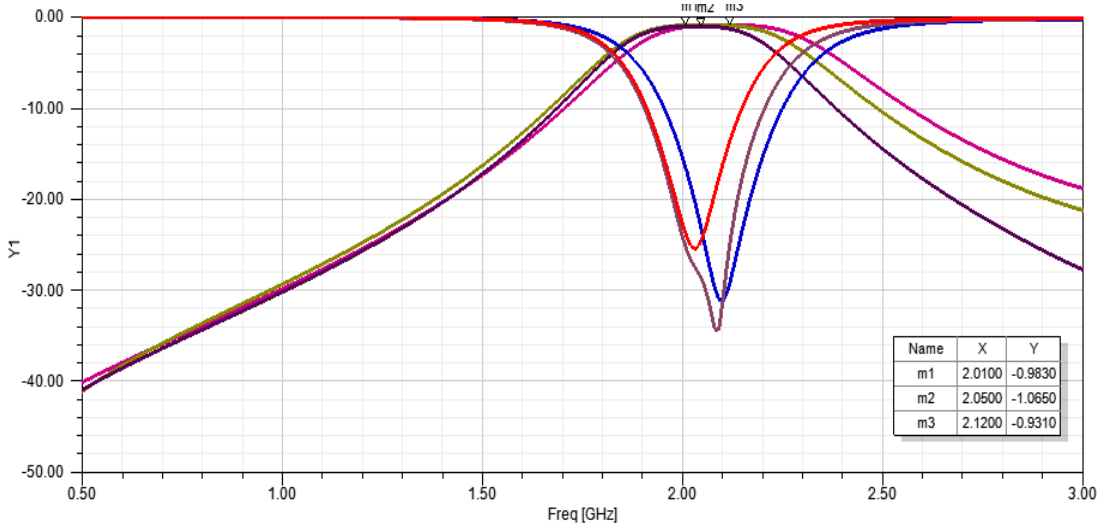

Fig 3.24: Simulated tunability of the second order BPF with different conventional gaps

From above figure, the filter is tuned at three different center frequencies which are at 2.01, 2.05 and 2.12 GHz. The achieved tunability in the second order BPF is noticed to be more than the first order BPF.

3.5.2. Calculated loaded and unloaded quality factor (QF). The loaded and unloaded quality factors of this filter are recorded as follow:

$$Q_L = \frac{2.04}{2.23 - 1.84} = 5.23$$

$$Q_u = \frac{2}{2.07 - 2.01} = 33.33$$

3.5.3. Simulated tuning for the 3D model filter in HFSS using the RF MEMS Varactor. The tuning process of this filter is implemented through loading the gap with the same RF MEMS varactor designed for the first order BPF with the same dimensions. The final design of the second order BPF with RF MEMS varactor is presented in Fig 3.25. First, the RF MEMS varactor is anchored on one side of the ring resonator while the tip of the cantilever beam is tuned to have different gaps with the other side of the ring. The RF performance is shown in Fig 3.26, through varying the gap between the tip of the cantilever beam and the bottom electrode that is the other side of the ring resonator as illustrated in Fig 3.27. The center frequency of the filter is varying between 1.95 GHz, 2 GHz and 2.05 GHz for gaps of the parallel plates are 2.5 μm, 2.03 μm and 1.8 μm.

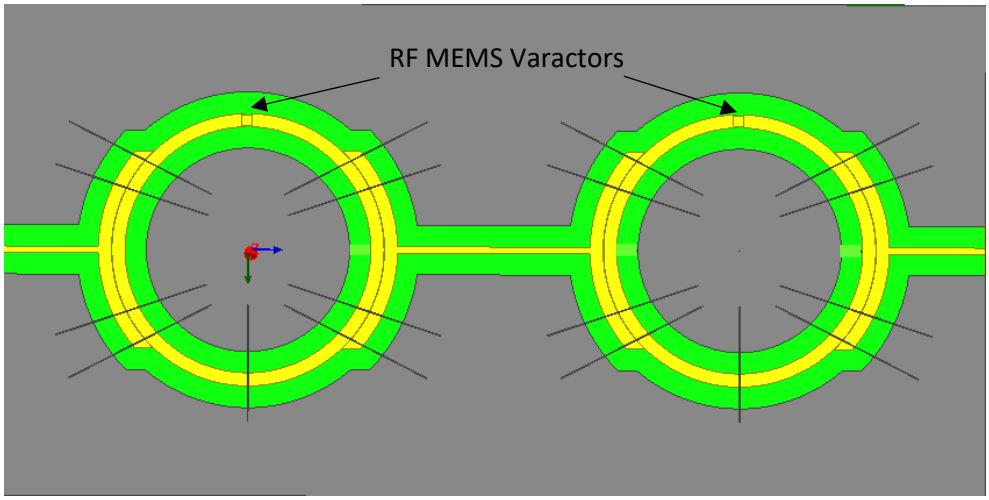

Fig 3.25: Final design of second order BPF with RF MEMS varactor

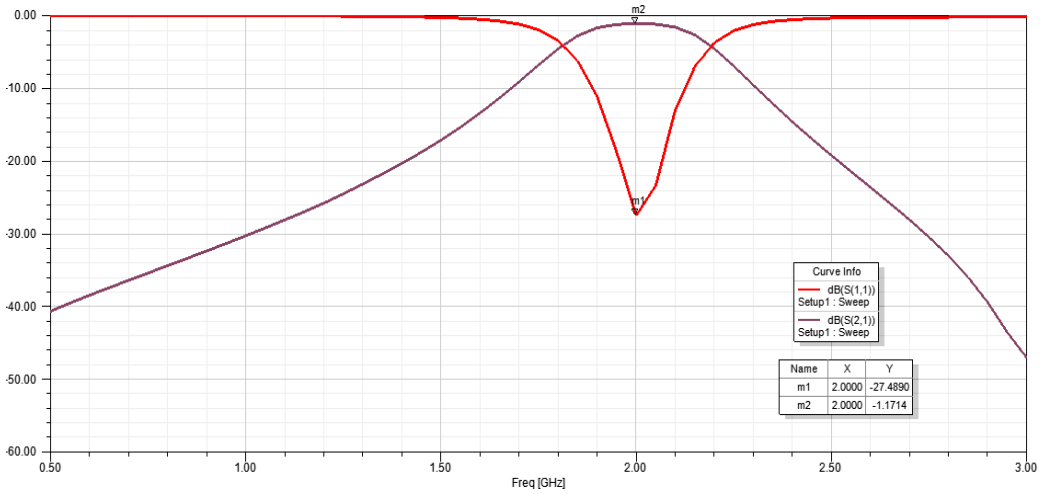

Fig 3.26: Simulated second order BPF with the varactor at a gap of 2.5 $\boldsymbol{\mu m}$

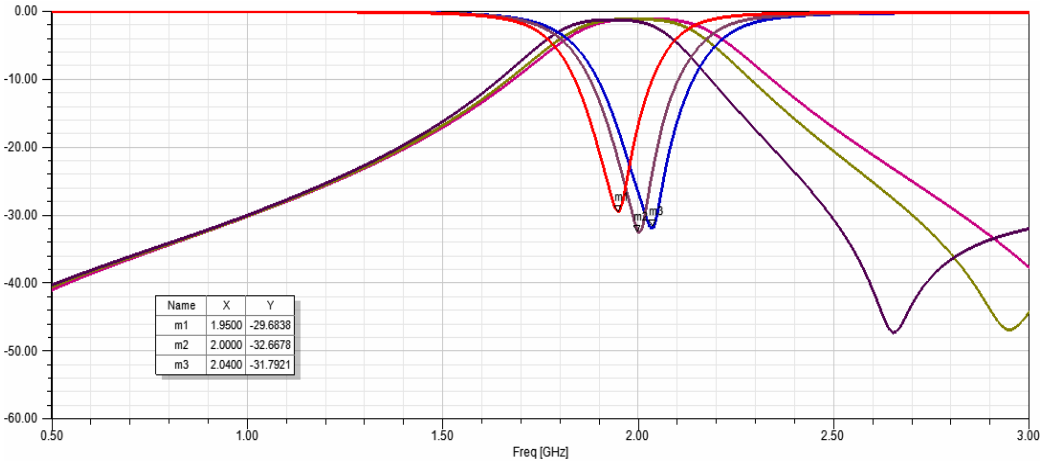

Fig 3.27: Simulated tunability of second order BPF using an RF MEMS varactor

3.6. Perfect Conductor Material

An idealized material which has infinite electrical conductivity or zero resistivity, is called a perfect conductor or perfect electric conductor (PEC). In reality, there is no perfect electrical conductor at ambient temperature, but this material can be used for modeling purposes including radiation and de-tuning effects. In this work, the perfect conductor is used to check the frequency response for the filter when there are no resistive losses. Using the perfect conductor material, the best possible RF response can be achieved. In the following sections, the effects of the perfect conductor for both first and second order BPF are showed.

3.6.1. First order bandpass filter using perfect conductor material. The perfect conductor is used for the conductor material in the first order BPF with the same dimensions to evaluate the frequency response of the filter. The filter is simulated in HFSS and ADS software and the results are shown in Fig 3.28 and Fig 3.29, respectively. The figures show the insertion loss of zero and return loss of 34 dB (HFSS) and 49 dB (ADS) for the same bandwidth, which are the best possible results for this filter design.

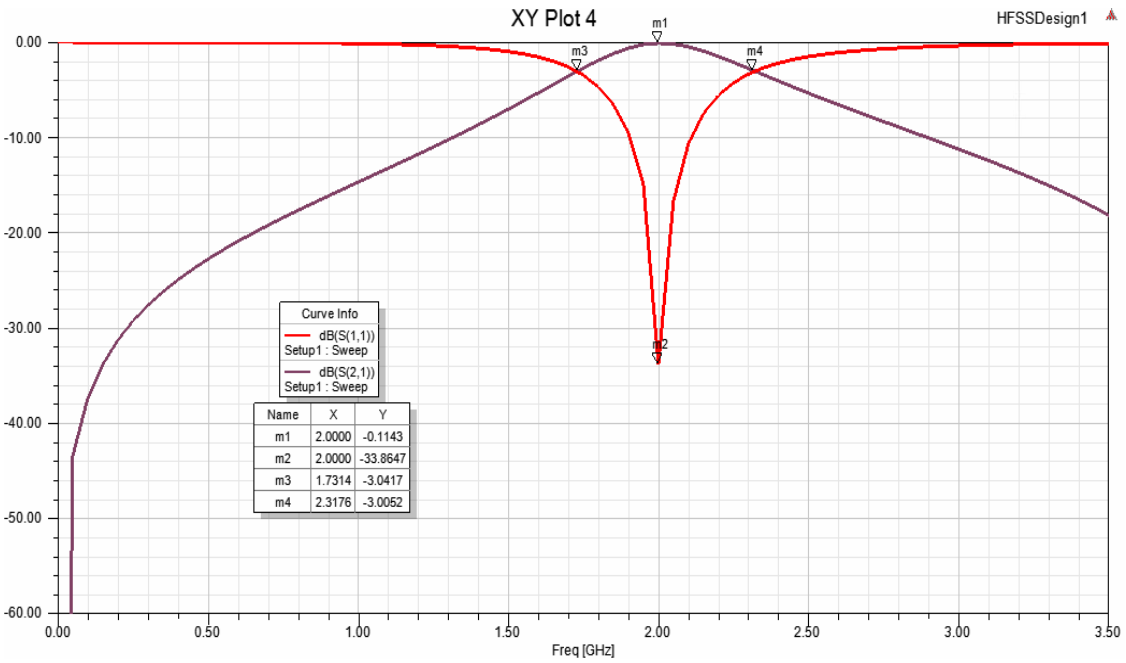

Fig 3.28: Simulated first order BPF using perfect conductor in HFSS

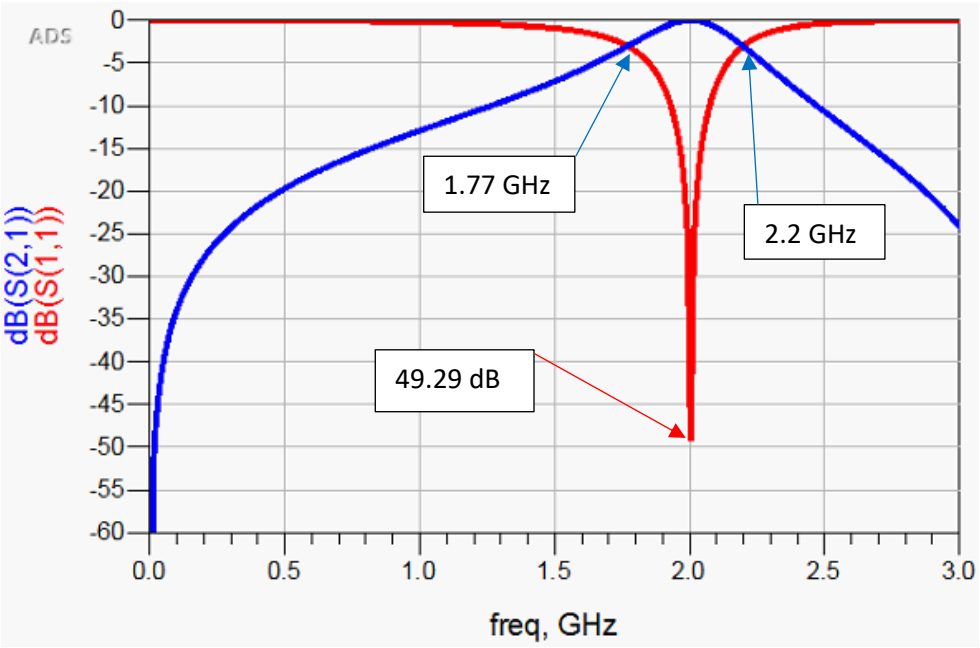

Fig 3.29: Simulated first order BPF using perfect conductor in ADS

3.6.2. Second order bandpass filter using perfect conductor material.

The same design and dimensions is simulated with perfect conductor material. The ideal frequency responses of this design are showed in Fig 3.30 and Fig 3.31, in HFSS and ADS software, respectively. Fig 3.30 the insertion loss, with zero losses, and a 26 dB of return loss for input matching. Similar response is obtained in ADS circuit simulator for the same modeled filter as shown in Fig 3.31.

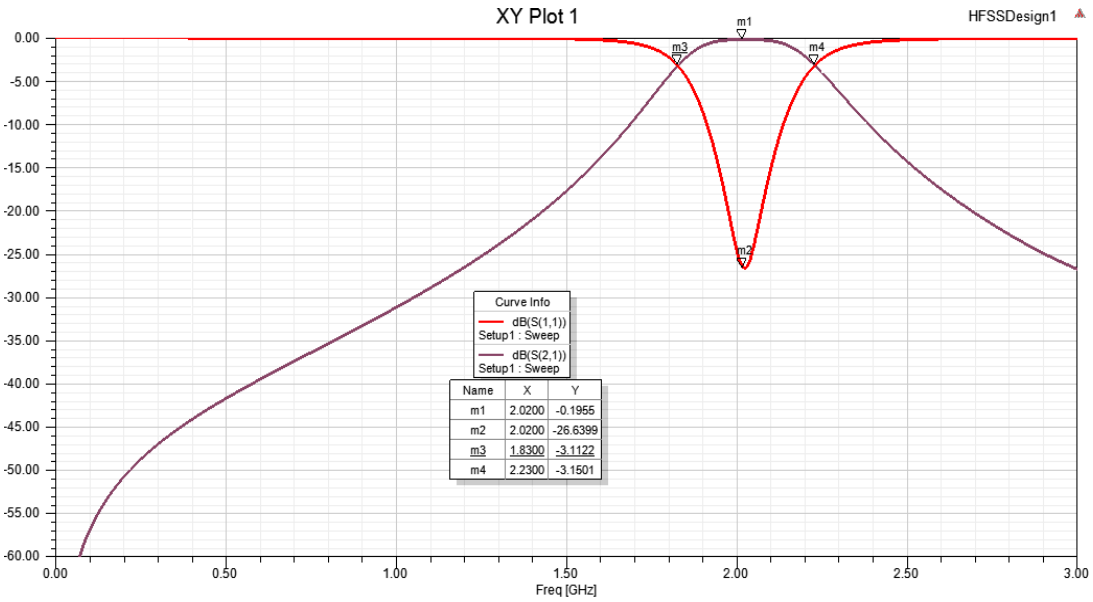

Fig 3.30: Simulated second order BPF using perfect conductor in HFSS

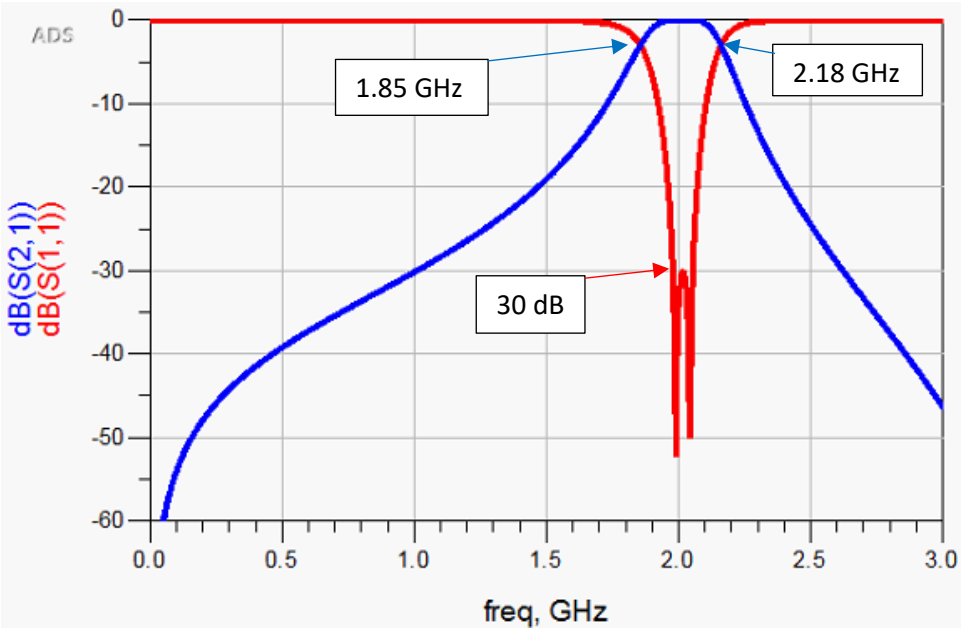

Fig 3.31: Simulated second order BPF using perfect conductor in ADS

Chapter 4: Tunable Bandpass Filter Using CPW Ring and RF MEMS Varactor Resonator for High Frequency

In this chapter, the same ring resonator topology was designed to operate at 2 GHz center frequency re-designed to operate at 20 GHz The circuit model of this filter is designed and simulated in ADS software, and the 3D model of the design is EM simulated in HFSS software.

4.1. Overall Design of Filter

The same CPW technology is used for designing the filter with the same model of bandpass filter using open ring resonator. Firstly, the first order bandpass filter is designed and simulated in both ADS and HFSS, and then the second order filter. For both filters, the dimensions of filters are designed for center frequency of 20 GHz and became smaller than the filter operating at lower center frequency. Since the resonators operate at higher frequency, there will be more loss due to the finite thickness of the used conductive material, and also resonators are closed to each other. As a result, higher insertion loss is expected to be found. The results in this chapter will show these losses.

4.2. First Order BPF Circuit Model

The circuit model of this BPF is designed and simulated using ADS software. The first step in this part is to change the radius of the ring resonator by using the value calculated in section 2.5.2 for filter to operate at center frequency of 20 GHz. Then, by running the simulation result in ADS, the frequency response of the filter is achieved. Finally, an optimization method is used to tune the dimensions of resonators for a better frequency response at the targeted 20 GHz center frequency.

4.2.1. Schematic circuit model of the resonator at 20 GHz. The circuit model of this filter is shown in Fig 4.1, which is similar to the first ring resonator operating at low center frequency however it has different dimensions for each components which are calculated such that to operate at 20 GHz center frequency. As explained before for the schematic diagram of the resonator at 2 GHz, the CPW transmission lines in ADS library is used to design the filter and the resonator uses edge coupling on an open ring resonator. The input/output ports are connected to the simple transmission lines for two ports network.

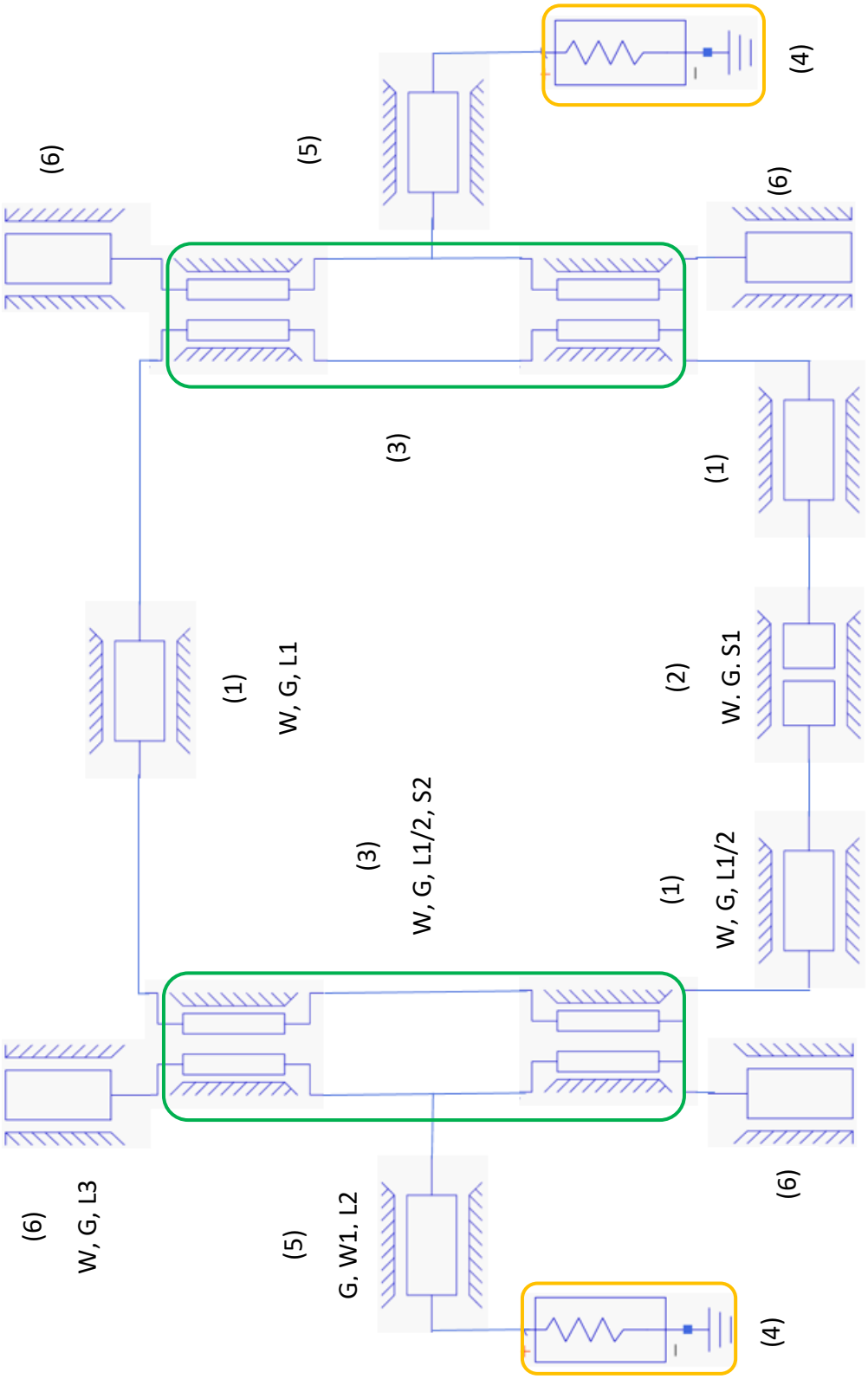

Fig 4.1: Circuit model of first order BPF in ADS

4.2.2. Simulation results of circuit model in ADS. The filter presented in Fig 4.1 is simulated in ADS, and the frequency response is depicted in Fig 4.2 at a center frequency of 20 GHz and a bandwidth of 2 GHz. Fig 4.3 shows the obtain insertion loss and the return loss of 1.57 dB and 15.83 dB, respectively.

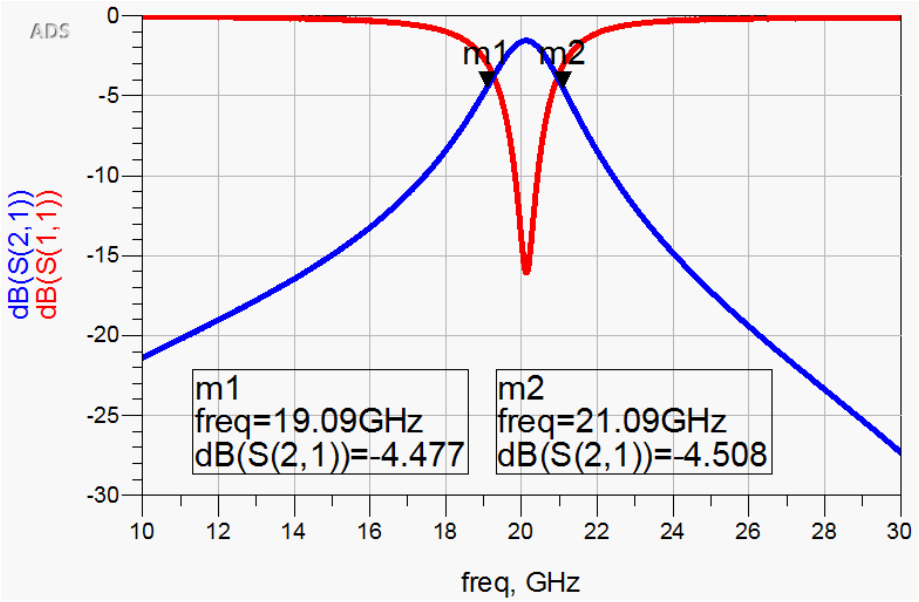

Fig 4.2: Extracted bandwidth of first order BPF

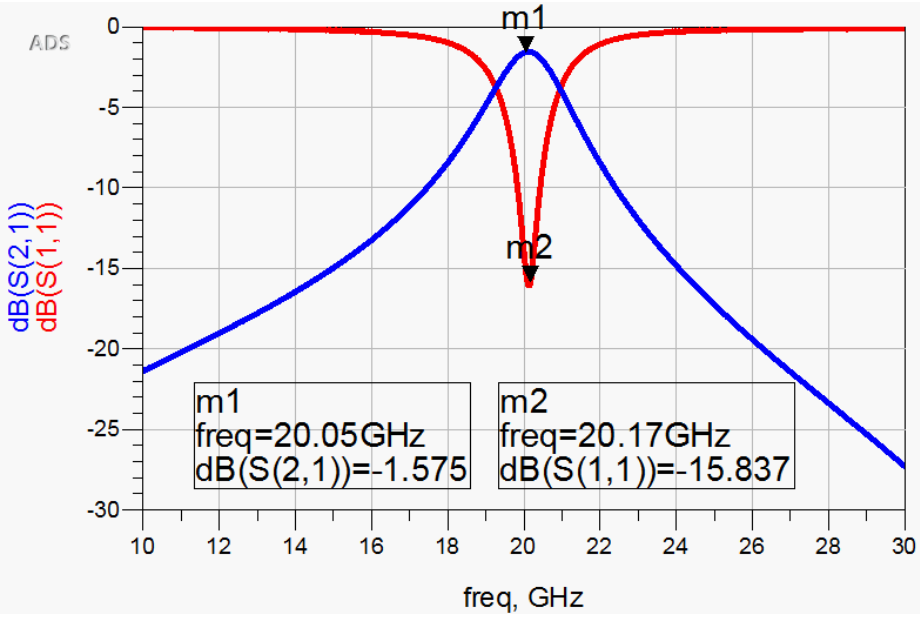

Fig 4.3: Extracted insertion loss and return loss of first order BPF

4.2.3. Simulated tuning BPF for circuit model in ADS. In this section, the tuning of first order BPF for high frequency is simulated and the result is shown in Fig 4.4. The gap in ring resonator has been changed from 50 µm to 250 µm with a step of 100 µm. From the simulated result, it clearly shows that the resonator's center frequency changes due to the change in the gap's spacing as 50 µm, 150 µm, and 250 µm to 19.5 GHz, 20.5 GHz and 21 GHz, respectively.

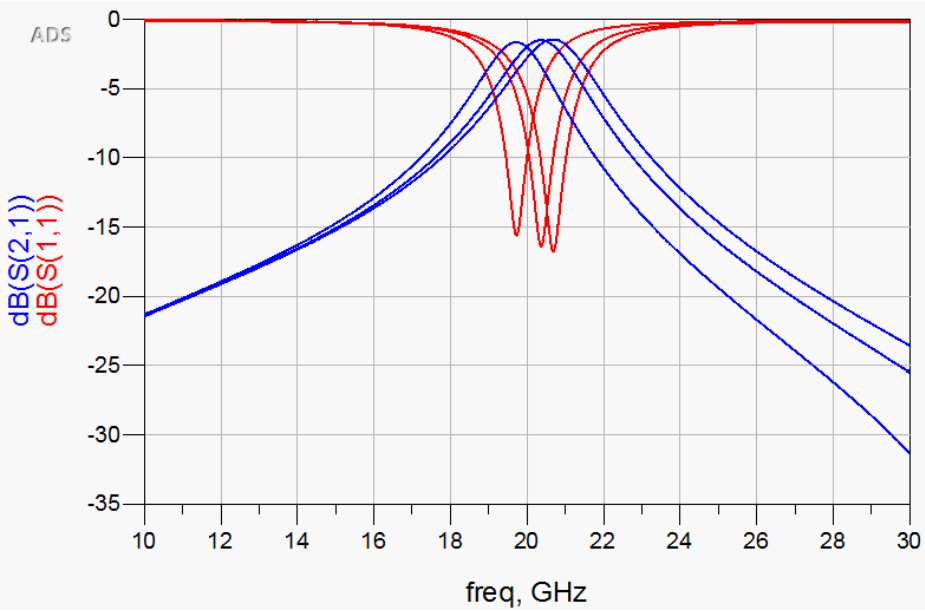

Fig 4.4: Simulated tunability of first order BPF at gap's spacing of 50 µm, 150 µm, and 250 µm

4.2.4. Calculated loaded and unloaded quality factor. The loaded and unloaded quality factor are calculated which are:

$$Q_L = \frac{20.17}{20.09 - 19.09} = 20.17$$

$$Q_u = \frac{20.17}{20.5 - 19.9} = 33.62$$

4.3. Second Order BPF Circuit Model

The modeling of second order BPF is implemented with two ring resonators that both have the same dimensions of the previously mentioned single resonator BPF connected by one CPW transmission line through two coupled line couplers. The overall design is displayed in Fig 4.5 in ADS software. Four coupled line couplers and two open ring resonators with a CPW transmission line composes the second order

BPF at 20 GHz. Moreover, an optimization method is used in the ADS software to tune the dimensions to get the best possible RF performance.

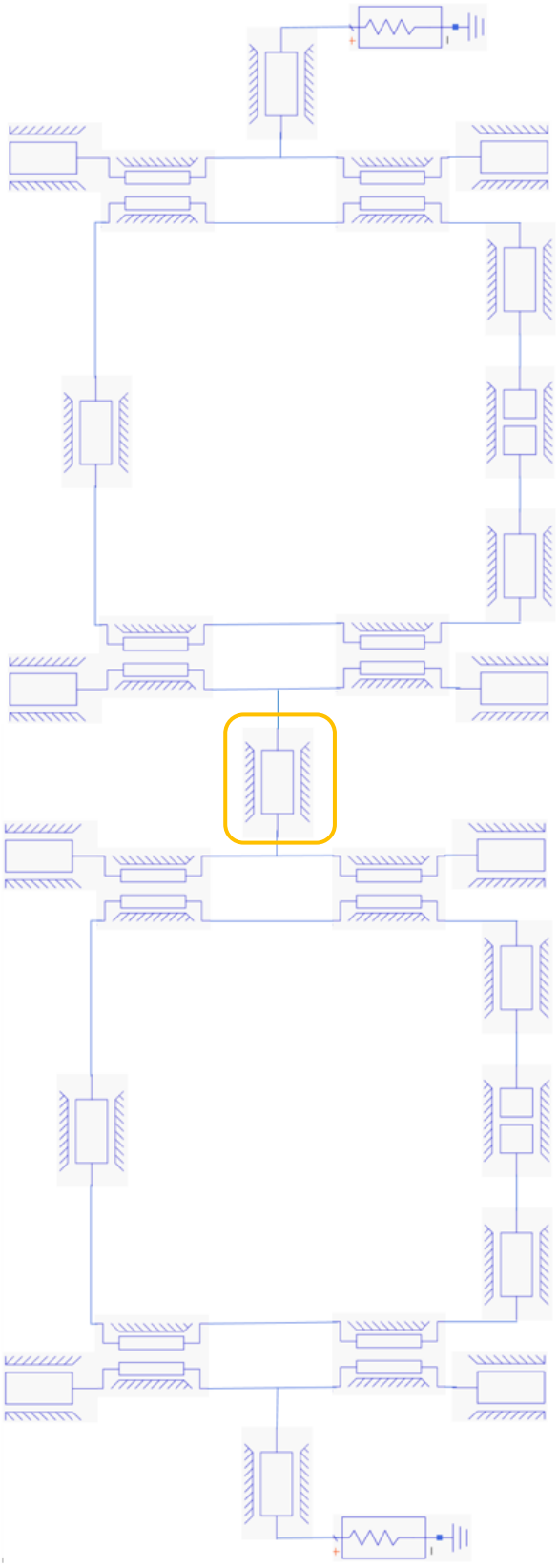

Fig 4.5: Second order BPF circuit model in ADS

4.3.1. Simulation results of circuit model. The second order BPF simulated in ADS software, and the result of frequency response is demonstrated in Fig 4.6. The center frequency appears at 20 GHz with bandwidth of 1.1GHz. The insertion loss and return loss of this filter are found by using the result showed in Fig 4.7. The insertion loss is 3.59 dB and return loss is 33.63 dB. The results proved that by increasing the number of order of filter, the performance of the filter will improve (better insertion and return loss).

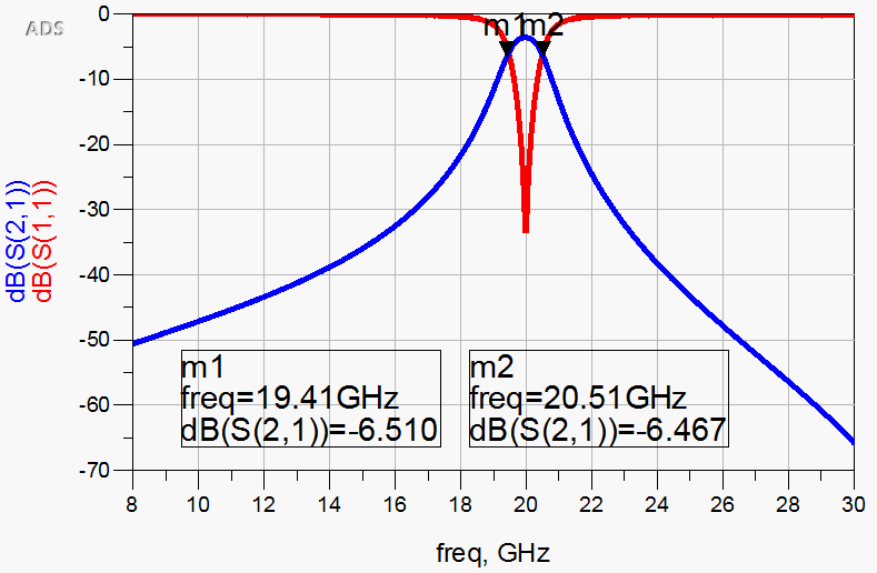

Fig 4.6: Extracted bandwidth of second order BPF

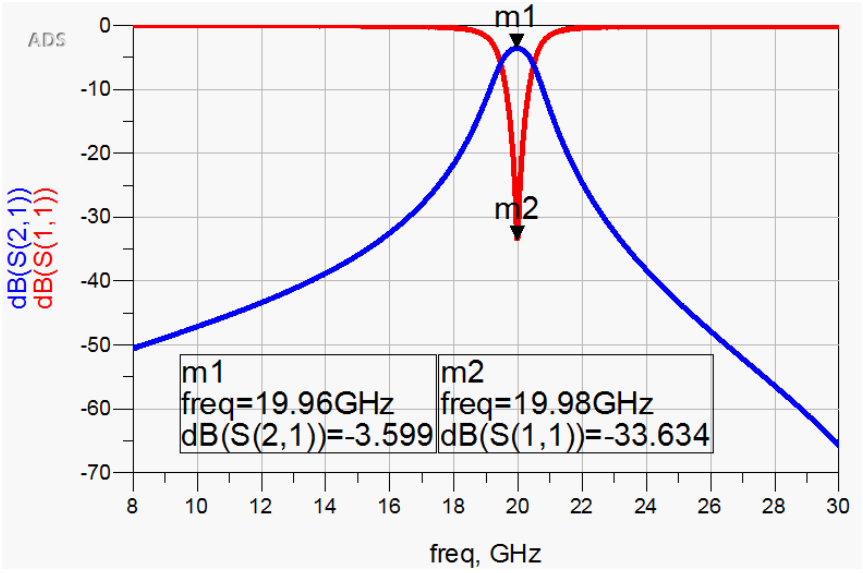

Fig 4.7: Extracted insertion loss and return loss of second order BPF

4.3.2. Calculated loaded and unloaded quality factor. In this section, the loaded and unloaded quality factors are calculated and the results are:

$$Q_L = \frac{20}{20.51 - 19.41} = 18.18$$

$$Q_u = \frac{20}{20.01 - 19.9} = 181.81$$

4.4. First Order BPF 3D Design in HFSS

For the EM simulation, the 3D model design is built in HFSS. The finalized values in ADS design circuit model are applied on the model in HFSS software. The radius of the ring, width of the conductor, coupled line coupler separation and the length are the parameters that were updated in the HFSS 3D model. The same thickness of signal, ground conductors and the substrate are implemented in the filter operating at 2 GHz. The thickness of signal and ground conductors is set to be 2 μm of gold material, and the material of the substrate is Alumina with thickness of 675 μm. The overall size of the first order BPF is 2.4 mm x 2 mm. Fig 4.8 and Fig 4.9 show the top and the side views of the filter designed in HFSS. The air box height is reduced for clarity purpose.

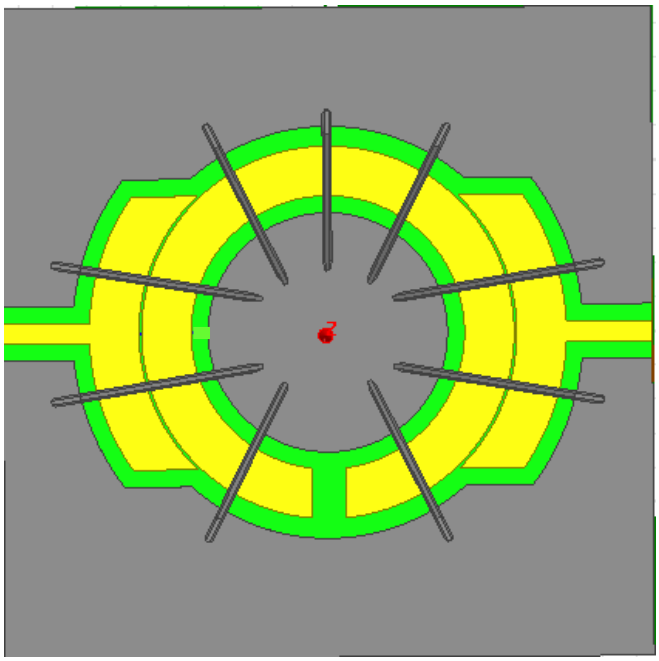

Fig 4.8: The top view of the first order BPF in HFSS

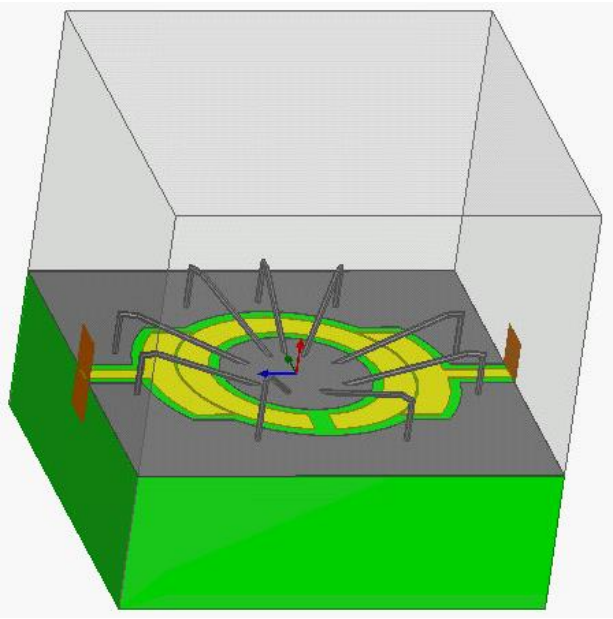

Fig 4.9: An angle view of the second order BPF in HFSS

4.4.1. EM simulation results of 3D design in HFSS. The filter is simulated in HFSS software, and the result of the frequency response is shown in Fig 4.10 over a frequency range from 10 to 30 GHz. The center frequency is at 20 GHz with a bandwidth of 2.61 GHz. Fig 4.11 shows a result 1.74 dB insertion loss and 17.53 dB return loss. Fig 4.12 shows the frequency response when the gap in the ring resonator is changed from 100 μm to 200 μm in a step of 25 μm.

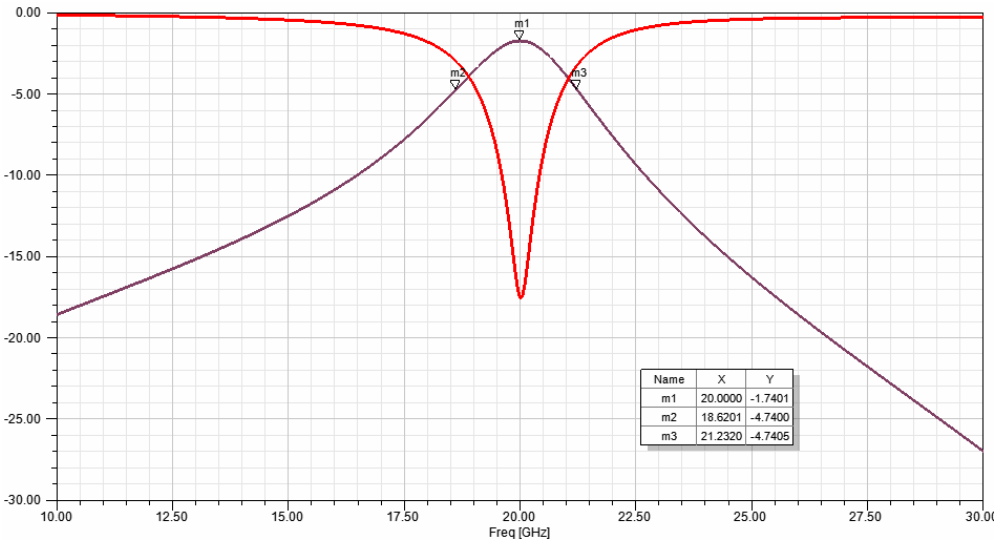

Fig 4.10: Simulated bandwidth of first order BPF in HFSS for a gap of 200 μm

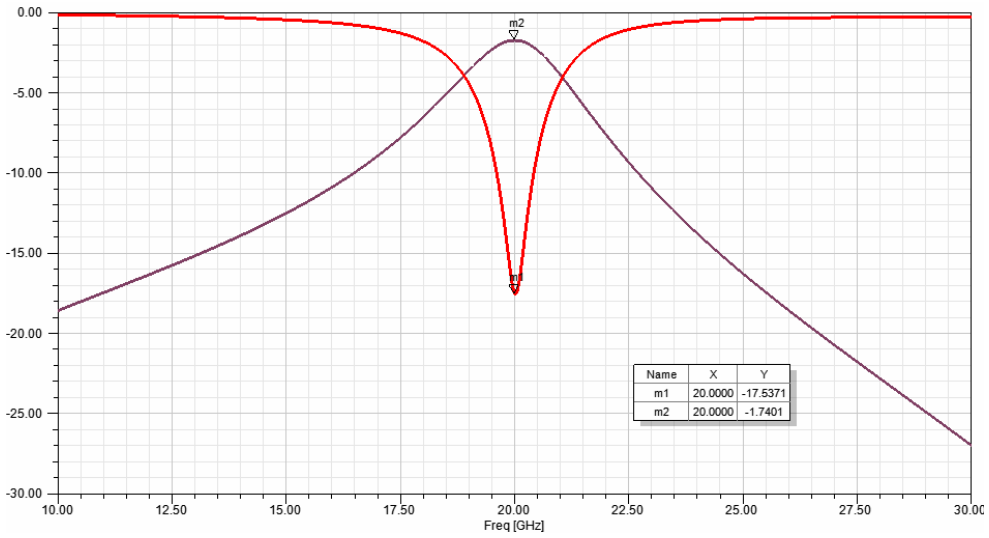

Fig 4.11: Simulated insertion loss and return loss of first order BPF for a gap of 200 μm

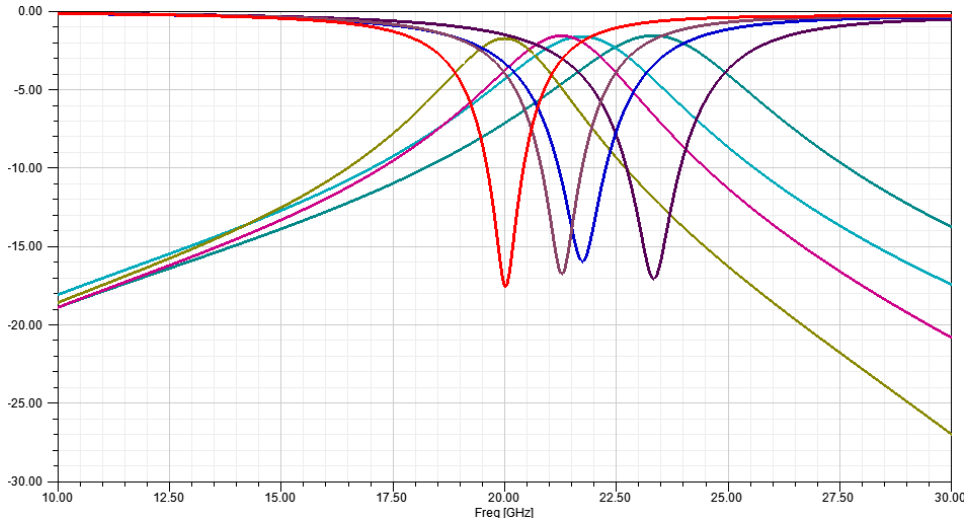

Fig 4.12: Simulated tunability of the first order BPF through varying the conventional gap from 100 µm to 200 µm in a step of 25 µm

4.4.2. Calculated loaded and unloaded quality factor (QF). The loaded and unloaded quality factors are extracted from the above figures and calculated to be as follow:

$$Q_L = \frac{20}{21.23 - 18.62} = 12.42$$

$$Q_u = \frac{20}{20.15 - 19.57} = 34.48$$

4.4.3. RF MEMS varactor design of filter layout design. The RF MEMS varactor for this first order BPF has different dimensions that the used varavtor in the lower frequency design. The cantilever beam is anchored on one side of the open ring and while the tip of the beam is overlapping with the other side of the ring. The separation distance between the tip and the other side of the ring can vary through different applied voltages and as a result tuning is achieved. The overall size of the RF MEMS varactor that is of cantilever shape is 160 μm x 100 μm, for the length and width, respectively while the overlapped area between the tip of the cantilever and the other side of the ring resonator is 40 μm x 100 μm.

The final design of the first order BPF with the RF MEMS varactor is illustrated in Fig 4.13. Fig 4.14 shows the frequency response of the filter with the RF MEMS varactor at a gap of 2.5 μm between the tip of the beam and the other ring side.

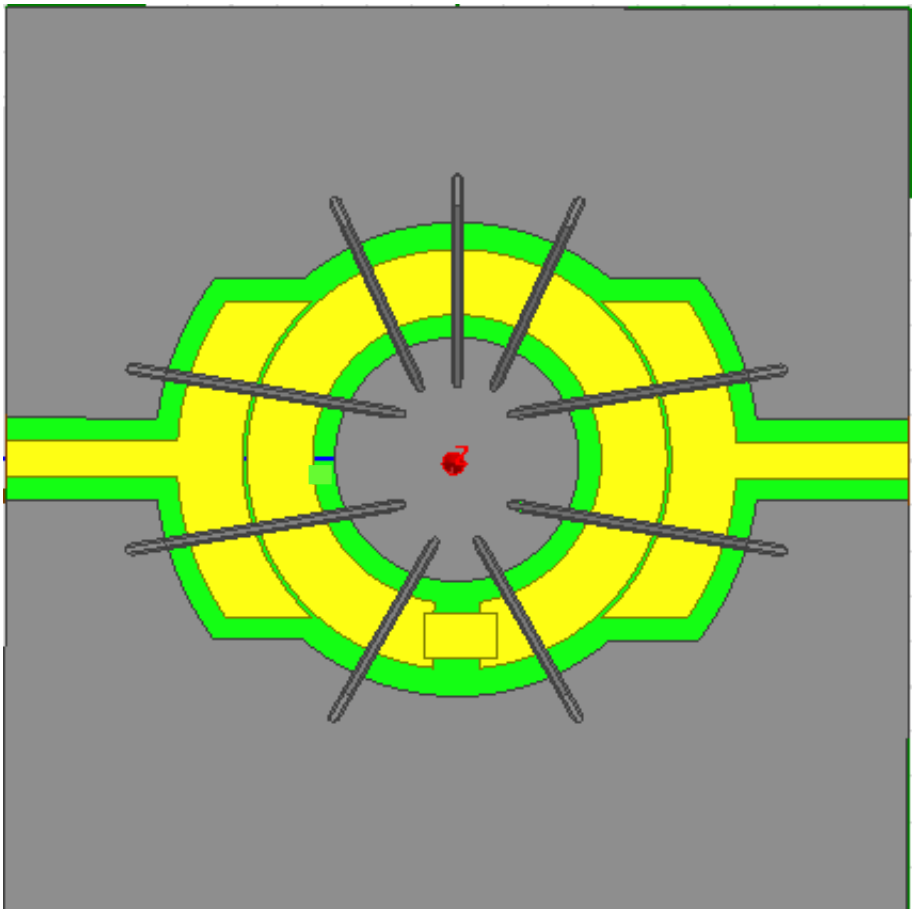

Fig 4.13: Final design of first order BPF with RF MEMS varactor

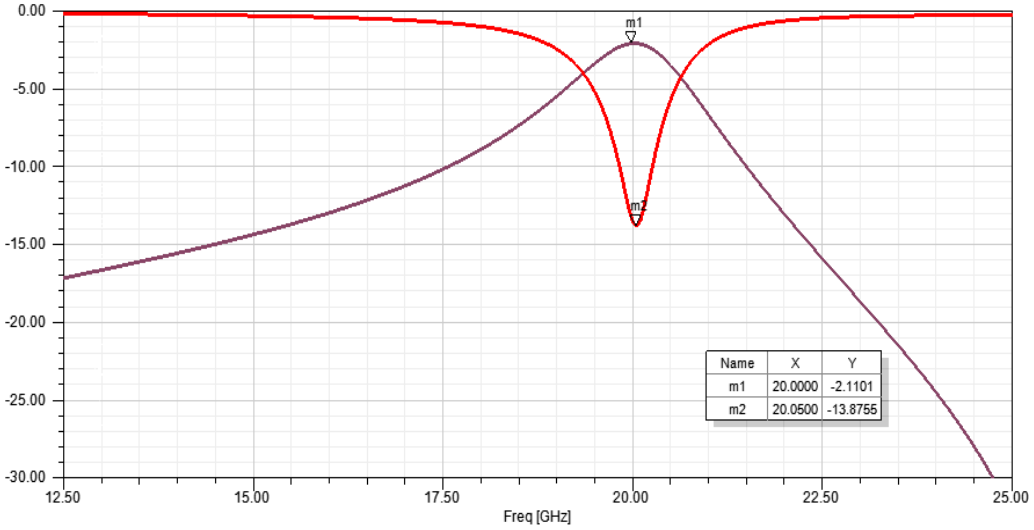

Fig 4.14: Simulated first order BPF with RF MEMS varactor at a gap of 2.5 μm

The tuning process is done by changing the gap from 2.8 µm to 1.4 µm. As a result, the frequency response of this tuning is shown in Fig 4.15. From the figure, the center frequency is tuned from 17.8 GHz to 20.15 GHz with an increase of loss of around 1 dB. The rejection band for each tuned filter is changed as a result.

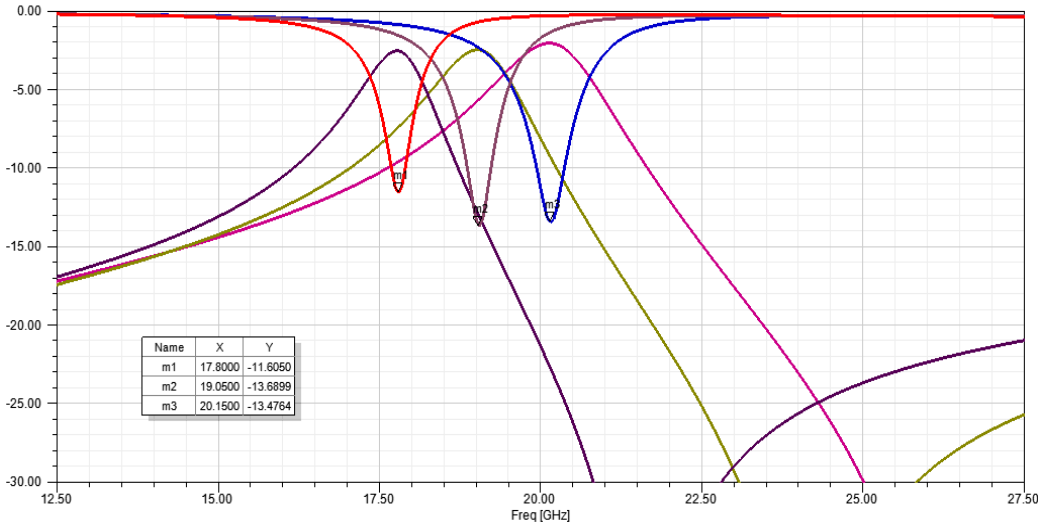

Fig 4.15: Simulated tunability of first order BPF with the RF MEMS varactor varying from 2.8 µm to 1.4 µm

4.5. Second Order BPF 3D Model Design in HFSS

The same values of circuit model design are used to design the 3D of the second order BPF in HFSS software. The design is based on using two ring resonators which are connected by one transmission line through coupled line couplers, Fig 4.16. All

the resonator sizes are the same as first order BPF with the same substrate and the same conductor's material. The air box that surrounds all over the filter design is from -3000 μm to 6000 μm. In general, the air box for each filter should be six times bigger than the substrate thickness. The filter is simulated without the RF MEMS varactor, only by creating the gap in the ring resonator, and then the simulation is continued by using an RF MEMS varactor to achieve tunability. The two ports of the filter are coupled through coupled line coupler to the two ports in HFSS software. The two ring resonators are separated by 280 μm transmission line and the overall size of the filter is 2 mm x 3.64 mm.

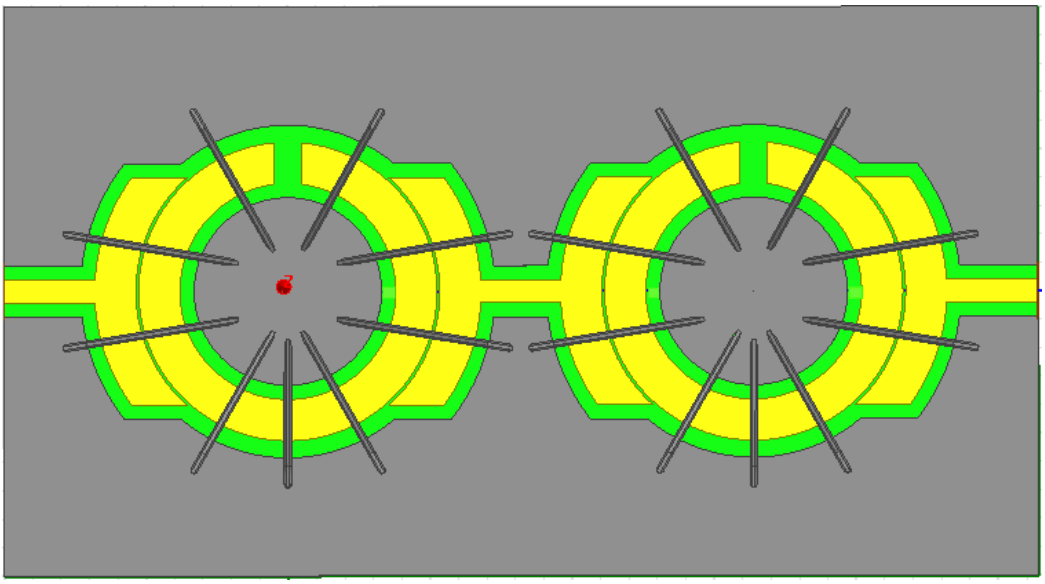

Fig 4.16: Top view of second order BPF with conventional gap

4.5.1. EM simulation results of the 3D model design in HFSS. The frequency response of the filter simulated above is displayed in Fig 4.17. The center frequency appears at 19.75 GHz with the return loss of 30.59 dB and the insertion loss of 2.9 dB. The bandwidth of this filter is 1.47 GHz, which is less than the first order BPF. The transmission line used in between the two ring resonators to adjust the bandwidth and the insertion loss. The tunability of the filter is evaluated by changing the gap in ring resonators equally as shown in Fig 4.18. The gap in ring resonator is changed from 100 μm to 200 μm with step of 50 μm. The tuning from 19.75 GHz to 20.85 GHz achieved from the HFSS simulation. The bandwidth of the filter is changed for each center frequency, because the gap is affect to the radius of the ring resonator which cause different bandwidth.

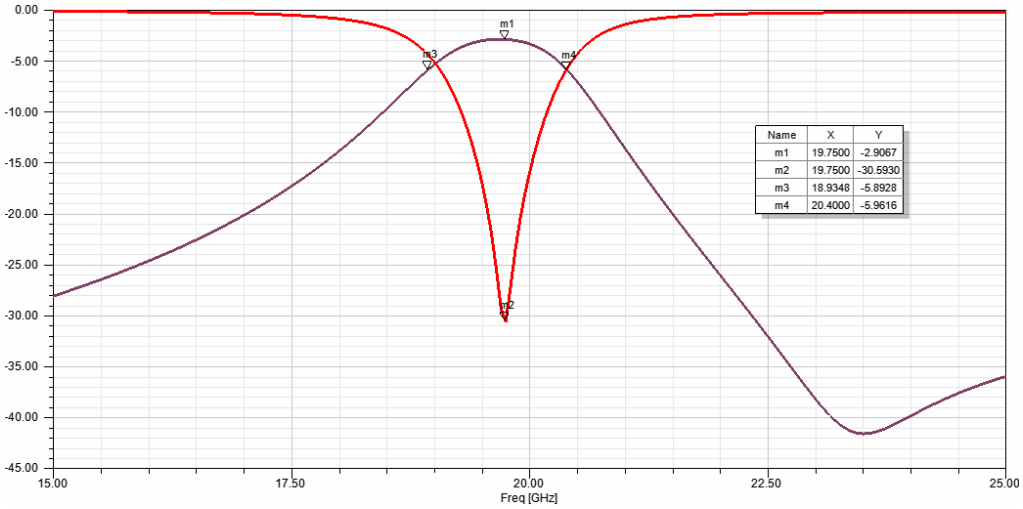

Fig 4.17: Simulated of second order BPF with conventional gap

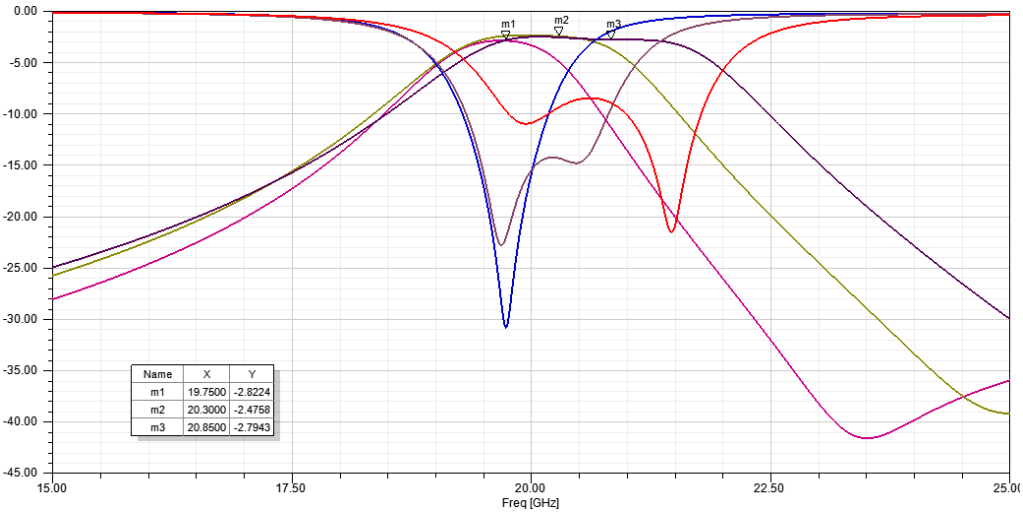

Fig 4.18: Simulated tunability of second order BPF with conventional gaps

4.5.2. Tuning with RF MEMS varactor for the 3D model design in HFSS.

The RF MEMS varcator is used to tune the second order BPF with the same dimensions. The final design of the second order BPF with RF MEMS varactor is presented in Fig 4.19 (the air box is reduced to show for illustration purposes). First, the RF MEMS varactor is placed at the ring resonator open area. The initial gap is designed such that the same center frequency is obtained in frequency performance which is showed in Fig 4.20, then tuning is achieved by changing the gap between the tip of the beam and the other side of the ring from 0.8 μm to 2.4 μm with step of 0.8 μm as shown in Fig 4.21. This results in center frequencies at 19.6 GHz, 19.9 GHz and 20.2 GHz, respectively with a tuned bandwidth as well. The bandwidth of the filter is changed for each center frequency.

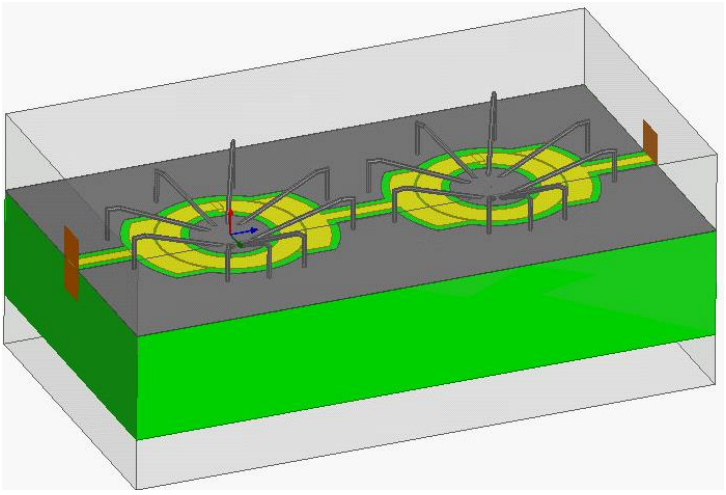

Fig 4.19: Final 3 D model design of second order BPF with the RF MEMS varactors

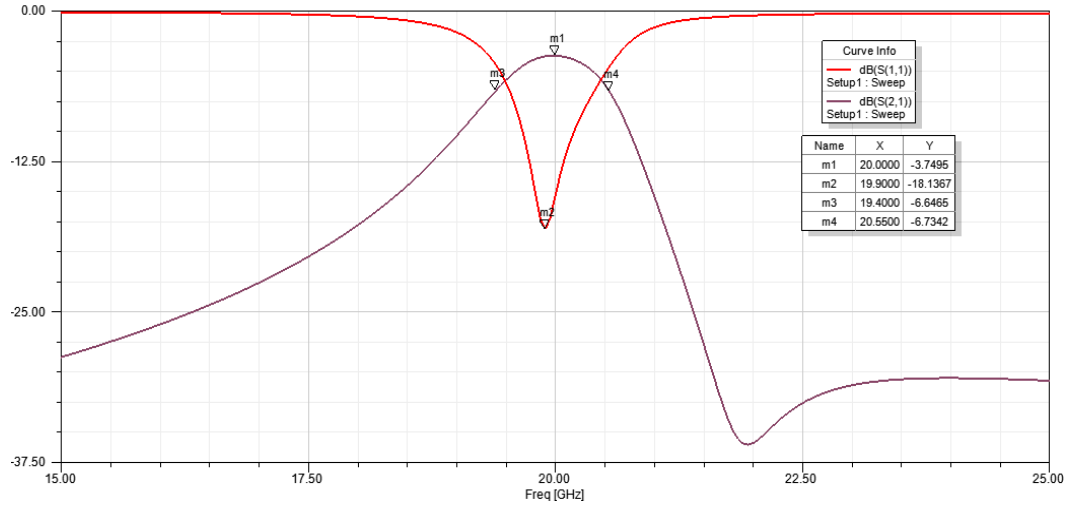

Fig 4.20: Simulated second order BPF with the RF MEMS varactors

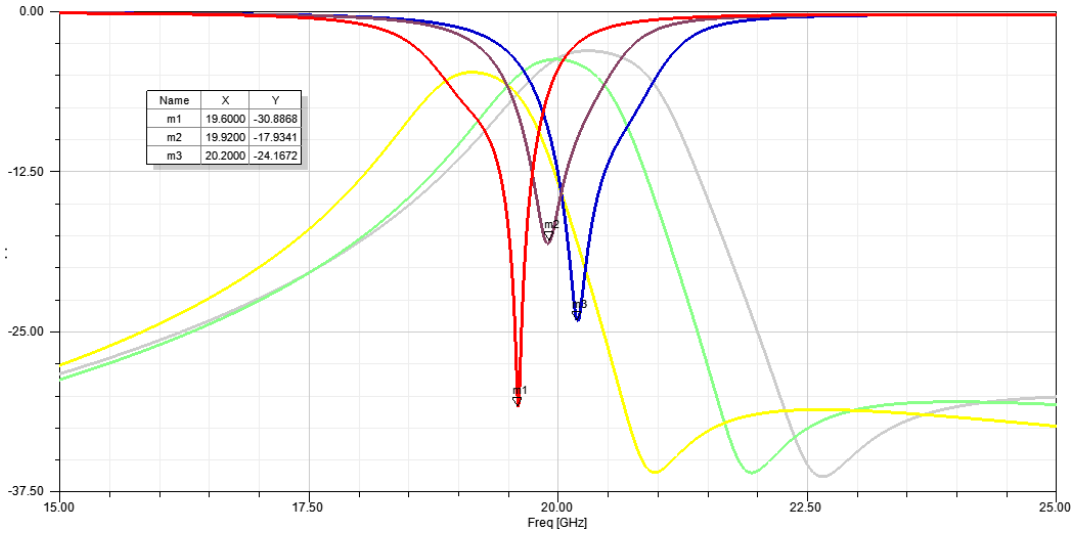

Fig 4.21: Simulated tunability of second order BPF with tuning the RF MEMS varcators

4.5.3. Calculated loaded and unloaded quality factor (QF). The loaded and unloaded quality factors of this filter are measured which are as follow:

$$Q_L = \frac{20}{20.55 - 19.4} = 17.39$$

$$Q_u = \frac{20}{20.1 - 19.8} = 66.66$$

4.6. Perfect Conductor Material

The perfect conductor is used to check the frequency response of the filter when there are no resistive losses. By using the perfect conductor, the best possible frequency response can be achieved. In the following sections, the effects of the perfect conductor for both first and second order BPF are showed for both circuit schematic and 3D design.

4.6.1. First order bandpass filter using perfect conductor material. The perfect conductor has been used for the conductor material in the first order BPF with the same dimensions, to check the frequency response of the filter. The filter was simulated in HFSS and ADS software, and its results are displayed in Fig 4.22 and Fig 4.23. The center frequency has been shifted to 20.4 GHz. The figures show the insertion loss of 0.61 dB (HFSS) and return loss of 21.1 dB (HFSS) and 49 dB (ADS), which are the best possible results for this filter design.

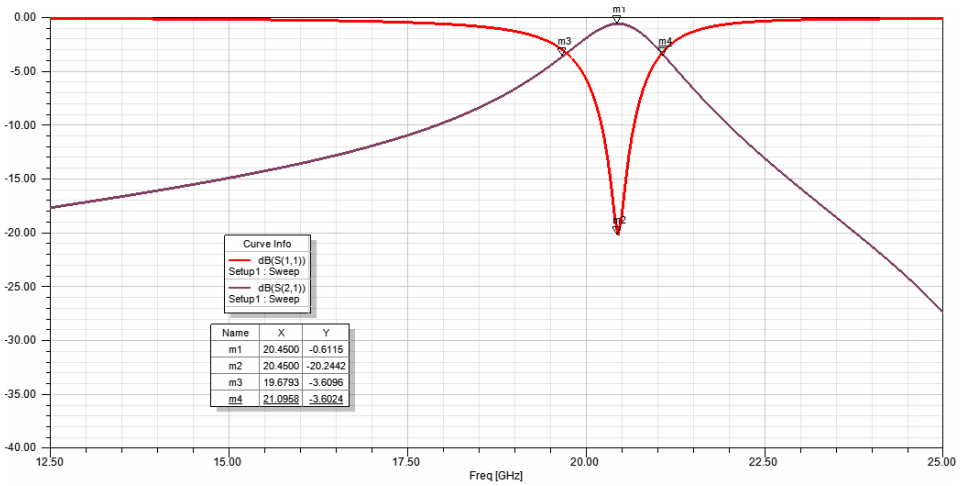

Fig 4.22: Simulated first order BPF with RF MEMS capacitive switches for perfect conductor in HFSS

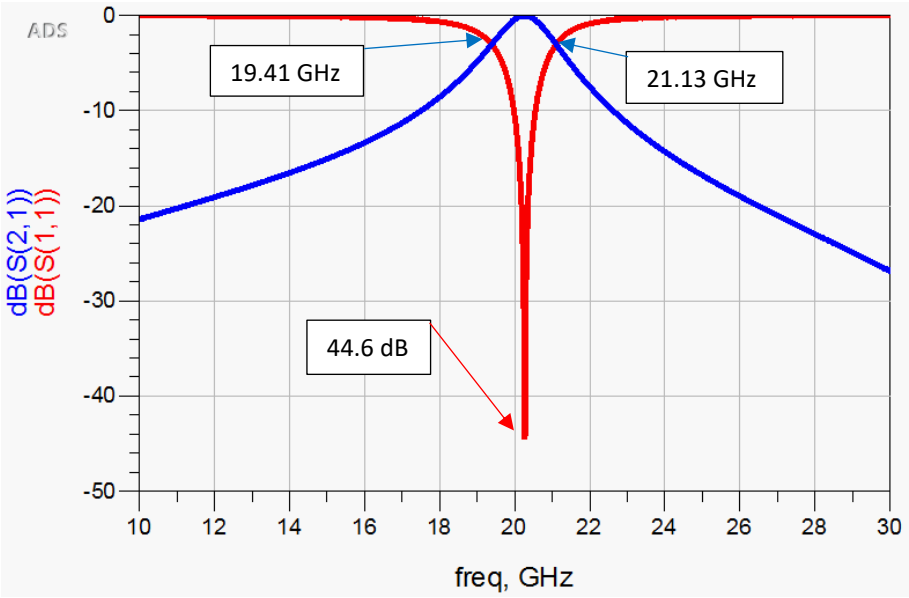

Fig 4.23: Simulated first order BPF for perfect conductor in ADS

4.6.2. Second order bandpass filter using perfect conductor material.

The same design and dimensions have been used for this part with perfect conductor material. The ideal frequency responses that can be achieved from this design are showed in Fig 4.24 and Fig 4.25, which are simulated in HFSS and ADS software. The insertion loss for HFSS simulation is 0.92 dB and for ADS simulation is zero. The return loss values are 16.7 dB (HFSS) and 26.7 dB (ADS), which is the best possible values obtained from fine tuning the parameters of the filter through optimization in ADS.

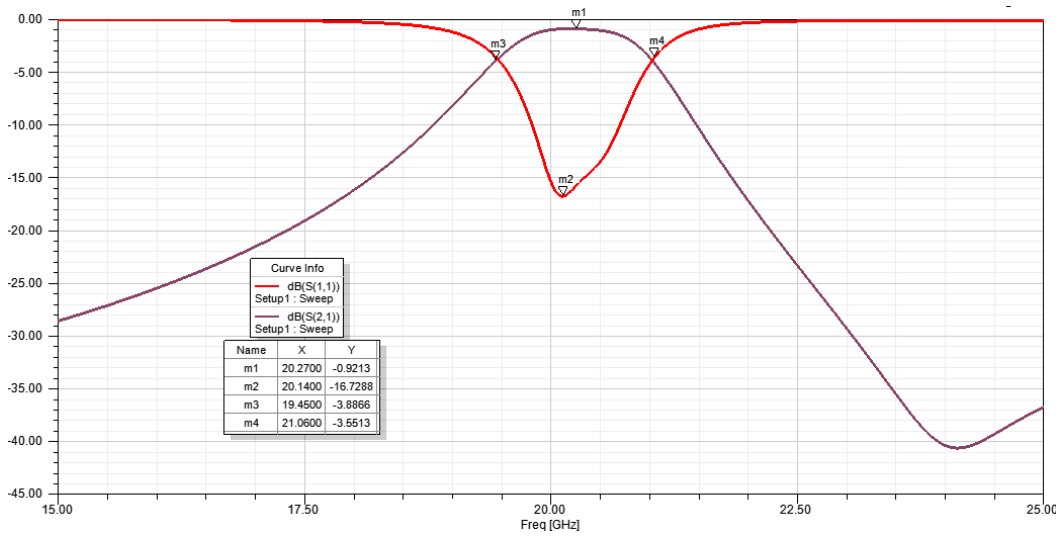

Fig 4.24: Simulated second order BPF for perfect conductor in HFSS

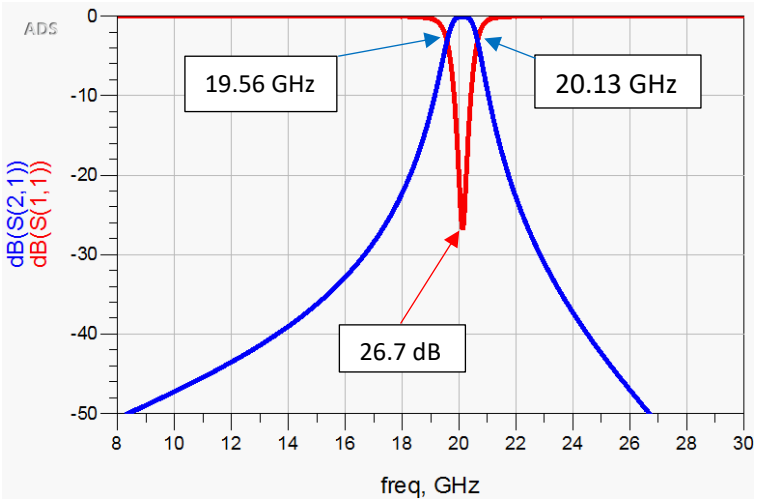

Fig 4.25: Simulated second order BPF for perfect conductor in ADS

Chapter 5: Results and Comparison

In this chapter, all the results of first and second order BPF are compared with perfect conductor materials and published papers. The benefits of using novel design of new technology are summarized in tables with the simulated results.

5.1. Results of the Low Frequency BPF

This section contains the summary of the results for first and second order BPF at low frequency for both ADS and HFSS simulation, which have been compared with the filter using perfect and gold conductor materials. The following tables display the results.

In Table 5.1, the simulated bandwidth for the first order filter using perfect conductor has wider bandwidth and as expected high quality factor the simulated results of this work for the second order filter for gold and perfect conductor material are in good agreement.

Table 5.1: Comparison of first order BPF with filter using perfect and gold conductor material at low frequency

	Bandwidth (GHz)	S11 (dB)	S21 (dB)	Q_L	Q_u
This work, gold (ADS)	0.3	23	0.5	6.78	40
This work, Perfect conductor (ADS)	0.43	49.29	0	4.65	181.81
This work, gold (HFSS)	0.59	25	0.5	3.38	33.33
This work, Perfect conductor (HFSS)	0.58	33.86	0.11	3.44	50

Table 5.2 is the summary of the second order BPF with the results of the filter using gold and perfect conductor. From the results, again the first order filter bandwidth is wider in case of perfect conductor; the loaded quality factor in case of gold for both ADS and HFSS simulations is higher than the perfect conductor, which is due to the narrower frequency response in the S_{11}.

Table 5.2: Comparison of second order BPF with filter using gold and perfect conductor material at low frequency

	Bandwidth (GHz)	S11 (dB)	S21 (dB)	Q_L	Q_u
This work, gold (ADS)	0.3	29.25	0.94	6.47	24.69
This work, Perfect conductor (ADS)	1.07	30	0	1.86	18.18
This work, gold (HFSS)	0.39	26.29	1.12	5.23	33.33
This work, Perfect conductor (HFSS)	0.4	26.64	0.19	5	22.22

5.2. Results of the High Frequency BPF

The results of the first and second order BPF with the same filter using perfect conductor material are summarized in this section. Table 5.3 shows that the bandwidth of both ADS and HFSS simulation of this work is wider than the filter using perfect conductor materials. The narrower the bandwidth, the better return loss can be achieved. As a result, the higher value of loaded quality factor can be obtained. The better return loss and loaded quality factor are obtained in second order BPF compared with perfect conductor material, which is clearly shown in

Table **5.4**.

Table 5.3: Comparison results of the first order BPF and the filter with gold and perfect conductor material at high frequency

	Bandwidth (GHz)	S11 (dB)	S21 (dB)	Q_L	Q_u
This work, gold (ADS)	2	15.83	1.57	20.17	33.62
This work, Perfect conductor (ADS)	1.72	49	0	11.74	100.5
This work, gold (HFSS)	2.61	17.53	1.74	12.42	34.48
This work, Perfect conductor (HFSS)	1.42	21.1	0.61	14.4	136.33

Table 5.4: Comparison results of the second order BPF and the filter with gold and perfect conductor material at high frequency

	Bandwidth (GHz)	S11 (dB)	S21 (dB)	Q_L	Q_u
This work, gold (ADS)	1.1	33.63	3.59	18.18	181.81
This work, Perfect conductor (ADS)	0.57	26.6	0	35.08	100
This work, gold (HFSS)	1.47	30.59	2.9	17.39	66.66
This work, Perfect conductor	1.61	16.7	0.92	12.42	28.57

(HFSS)					

5.3. Results and Comparison of Expectation

The expectation results of designing this filter are summarized in Table 2.1. In this section, the final 3D model (HFSS) results of second order BPF for both low and high center frequency are compared with the expectation results.

Table 5.5: Results of second order BPF for both low and high frequency and specifications

Design Parameters	Specificatios	2 GHz	20 GHz
Technology	CPW	CPW	CPW
Center Frequnecy (GHz)	2 and 20	2	20
Bandwidth (GHz)	0.5 (Low Freq.) and 1 (High Freq.)	0.39	1.47
Return Loss (dB)	< -20	26.29	30.59
Insertion Loss (dB)	>-2	1.12	2.9
Quality Factor	-	33.33	66.66
Input port (Impedance)	50 Ohm	50 Ohm	50 Ohm
Output port (Impedance)	50 Ohm	50 Ohm	50 Ohm

The second order BPF for high center frequency has better return loss. On the other hand, the insertion loss of the filter with low center frequency is lower than the filter at high center frequency. The quality of the filter is also shown in the table which is the loaded quality factor. For all 3D model designs, the input and output ports are normalized to 50 Ohm.

5.4. Published Papers Results

In this section, the published papers results are summarized and compared with the final design of the BPF for both low and high center frequencies. All the published papers are designed the filter with microstrip technology, but the center

frequency are closer to the proposed targeted frequencies in this work. Table 5.6 shows the benefit of using the CPW technology by comparing between the simulated results of different published papers to this work.

Table 5.6: Results and comparison of literature and this work

Reference	Technology	Order	F_c (GHz)	BW	Return Loss (dB)	Insertion Loss (dB)	Q	Size (mm)
[9]	Microstrip	3	4.25	2.7	20	0.9	-	20 x 15
[10]	Microstrip	2	2.45	0.38	16.9	0.66	16	68 x 50
[11]	Microstrip	3	4.3	0.42	17	1.3	10.8	30 x 20
[12]	Microstrip	2	1.78	0.4	19.3	0.31	12.5	19.4 x 30.4
[13]	Microstrip	4	2.6	0.1	42	1.8	30	76 x 45
[14]	Microstrip	1	2.5	1.8	18.6	0.35	18.9	53.8 x 54.4
[15]	Microstrip	1	2.5	1.31	10.9	0.54	11.4	41.02 x 15.42
[16]	Microstrip	2	2.38	0.26	15	2	20	21.82 x 17.31
[17]	Microstrip	1	1	0.2	15	3.3	18.4	440 x 350
[18]	Microstrip	1	4.6	0.7	18	3.6	19.5	24 x 18
[19]	Microstrip	1	25	7.1	15	2.7	-	9.85 x 9.85
This work (HFSS)	CPW	1	2	0.59	25	0.5	33.33	15 x 15
This work (HFSS)	CPW	1	20	2.61	17.53	1.74	34.48	2 x 2.4
This work (HFSS)	CPW	2	2	0.39	26.29	1.12	33.33	15 x 30
This work (HFSS)	CPW	2	20	1.47	30.59	2.9	66.66	2 x 3.69

In all filter designs in the literature, the overall size of the reported filters are bigger than the proposed designs in this thesis. The achieved simulated quality factor shows a high potential of superior RF performance than the reported RF performances in the literature, which fulfills the aim of this thesis. Utilizing the CPW technology in the proposed designs contributed to the achieved compact size of the filter. For the filter design at 20 GHz, the overall size of the filter becomes really small in comparison with the reported filter in [19]. This work can be designed for the center frequency up to 40 GHz, however for frequency more than 40 GHz higher losses will be obtained. It is also notable that the obtained Return Loss for the proposed filters are better what are in the literature when simulations are compared.

Chapter 6: Conclusions and Future Work

6.1. Conclusions

A tunable CPW ring resonator bandpass filter is designed using RF MEMS varcators in both ADS and HFSS software for its circuit model and 3D design, respectively. Filters have been simulated for both low (at 2 GHz) and high (20 GHz) frequencies.

The first tunable ring resonator has been designed and simulated for 2 GHz and 20 GHz center frequencies, with an overall filters size of 15 mm x 15 mm and 2.4 mm x 2 mm, respectively. The unloaded and loaded quality factors of 33.33 and 3.38 for 2 GHz center frequency, and 34.48 and 12.42 for 20 GHz center frequency have been achieved, respectively. RF MEMS capacitive switches have been integrated in the ring resonator, and the tuning variations of 1.7 GHz to 2 GHz (2 GHz center frequency) and 17.8 GHz to 20.15 GHz (20 GHz center frequency) have been obtained.

Second order tunable BPF that is based on two coupled ring resonators has been designed and simulated for both center frequencies of 2 GHz and 20 GHz. An overall filter size of 15 mm x 30 mm in the case of 2 GHz center frequency and 2 mm x 3.64 mm in the case of 20 GHz center frequency have been achieved. The unloaded and loaded quality factors of 33.33 and 5.23 for center frequency of 2 GHz and 66.66 and 17.39 for center frequency of 20 GHz, respectively. RF MEMS varactors have also been integrated in the both ring resonators, and the tuning variations of 1.95 GHz to 2.05 GHz (2 GHz center frequency) and 19.6 GHz to 20.2 GHz (20 GHz center frequency) have been obtained.

In case of using perfect conductor material for signal plane, the resistive losses disappeared as shown in simulation results for both schematic and layout designs. All the dimensions of filters were obtained using optimization method on the circuit model, then these dimensions were transferred to HFSS software to verify the RF simulation.

6.2. Future Works

RF MEMS varactors based on cantilever beams will be integrated on the novel CPW based ring resonators and filters to achieve the targeted RF performance. Micro-

fabrication and hybrid and/or monolithic integration of the RF MEMS varactors are possible options. Moreover, an open ring resonator will be designed for 5G applications at the center frequency of 28 GHz and above.

References

[1] D. M. Pozar, *Microwave Engineering*. Wiley, 2005.

[2] A. E. Atia and A. E. Williams, "Narrow-bandpass waveguide filters*," IEEE Trans. Microwave Theory Tech*., vol. 20, no. 4, pp. 258–265, Apr. 1972.

[3] Lei Zhu and W. Menzel, "Broad-band microstrip-to-CPW transition via frequency-dependent electromagnetic coupling," *in IEEE Transactions on Microwave Theory and Techniques*, vol. 52, no. 5, pp. 1517-1522, May 2004.

[4] L.-H. Hsieh and K. Chang, "Tunable microstrip bandpass filters with two transmission zeros," *IEEE Trans. Microw. Theory Tech*., vol. . . . 51, no. 2, pp. 520–525, Feb. 2003.

[5] A. A. Oliner, "Historical perspectives on microwave field theory," *IEEE Transactions on Microwave Theory and Techniques*, vol. MTT-32, pp. 1022–1045, September 1984.

[6] Y. S. Lin and C. C. Cheng, "Miniature CPW parallel-coupled bandpass filter based on inductive loaded coupled-lines and lumped-element J-inverters," *in IEEE Microwave and Wireless Components Letters*, vol. 17, no. 5, pp. 343-345, May 2007.

[7] B. D. Braaten, M. A. Aziz, M. J. Schroeder and Hongxiang Li, "Meander open complementary split ring resonator (MOCSRR) particles implemented using coplanar waveguides," Wireless Information Technology and Systems (ICWITS), *2010 IEEE International Conference on, Honolulu, HI,* 2010, pp. 1-4.

[8] G. F. Craven and C. K. Mok, "The design of evanescent mode waveguide bandpass filter for a prescribed insertion loss characteristic," *IEEE Trans. Microwave Theory Tech.*, vol. 19, no. 3, pp. 295–308, Mar. 1971.

[9] S. Sun and L. Zhu, "Wideband microstrip ring resonator bandpass filters under multiple resonances," *in IEEE Transactions on Microwave Theory and Techniques*, vol. 55, no. 10, pp. 2176-2182, Oct. 2007.

[10] U. H. Lok, Y. C. Chiou and J. T. Kuo, "Quadruple-mode coupled-ring resonator bandpass filter with quasi-elliptic function passband," *in IEEE Microwave and Wireless Components Letters*, vol. 18, no. 3, pp. 179-181, March 2008.

[11] H. Xu, K. Xu, Y. Liu and Q. H. Liu, "Compact triple-mode bandpass filter using short- and open-stub loaded spiral resonator," *2016 IEEE/ACES International Conference on Wireless Information Technology and Systems (ICWITS) and Applied Computational Electromagnetics (ACES), Honolulu, HI*, 2016, pp. 1-2.

[12] M. Li, K. Xu, Y. Bai, Y. Liu and Q. H. Liu, "Planar microstrip tri-mode bandpass filter using center-stub-loaded spiral resonator," *2016 IEEE/ACES*

International Conference on Wireless Information Technology and Systems (ICWITS) and Applied Computational Electromagnetics (ACES), Honolulu, HI, 2016, pp. 1-2.

[13] M. Ohira, T. Kato and Z. Ma, "A novel microstrip filter structure consisting of transversal resonator array and its fully canonical bandpass filter design," *2015 IEEE MTT-S International Microwave Symposium, Phoenix*, AZ, 2015, pp. 1-3.

[14] S. Arain, M. A. B. Abassi, S. Nikolaou and P. Vryonides, "A square ring resonator bandpass filter with asymmetrically loaded open circuited stubs," 2016 5th International Conference on Modern Circuits and Systems Technologies (MOCAST), Thessaloniki, 2016, pp. 1-4.

[15] C. H. Kim, K. Chang and X. Liu, "Varactor tuned ring resonator filter with wide tunable bandwidth," *2015 IEEE Radio and Wireless Symposium (RWS), San Diego*, CA, 2015, pp. 141-143.

[16] S. Luo, L. Zhu and S. Sun, "A dual-band ring-resonator bandpass filter based on two pairs of degenerate modes," *in IEEE Transactions on Microwave Theory and Techniques*, vol. 58, no. 12, pp. 3427-3432, Dec. 2010.

[17] F. Lin and M. Rais-Zadeh, "A tunable 0.6 GHz – 1.7 GHz bandpass filter with a constant bandwidth using switchable varactor-tuned resonators," *2015 IEEE MTT-S International Microwave Symposium*, Phoenix, AZ, 2015, pp. 1-4.

[18] H. A. Atallah, A. B. Abdel-Rahman, K. Yoshitomi and R. K. Pokharel, "New compact tunable filter-antenna using varactor loaded ring resonator for cognitive radio front end system," *2016 IEEE/ACES International Conference on Wireless Information Technology and Systems (ICWITS) and Applied Computational Electromagnetics (ACES)*, Honolulu, HI, 2016, pp. 1-2.

[19] Peng Cai, Zhewang Ma, Xuehui Guan, Yoshio Kobayashi, Tetsuo Anada and Gen Hagiwara, "Compact millimeter-wave ultra-wideband bandpass filter using dual-mode ring resonator and multiple- mode parallel-coupled line structure," *2006 Asia-Pacific Microwave Conference*, Yokohama, 2006, pp. 163-166.

[20] J.-S. Hong, "Microstrip filters for RF/microwave application," Second Edition, *Wiley-IEEE Press*, 2010.

[21] I. Hunter, "Theory and design of microwave filters," *The Institution of Electrical Engineers*, London, 2001.

[22] Peng Wen Wong, E. Zee, S. Soeung and S. Cheab, "A new class of microwave dual-band filter based on hybrid Chebyshev polynomials," *2016 IEEE MTT-S International Microwave Symposium (IMS), San Francisco*, CA, 2016, pp. 1-3.

[23] Young-Ho Cho; Rebeiz, G.M., "Tunable 4-pole dual-notch filters for cognitive Radios and carrier aggregation systems," in Microwave Theory and Techniques, *IEEE Transactions on* , vol.63, no.4, pp.1308-1314, April 2015.

[24] Robert E. Collin, "Periodic structures and filters," in Foundations for Microwave Engineering, 1, *Wiley-IEEE Press*, 2001, pp.550-647.

[25] M. Ohira and Z. Ma, "An efficient design method of microstrip filtering antenna suitable for circuit synthesis theory of microwave bandpass filters," *2015 International Symposium on Antennas and Propagation (ISAP)*, Hobart, TAS, 2015, pp. 1-4.

[26] H. Y. A. Yim, F. L. Wong and K. K. M. Cheng, "A new synthesis method for dual-band microwave filter design with controllable bandwidth," *2007 Asia-Pacific Microwave Conference*, Bangkok, 2007, pp. 1-4.

[27] H. Meng, P. Zhao, K. L. Wu and G. Macchiarella, "Direct synthesis of complex loaded chebyshev filters in a complex filtering network," *in IEEE Transactions on Microwave Theory and Techniques*, vol. 64, no. 12, pp. 4455-4462, Dec. 2016.

[28] M. Caenepeel, F. Seyfert, Y. Rolain and M. Olivi, "Parametric modeling of the coupling parameters of planar coupled-resonator microwave filters," *2015 European Microwave Conference (EuMC)*, Paris, 2015, pp. 538-541.

[29] V. Miraftab and M. Yu, "Generalized lossy microwave filter coupling matrix synthesis and design," *2008 IEEE MTT-S International Microwave Symposium Digest*, Atlanta, GA, 2008, pp. 627-630.

[30] M. Pagani, E. H. W. Chan and R. A. Minasian, "A study of the linearity performance of a stimulated brillouin scattering-based microwave photonic bandpass filter," *in Journal of Lightwave Technology*, vol. 32, no. 5, pp. 999-1005, March1, 2014.

[31] M. A. Jamlos, M. F. Jamlos and A. H. Ismail, "High performance novel UWB array antenna for brain tumor detection via scattering parameters in microwave imaging simulation system," *2015 9th European Conference on Antennas and Propagation (EuCAP)*, Lisbon, 2015, pp. 1-5.

[32] P. Kumar, "Design of dual-band band pass filter using transmission line sections," *2015 Annual IEEE India Conference (INDICON)*, New Delhi, 2015, pp. 1-4.

[33] H. G. Momen and R. Kopru, "A method for low-pass filter designing by commensurate transmission lines," *2016 39th International Conference on Telecommunications and Signal Processing (TSP)*, Vienna, 2016, pp. 239-242.

[34] Y. H. Chun and J.-S. Hong, "Electronically reconfigurable dual-mode microstrip open-loop resonator filter," *IEEE Microw. Wireless Compon.* Lett., vol. 18, no 7, pp. 449-451, Jul. 2008.

[35] P. Sarafis and A. G. Nassiopoulou, "Cu nanolines in coplanar waveguide transmission lines," *EUROSOI-ULIS 2015: 2015 Joint International EUROSOI Workshop and International Conference on Ultimate Integration on Silicon*, Bologna, 2015, pp. 257-260.

[36] Yo-Shen Lin, Min-Shun Hsu, Chi-Hsueh Wang and Chun Hsiung Chen, "Millimeter-wave coplanar-waveguide parallel-coupled bandpass filters with

lumped-element K-inverters," *2005 European Microwave Conference*, 2005, pp. 4 pp.-.

[37] Y. C. Chen and Y. S. Lin, "Coplanar waveguide bandpass filter with hollow-T shaped transmission-line resonator for multiple spurious suppression," *2013 Wireless and Microwave Conference (WAMICON)*, Orlando, FL, 2013, pp. 1-3.

[38] S. Luo, L. Zhu and S. Sun, "A dual-band ring-resonator bandpass filter based on two pairs of degenerate modes," *in IEEE Transactions on Microwave Theory and Techniques*, vol. 58, no. 12, pp. 3427-3432, Dec. 2010.

[39] Jan-Dong Tseng, "The characteristics of parallel-connected transmission lines," *Progress in Electromagnetics Research Symposium 2005*, Hangzhou, China, August 22-26.

[40] I. Wolff, "Microstripbandpass filter using degenerate modes of a microstrip ring resonator," *Electron. Lett*., vol. 8, no. 12, pp. 29-30, 1972.

[41] A. M. Elelimy, H. N. Ahmed and A. M. El-Tager, "A low phase noise microwave oscillator based on a planar microstrip spiral resonator*," IEEE Middle East Conference on Antennas and Propagation* (MECAP 2010), Cairo, 2010, pp. 1-5.

[42] X. Cao, Y. Wu, Z. Tang and B. Zhang, "Influence of CPW dimension on quality factor in microwave measurement," *2012 IEEE 12th International Conference on Computer and Information Technology*, Chengdu, 2012, pp. 990-993.Jr.

[43] X. Liu et al., "Tunable microwave phase shifter with low RF-power variation based on high-Q epitaxial AlN ring resonator*," 2016 Conference on Lasers and Electro-Optics (CLEO)*, San Jose, CA, 2016, pp. 1-2.

[44] A. Cazzorla, R. Sorrentino and P. Farinelli, "Double-actuation extended tuning range RF MEMS varactor," *2015 European Microwave Conference (EuMC)*, Paris, 2015, pp. 937-940.

[45] S. Lakshmi, S. Rao, P. Manohar and P. N. Sayanu, "Design and simulation of multi-beam RF MEMS varactor," *International Conference on Circuits, Communication, Control and Computing*, Bangalore, 2014, pp. 308-311.

[46] P. Gupta, P. Singh, R. K. chaudhry and P. Srivastava, "Design and analysis of RF MEMS varactor for extended tuning range," *2013 International Conference on Control, Computing, Communication and Materials (ICCCCM)*, Allahabad, 2013, pp. 1-4.

[47] D. Girbau, N. Otegi, L. Pradell and A. Lazaro, "Study of intermodulation in RF MEMS variable capacitors," *in IEEE Transactions on Microwave Theory and Techniques*, vol. 54, no. 3, pp. 1120-1130, March 2006.

[48] S. H. Pu et al., "RF MEMS zipping varactor with high quality factor and very large tuning range," *in IEEE Electron Device Letters*, vol. 37, no. 10, pp. 1340-1343, Oct. 2016.

Vita

Ahlam Mohammad Ebrahim Pish Dast was born in 1989 in Dubai, UAE. Her primary and secondary school education was from Towheed Iranian Girls School in Dubai, UAE. She started her bachelor at the department of Electrical Engineering in 2008 at Ajman University of Science and Technology (AUST). In 2012, she graduated with a Bachelor of Science degree in Electrical and Electronics Engineering. She started her Master of Science degree in Electrical Engineering (MSEE) at the American University of Sharjah (AUS) in fall 2012. The research and analysis areas which she is interested in are Microwave engineering, RF MEMS Devices, Microelectronics and circuit design.